Multi-Terminal VSC-Based HVDC Systems for Offshore Wind Energy Systems Integration

A Thesis

Presented in Partial Fulfillment of the Requirements for the

Degree of Master of Science

with a

Major in Electrical Engineering

in the

College of Graduate Studies

University of Idaho

by

AlMutasim AlSammari

May 2014

Major Professor: Brian Johnson, Ph.D.

AUTHORIZATION TO SUBMIT THESIS

This thesis of AlMutasim AlSammari for the degree of Master of Science with a Major in Electrical Engineering and titled "Multi-Terminal VSC-Based HVDC Systems for Offshore Wind Energy Systems Integration," has been reviewed in final form. Permission, as indicated by the signatures and dates below, is now granted to submit final copies to the College of Graduate Studies for approval.

Major Professor:

_____Date_____

Brian Johnson, Ph.D.

Committee

Members:

_____Date_____

Herbert Hess, Ph.D.

_____Date_____

Michael Dixon, Ph.D.

Department

Administrator:

_____Date_____

Fred Barlow, Ph.D.

Discipline's

College Dean:

_____Date_____

Larry Stauffer, Ph.D.

Final Approval and Acceptance:

Dean of the College

Of Graduate Studies:

_____Date_____

Jie Chen, Ph.D.

ABSTRACT

The installation of wind energy generation has rapidly increased in the last decade, especially in countries in Europe, North America, and East Asia. Offshore wind energy is expected to be one of the major power generation sources in Europe in the near future. However, the integration of offshore wind plants into onshore ac grids remains a challenge in both technical and economic terms.

Offshore wind plants can be connected to ac grids using ac or dc transmission systems. HVDC transmission is favored over HVAC transmission as the transmission distance increases. Recently, with the improvement in the field of semiconductor power devices, it became possible to build a cost-effective VSC-based HVDC system providing many benefits including the ability to independently control reactive power on the ac side of each converter in addition to active power transfer. VSC-based Multiterminal HVDC (MTDC) transmission systems allow the interconnection of multiple offshore wind farms with multiple locations on one or more onshore ac grids, maximizing the use of the limited space for on-shore connection points. The challenges of designing and controlling MTDC systems has been a hot topic in the past years and it appears this will continue into the future. Different control schemes based on droop characteristics have been presented as a means to regulate the dc voltage and control the power flow in MTDC transmission systems to maximize performance in a stable fashion.

In this thesis, the control and steady state operation of VSC-based MTDC systems is studied. A generalized control scheme based on droop characteristics is presented. The control methodology is based on the design of the droop constants to control the grid side VSCs for three different operational modes taking into consideration the varying output of the wind

generators. The three operational modes differ in how the generated wind power is distributed between the ac grids in the MTDC system, but all are designed to minimize transmission losses while meeting the system constraints.

The difficulties and challenges of adding tap stations on existing HVDC lines in MTDC systems is also discussed in the thesis. A new control scheme approach for adding and defining control requirements for an arbitrary number of tap connections on HVDC lines in MTDC systems is presented.

MTDC test systems are built in Matlab/Simulink software to evaluate the performance of the control schemes. The system model uses switching models of two-level VSC. The models are simulated for different case scenarios and verify the performance of the control scheme for normal operation of the systems.

ACKNOWLEDGMENTS

First of all, I would like to express my deepest gratitude to my major professor and advisor Dr. Brian Johnson, not only for his guidance and encouragements throughout my research work, but also for transferring his knowledge through teaching many courses throughout my master's program.

I would also like to thank my thesis committee members, Dr. Herbert Hess and Dr. Mike Dixon for their valuable input and advice reviewing my thesis. The appreciation also goes to my professors, Fred Barlow, Jim Alves-Foss, and Paul Ortmann for their generosity in passing their knowledge and expertise in their courses.

This thesis would not have been possible without Dr. Ahmed Massoud in Qatar University at Qatar. His help, guidance, patience, and encouragement were continuous throughout my research despite his busy schedule. Working under his guidance was a great opportunity to be enlightened by his knowledge and expertise.

I am also indebted to many of my colleagues and superiors in BeIN Sports for all the support they provided throughout my masters. All respect to Mr. Ihsan Ali, Mr. Salaheddine Awad, Mr. Ayman AlGhoutani, and Mr. Mohammed Rashad. I don't want to forget my friends who were supportive all the time.

Last but not least, a special thanks to my family for their support and love. Words cannot express how grateful I am to my dad, my mom, and my brother for their encouragement and patience in all the difficult times.

DEDICATION

This work is dedicated to my special Mom, Dad and Brother for their endless love, support, and encouragement.

TABLE OF CONTENTS

Authorization to Submit Thesis ii
Abstract iii
Acknowledgments v
Dedication vi
Table of Contents vii
List of Figures ix
List of Tables xiii
Acronyms xiv

1.Chapter 1: Introduction 1
1.1.Background 1
1.2.HVDC Converter Technologies 2
1.3.Multiterminal HVDC Systems 5
1.4.Scope of the Thesis Work 6

2.Chapter 2: Two-Terminal VSC-HVDC – Control and Principle of Operation 8
2.1.Basic Concept and Study System Model 8
2.1.1.Transformer 8
2.1.2.Phase Reactor 9
2.1.3.AC Filter 9
2.1.4.DC Capacitors 10
2.1.5.DC Transmission Line 10
2.2.Overview of Voltage Sourced Converters 10
2.2.1.Operating Principles of a VSC 11
2.2.2.Two-Level, Six-Pulse Bridge VSC 14
2.2.3.Three-Level Neutral Point Clamped VSC 15
2.2.4.Modular Multi-Level Converters 16
2.3.Control Objectives and Techniques 18
2.3.1.Control Circuit of GSC 18
2.3.2.Control Circuit of WPPC 22

*3.*Chapter 3: Two-Terminal VSC-HVDC – Simulation Results 24
3.1.System Design 24
3.2.Simulation Results 26

4.Chapter 4: Multi-Terminal VSC-HVDC 32
4.1.Three-Terminal HVDC System Consisting of Two Wind Power Plants and One AC Grid 32
4.1.1.Basic Concept and System Diagram 32
4.1.2.Droop Characteristics 34

4.1.3.Logic Flowchart of Active Power Distribution Based on Droop characteristics and WPPs Generation Limits 36
4.1.4.Case Studies 38
4.2.Three-Terminal HVDC System Consisting of One Wind Power Plant and Two AC Grids 44
4.2.1.Basic Concept and Block Diagram 44
4.2.2.Case 1 – Potential Modes of Operation 46
4.2.3.Case Studies 53
4.3.General Control Approach for Multi-Terminal HVDC Systems 60
4.3.1.Control of VSCs that Provide Active Power in MTDC Systems 61
4.3.2.Control of VSCs that Receive Active Power in MTDC Systems 63
4.4.Summary 65

5.Chapter 5: Adding Single Taps on Lines in Multiterminal HVDC Systems 66
5.1.Introduction 66
5.2.Tapping on MTDC systems – Case Studies. 68
5.2.1.Case A – Offshore Oil Rig Located near AC Grid 70
5.2.2.Case B – Offshore Oil Rig Located near Wind Power Plant 1 73

6.Chapter 6: Multi-Tapping on HVDC Lines in MTDC Systems 76
6.1.Introduction 76
6.2.Control Schemes of Multi-Tapping in MTDC Systems 77
6.2.1.Approach Description 77
6.2.2.Control Scheme A 79
6.2.3.Control Scheme B 80
6.2.4.Control Scheme C 81
6.3.Case Studies of Multi-Tapping in MTDC Systems 82
6.3.1.MTDC System Configuration 82
6.3.2.Case A 82
6.3.3.Case B 85
6.3.4.Case C 88
6.4.Summary 91

7.Chapter 7: Summary, Conclusion, and Future Work 92
7.1.Summary 92
7.2.Conclusion 93
7.3.Future Work 93

References……. 95

Appendix A: Park's Transformation……. 99

LIST OF FIGURES

Figure 1.1 New Installed Offshore Wind Capacity in Europe in MW 1
Figure 1.2 Series MTDC System Configuration 5
Figure 1.3 Parallel MTDC System Configuration 5
Figure 2.1 Typical Architecture of a Two-Terminal VSC-HVDC System 8
Figure 2.2 Buck DC-DC Converter 11
Figure 2.3 Boost DC-DC Converter 11
Figure 2.4 Bidirectional DC-DC Converter 12
Figure 2.5 Rearrangement of Bidirectional DC-DC Converter 12
Figure 2.6 Two-Level VSC 14
Figure 2.7 Three-Level Neutral Point Clamped VSC 16
Figure 2.8 Half-Bridge Sub-Module Circuit Diagram 16
Figure 2.9 Two Sub-Modules MMC 17
Figure 2.10 Block Diagram for PLL Implemented in this Study 19
Figure 2.11 Inner Controller Block Diagram 21
Figure 2.12 DC Voltage Controller Block Diagram 21
Figure 3.1 Two-Terminal VSC-HVDC system built in Simulink 26
Figure 3.2 VSC Station – Snapshot from Simulink 26
Figure 3.3 Graph of the active and reactive power delivered by WPP versus time 28
Figure 3.4 Graph of the active and reactive power received by the ac grid versus time 28
Figure 3.5 Graph of I_d and I_q transmitted from the WPP to the dc line 28
Figure 3.6 Graph of I_d and I_q received by AC grid from the dc line 28
Figure 3.7 Graph of dc voltage at the WPP converter terminal versus time 29
Figure 3.8 Graph of dc voltage at the GS converter terminal versus time 29
Figure 3.9 Equivalent dc circuit of the system 29
Figure 3.10 Graph of the current in the dc line versus time 29
Figure 3.11 Graph of 3 cycles of the ac voltages of the WPP versus time 30
Figure 3.12 Graph of 3 cycles of the ac currents of the WPP versus time 30
Figure 3.13 Graph of 3 cycles of the ac voltages of the ac grid versus time 30

Figure 3.14 Graph of 3 cycles of the ac currents of the ac grid versus time..... 30
Figure 4.1 Three-Terminal VSC-HVDC System consisting of Two Wind Power Plants and One AC grid..... 33
Figure 4.2 Equivalent DC circuit of the system..... 35
Figure 4.3 Logic Flowchart Determining the Active Power Provided by WPP1..... 37
Figure 4.4 Logic Flowchart Determining the Active Power Provided by WPP2..... 37
Figure 4.5 Graph of the Active and Reactive Power Delivered by WPP1 versus time..... 40
Figure 4.6 Graph of the Active and Reactive Power Delivered by WPP2 versus time..... 40
Figure 4.7 Graph of the Active and Reactive Power Received by the AC grid versus time..... 41
Figure 4.8 Graph of DC voltage at the GS converter terminal versus time 41
Figure 4.9 Graph of DC voltages at WPP1 and WPP2 converter terminals versus time..... 41
Figure 4.10 Graph of the Active and Reactive Power Delivered by WPP1 versus time..... 42
Figure 4.11 Graph of the Active and Reactive Power Delivered by WPP2 versus time..... 42
Figure 4.12 Graph of the Active and Reactive Power Received by the AC grid versus time..... 43
Figure 4.13 Graph of DC voltage at the GS converter terminal versus time 43
Figure 4.14 Graph of DC voltages at WPP1 and WPP2 converter terminal versus time 43
Figure 4.15 Three-Terminal VSC-HVDC System consisting of One Wind Power Plant and Two AC grids 44
Figure 4.16 Equivalent DC circuit of the system..... 45
Figure 4.17 DC Voltage Controller with Converter Current Limiter Block 47
Figure 4.18 VI Characteristics for GSVSC1 48
Figure 4.19 VI Characteristics of the Two GSVSCs..... 49
Figure 4.20 DC Voltage Controller of GSVSC1 operated in Mode3..... 51
Figure 4.21 DC Voltage Controller of GSVSC2 operated in Mode3..... 51
Figure 4.22 VI Characteristics of the Two GSVSCs..... 51
Figure 4.23 Graph of the Active and Reactive Power Delivered by WPP versus time..... 55
Figure 4.24 Graph of DC voltage at the WPP converter terminal versus time 55
Figure 4.25 Graph of the Active and Reactive Power received by AC grid1 versus time 56
Figure 4.26 Graph of the Active and Reactive Power received by AC grid2 versus time 56

Figure 4.27 Graph of DC voltage at the AC grid 1 converter terminal versus time 57
Figure 4.28 Graph of DC voltage at the AC grid 2 converter terminal versus time 57
Figure 4.29 Graph of the Active and Reactive Power Delivered by WPP versus time..... 58
Figure 4.30 Graph of the Active and Reactive Power received by AC grid1 versus time 59
Figure 4.31 Graph of the Active and Reactive Power received by AC grid2 versus time 59
Figure 4.32 Graph of DC voltage at the AC grid 1 converter terminal versus time 59
Figure 4.33 Graph of DC voltage at the AC grid 2 converter terminal versus time 59
Figure 4.34 MTDC system consisting of n WPPs and m AC grids 60
Figure 4.35 Equivalent DC circuit of the system..... 61
Figure 4.36 Logic Flowchart Determining the Active Power Provided WPPs and AC grids..... 62
Figure 5.1 Two-Terminal HVDC System with an Inserted Tap Station. 66
Figure 5.2 DC Equivalent Circuit of the Two-Terminal HVDC System with an Inserted Tap Station as shown in Figure 5.1..... 67
Figure 5.3 MTDS System consisting of Two Wind Power Plants and One grid 69
Figure 5.4 Case A System Diagram 71
Figure 5.5 Graph of the Active and Reactive Power Received by the AC grid versus time for the case with a tap station. 71
Figure 5.6 Graph of the Active and Reactive Power Received by the AC grid versus time for the case without a tap station. 71
Figure 5.7 Graph of DC voltage at the AC grid converter terminal versus time for the case with a tap station 72
Figure 5.8 Graph of DC voltage at the AC grid converter terminal versus time for the case without a tap station..... 72
Figure 5.9 Graph of DC voltage at the WPP1 converter terminal versus time for the case with a tap station 73
Figure 5.10 Graph of DC voltage at the WPP1 converter terminal versus time for the case without a tap station 73
Figure 5.11 Case B System Diagram 73
Figure 5.12 Graph of the Active and Reactive Power Received by the AC grid versus time for case B simulation 74

Figure 5.13 Graph of DC voltage at the AC grid converter terminal versus time for case B simulation 74
Figure 5.14 Graph of DC voltage at the WPP1 converter terminal versus time for case B simulation 74
Figure 6.1 Two-Terminal HVDC System with Two Tapping Stations. 77
Figure 6.2 DC Equivalent Circuit of the System in Figure 6.1 78
Figure 6.3 MTDC system consisting of 1 WPP, 1 AC grid, and *r* tap stations 79
Figure 6.4 DC Equivalent Circuit of the System shown in Figure 6.3 80
Figure 6.5 Case A System Diagram 83
Figure 6.6 Graph of the Active and Reactive Power Delivered by WPP 84
Figure 6.7 Graph of the Active and Reactive Power Received by the AC grid versus time 84
Figure 6.8 Graph of the DC voltages at Different Locations in the HVDC Line. 84
Figure 6.9 Graph of the DC currents through the HVDC line at different locations. 85
Figure 6.10 Graph of the Active and Reactive Power Delivered by WPP 86
Figure 6.11 Graph of the Active and Reactive Power Received by the AC grid versus time 86
Figure 6.12 Graph of the DC voltages at Different Locations in the HVDC Line. 87
Figure 6.13 Graph of the DC currents through the HVDC line at different locations. 87
Figure 6.14 Case C System Diagram 88
Figure 6.15 Graph of the Active and Reactive Power Delivered by WPP versus time 89
Figure 6.16 Graph of the Active and Reactive Power Received by the AC grid versus time 89
Figure 6.17 Graph of the DC voltages at Different Locations in the HVDC Line. 90
Figure 6.18 Graph of the DC currents through the HVDC line at different locations 90

LIST OF TABLES

Table 3.1 Parameters used in the system design 24

Table 4.1 Operating Scenarios for active power sharing in a three-terminal system that consist of two wind power plants and one ac grid 33

Table 4.2 Cases of active power distribution through the dc transmission system in a three-terminal HVDC system consisting of terminals for one wind power plant and two ac grids 46

ACRONYMS

HVDC	----	High Voltage Direct Current
HVAC	----	High Voltage Alternating Current
VSC	----	Voltage Source Converters
MTDC	----	Multi-Terminal High Voltage Direct Current
LCC	----	Line Commutated Converters
PWM	----	Pulse Width Modulation
DC	----	Direct Current
WPP	----	Wind Power Plant
IGBT	----	Insulated-Gate Bipolar Transistor
AC	----	Alternating Current
MMC	----	Modular Multi-Level Converter
NPC	----	Neutral Point Clamped
WPPC	----	Wind Power Plant Converter
GSC	----	Grid Side Converter
PLL	----	Phase Locked Loop
GSVSC	----	Grid Side Voltage Source Converter

1. Chapter 1: Introduction

1.1. Background

Despite its unique output power characteristics, which make its integration to power grids a challenge in technical and economic terms, wind energy is expected to be one of the major power generation sources in many areas of the world in the near future. The *European Wind Energy Association* estimates that wind power will provide 10% of the installed generation capacity in the next two decades with an estimated generation of 120 GW [1]. Currently, wind power provides around 1.92% of the world's electricity [2]. Figure 1.1 shows the annual new installed offshore wind capacity in Europe from 2000 through 2013 in MW. From the figure we can see that the capacity of the installed wind power plants is increasing significantly every year.

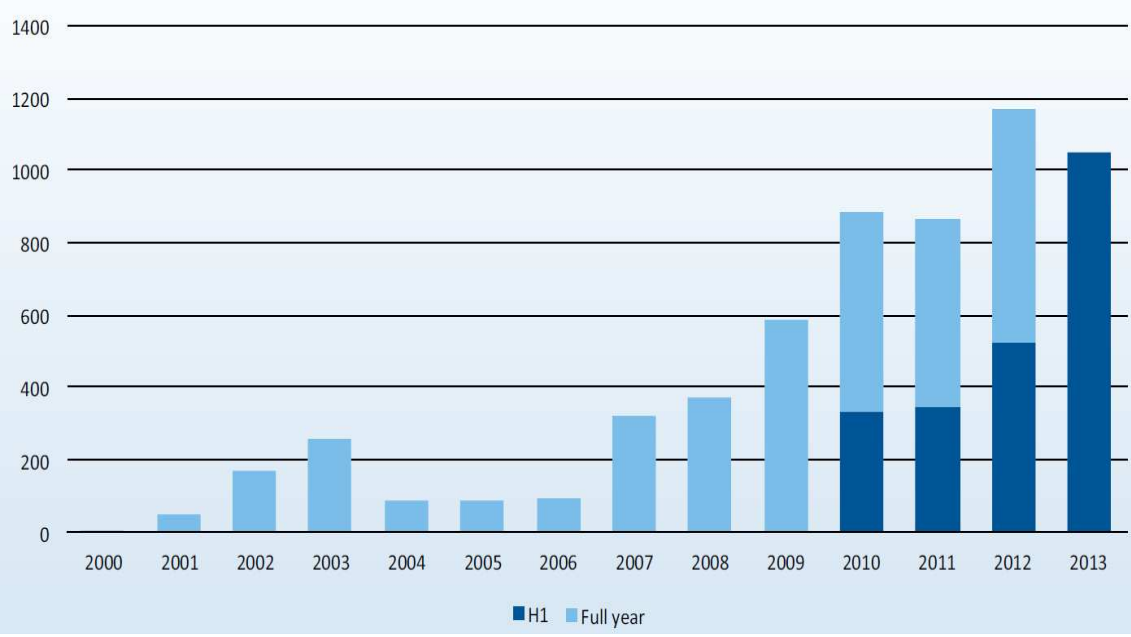

Figure 1.1 New Installed Offshore Wind Capacity in Europe in MW. H1: First Half of the Year [1]

Recently in Europe, the power production from offshore wind plants overtook that from the

onshore wind plants. The reasons for this is two-fold. First, onshore wind plants are considered unsightly by the public and also contribute to noise disturbance, especially in areas with high population density such as many countries in Europe. Second, offshore locations are characterized by higher speed and more stable wind flow than onshore locations [3]. But offshore wind farms are more expensive to install and maintain.

However, integration of offshore wind farms to existing ac grids is a major challenge to the power industry. Offshore wind farms are usually located at a remote location of at least 10km away from the shore. This fact makes HVDC transmission more favorable than the conventional HVAC transmission for connecting offshore wind energy plants to onshore ac grids. The capacitive charging currents for ac cables limits HVAC transmission in terms of distance and capacity. Installing shunt reactors to compensate for this is possible, but is not an economical option, especially for offshore installations [4]. As transmission distance increase, transmission losses become a greater concern, which is another factor favoring HVDC transmission over the HVAC transmission. In fact, dc transmission is significantly more efficient in terms of line losses than ac transmission. On the other hand, dc transmission will require converter stations, which will have their own conversion losses and installation costs [2, 4, 5]. One challenge for offshore wind generation is the limited number of locations where transmission line can come on shore, creating a need to create a multiterminal offshore dc system.

1.2. HVDC Converter Technologies

The majority of existing HVDC systems are based on line commutated converters (LCCs) which use thyristors bridges for AC/DC rectification and DC/AC inversion. LCCs are a well-established and proven technology and have been deployed in many existing projects.

However, due to the great development in the field of power semiconductor devices, voltage source converters (VSCs) have recently been considered as an attractive alternative to LCCs for several classes of applications. Two-level bridge based VSCs and three-level converter based VSCs use the pulse width modulation (PWM) based switching techniques for controlling the dc voltage and the ac phase voltages. Most early VSC HVDC schemes utilize two-level bridges, and a few use three-level converters. Newer installations appear to be going over to modular multilevel converters (MMCs). MMCs consist of hundreds of single phase VSC modules in series on each phase, and switch modules in and out of the circuit to produce a controlled magnitude and phase angle for the ac voltage.

VSC-based HVDC systems have the following advantages over the conventional LCC-based HVDC systems [4-7]:

- Modern switching schemes or converter topologies allow VSC to be controlled to provide an independent decoupled control of active and reactive power injection.
- Each converter has the ability to reverse the direction of power flow within milliseconds by reversing the direction of dc current flow without altering the dc voltage polarity or causing any interruption in service, which is important for parallel connected multiterminal systems. The direction of power flow is reversed in a LCC by reversing the voltage polarity which works well in series connected multiterminal systems, but not for parallel or mesh connected systems.
- With appropriate converter rating and controls, the VSC can provide dynamic voltage support to the ac system. LCC converters require extensive reactive power support, and often need dynamic reactive power support.

- VSC systems can operate with very weak ac systems, while LCCs require relatively stiff ac systems, especially at an inverter terminal.
- The harmonic filters needed for VSC-based HVDC systems are more compact in comparison to those needed for LCC-based HVDC systems, resulting in a smaller substation. In addition, MMC VSC based HVDC systems require little or no harmonic filters at all.

On the other hand, VSCs have the following disadvantages compared to LCC based systems [4-7]:

- VSC stations have higher capital costs than LCC stations with an equivalent MW rating.
- Converter station losses for MMC based VSCs are approximately double those of LCC stations. Conversion losses for two level PWM based VSCs are approximately double those of MMC VSC stations.
- The maximum VSC voltage and current ratings are lower than those for LCCs, with maximum MW ratings for LCC systems approximately eight times those of VSC installations.
- Most converter topologies for VSCs require either ac or dc circuit breakers to interrupt dc faults since the converter diodes are not able to interrupt reverse dc fault currents.

Despite all of these advantages, there are only a few existing VSC-HVDC systems worldwide, largely because of higher operational costs and limited power transfer limits. However, as the technology has improved, the number of studies for potential VSC-HVDC applications has increased. This includes a large number of VSC-HVDC systems connecting offshore wind

farms to ac grids that are under study for installation in the near future. There are also studies under way for a trans-European underground HVDC grid based on VSC converters [8].

1.3. Multiterminal HVDC Systems

Figures 1.2 and 1.3 show two configurations for MTDC systems: series MTDC system and parallel MTDC system, respectively. A parallel configuration is more practical for MTDC systems due to the following advantages it has over series configuration [9, 10]:

- Transmission losses in series configuration are higher than that in parallel configuration, especially if the system is expanded to a mesh configuration.
- Insulation requirement is more complex in series configuration since the voltage across the terminals varies with power variation.
- Expansion to a mesh connected system allows redundant transmission paths, improving reliability.

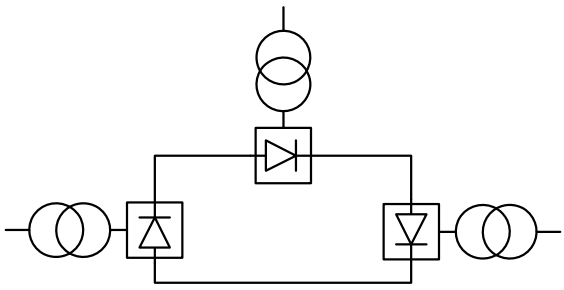

Figure 1.2 Series MTDC System Configuration

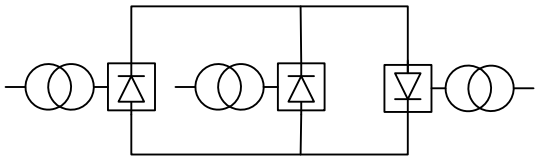

Figure 1.3 Parallel MTDC System Configuration

On the other hand, parallel connected systems do have some disadvantages. The most challenging one is the need to have some form of fast acting DC circuit breaker to isolate faulted lines. Studies have recommended clearing times as low as 4 milliseconds for parallel

connected schemes based on VSCs. Prototype designs capable of meeting this requirement have announced recently, but are not commercially proven [11].

The implementation of parallel connected MTDC grids with many terminals is under serious consideration in Europe and Southeast Asia. As noted above, VSCs lend themselves better to parallel connected systems than LCCs do.

The MTDC systems could connect possibly tens or hundreds of terminals through ac to dc conversion stations. These terminals could be connecting ac grids, offshore wind farms, or other types of distributed generation and energy storage devices. However, they are not in common use for two reasons. First of all, LCCs are not suitable for MTDC system with more than three terminals. Second, VSCs are not yet proven technology in this application.

The dc voltage level of the dc transmission network and the active power transfers at the ac terminals are controlled by the control circuits of the VSCs along with ac voltage magnitude or reactive power. VSC based MTDC grids have been a hot research topic in the past few years and it appears this will continue into the future [5, 12, 13].

1.4. Scope of the Thesis Work

This thesis focuses on the control and steady state operation of VSC-based MTDC systems. A comprehensive study of MTDC systems' control schemes based on droop characteristics is presented. Simulink software is used to build a switching model of the MTDC systems discussed throughout the thesis. The systems are simulated for different case scenarios to verify the functionality of the control schemes.

The thesis also examines tapping on HVDC lines in MTDC systems and its technical challenges. A new control scheme approach for adding multiple taps on HVDC lines in MTDC systems is presented. Various case studies were simulated to test the operation of MTDC

systems in the presence of single and multiple tapping stations.

The outline of the next chapters is as follows:

- Chapter 2 discusses the control and principle of operation of two-terminal HVDC systems. The dc system model, components, and control circuit are presented in this chapter.
- Chapter 3 presents the design parameters and assumptions of the switching model built in Simulink software. The chapter also present the simulation results of a two-terminal HVDC system case study.
- Chapter 4 discusses multiterminal HVDC systems. The chapter begins by discussing three-terminal HVDC systems integrating two wind plant and one ac grid. Following that, the case of integrating one wind plant and two points on an ac grid is presented. Finally, a general MTDC system with an arbitrary number of wind plants and ac grids is discussed. Throughout the chapter, different case studies are simulated.
- Chapter 5 introduces the concept of adding single taps on HVDC lines in MTDC systems.
- Chapter 6 discusses adding multiple taps on HVDC lines in MTDC systems. A new control scheme approach is presented and several case studies are simulated.
- Chapter 7 summarizes the work presented in this thesis and suggests avenues for future work.

2. Chapter 2: Two-Terminal VSC-HVDC – Control and Principle of Operation

2.1. Basic Concept and Study System Model

Figure 2.1 shows a block diagram of a typical architecture of a two-terminal VSC-HVDC system connecting a wind power plant (WPP) to an ac grid [14]. This model is not limited to WPP applications. In this simple topology, two VSCs are used. One VSC will rectify the ac power generated by the WPP to dc power, which will be transmitted to the second VSC through the HVDC transmission cable. The second VSC will invert the dc power back to ac power and supply it to the ac grid. The following sub-sections describe the different components of the two-terminal VSC-HVDC excluding the VSCs themselves, which will be explained separately in Section 2.2.

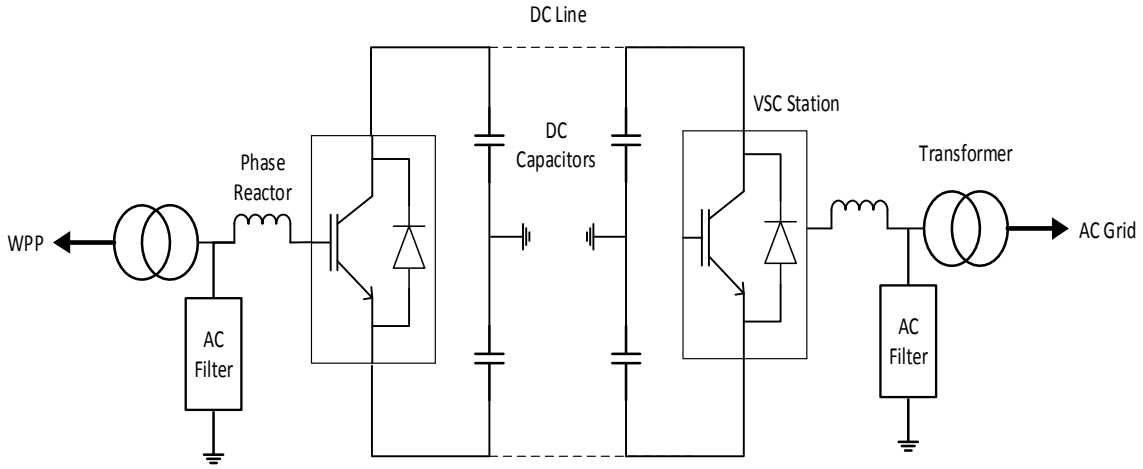

Figure 2.1 Typical Architecture of a Two-Terminal VSC-HVDC System

2.1.1. Transformer

Usually, VSCs are connected to the ac system, whether it is the WPP or the ac grid, through transformers. The objective of these transformers is to transform the ac voltage to a level that is suitable for the VSC. Depending on the converter topology, the transformer might also provide an isolated neutral to the converter [15].

2.1.2. Phase Reactor

Phase reactors are connected between the transformers and the VSCs for two important reasons. First, the reactors limit the rate of rise of currents through the power electronic devices to protect them. Second, they act as a low pass filter reducing the harmonic components in the ac voltage [15].

It is important to note that transformers have a leakage reactance in the range of 0.1 to 0.2 pu [15]. This value should be subtracted from the desired total inductance prior to selecting the phase reactor inductance.

2.1.3. AC Filter

Due to the switching behavior of the IGBTs in the VSCs, the ac voltage will contain voltage harmonic components. The series reactor acts as a low pass filter to help remove these harmonic components. AC current harmonics are also produced as a secondary effect of the voltage harmonics. Tuned ac filters are usually installed on the ac side of the VSCs to prevent these harmonics from entering and, therefore, affecting the ac network, for both the ac grid and the WPP. For VSCs, the current harmonics on the ac side are at odd multiples of the PWM switching frequency [15]. If a MMC topology is used, the number of levels determines the effective switching frequency and, therefore, the harmonic content. Therefore, if the switching is at a high frequency, just a high pass filter needs to be installed in VSC-HVDC systems, with a low current rating, which results in a smaller filtering requirement relative to the amount of filtering installed in LCC-HVDC systems. In addition, the harmonic filters do not need to be sized to provide significant capacitive reactive power at fundamental frequency. The first initial MMC installations have a sufficient number of levels to eliminate the need for ac harmonic filters.

2.1.4. DC Capacitors

DC capacitors are added to act as filters to reduce the amplitude of the ripple in the dc voltage. The larger the dc capacitors are, or the higher the switching frequency is, the smaller the amplitude of the ripple. However, the larger capacitors increase the cost and the stored energy which is discharged into a fault. Therefore, the dc capacitors' value should be chosen carefully. Two level converters often require only one or two capacitors, while MMC topologies will have smaller, individual capacitors for each sub-module on each phase, which can lead to a converter with several hundred separate capacitors. Balancing of the voltage between the capacitors in a MMC is handled through a supplemental control loop [15].

2.1.5. DC Transmission Line

The dc transmission line between the two VSCs, which can be some combination of overhead lines, underground cables or underwater cables, is usually modeled as a single pi section with series resistance and shunt capacitance split between the two ends of the line. The line inductance is neglected for steady-state and quasi-steady-state operating scenarios where the line inductance does not impact the results. The shunt capacitance will be lumped to the dc capacitors at the converters and the rest of the dc line will be represented as a series resistance connecting the converter stations [15].

2.2. Overview of Voltage Sourced Converters

There are many different topologies of three-phase VSCs that can be used in a two-terminal HVDC transmission system. The basic concept of a VSC is explained in the sub-section 2.2.1. The following sub-sections will highlight some of the different VSC topologies.

2.2.1. Operating Principles of a VSC

To understand how a VSC works, it is useful to first look at the simple buck and boost DC-DC converter topologies. Figures 2.2 and 2.3 show the circuit diagrams of unidirectional buck and boost DC-DC converters respectively [16].

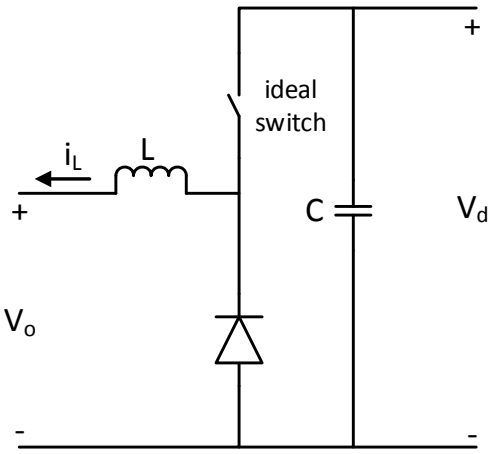

Figure 2.2 Buck DC-DC Converter

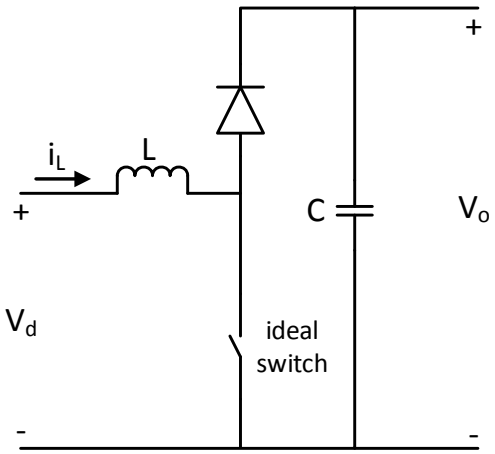

Figure 2.3 Boost DC-DC Converter

A buck converter is a converter that steps the voltage down. In this converter, the relationship between the average output voltage and the average input voltage is determined by the following equation:

$$V_o = D \cdot V_d \tag{2.1}$$

$$D = Duty\ Ratio = \frac{T_{on}}{T_s} \tag{2.2}$$

While a buck converter steps the voltage down, a boost converter steps the voltage up and the average output voltage and input voltage are related by the following equation:

$$V_o = \frac{V_d}{(1 - D)} \tag{2.3}$$

Power transfer in these buck and boost DC-DC converters topologies is unidirectional as shown in Figures 2.2 and 2.3. Combining both converters as shown in Figure 2.4 will allow

bidirectional power transfer, which comes from the ability to reverse the current in the circuit. Only one control signal in the bi-directional DC-DC converter is needed in the bidirectional DC-DC converter since the switch ON and OFF states will be exactly the opposite.

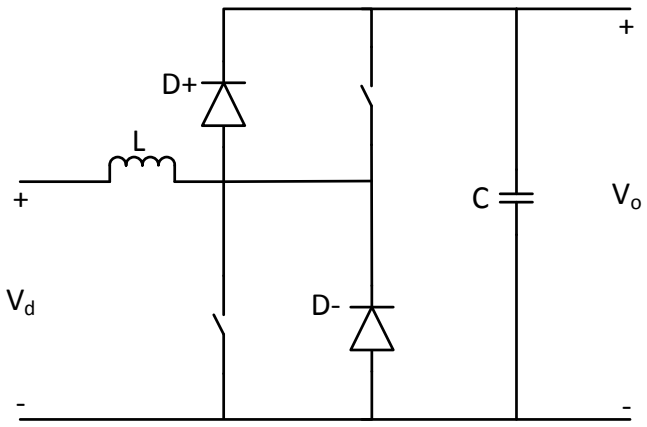

Figure 2.4 Bidirectional DC-DC Converter

Redrawing the bidirectional DC-DC converter as shown in Figure 2.5, a phase voltage, V_{ph}, can be defined as the voltage at the point X with reference to the ground.

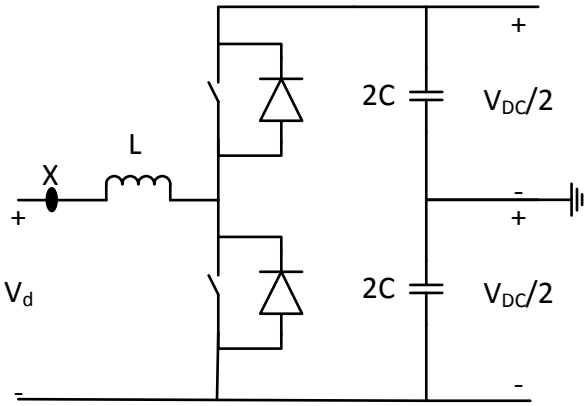

Figure 2.5 Rearrangement of Bidirectional DC-DC Converter

The phase voltage will have the following equation:

$$V_{ph} = V_d + \frac{-V_{DC}}{2} \qquad \textbf{(2.4)}$$

Replacing V_d and simplifying the equation, results in the following:

$$V_{ph} = D_1 \cdot V_{DC} + \frac{-V_{DC}}{2} \quad \textbf{(2.5)}$$

$$V_{ph} = (2D_1 - 1)\frac{V_{DC}}{2} \quad \textbf{(2.6)}$$

Now, a variable K can be defined as:

$$K = 2D_1 - 1, \qquad -1 \leq K \leq 1 \quad \textbf{(2.7)}$$

Replacing the variable K with a sinusoidal function of variable amplitude and angle, results in a sinusoidal phase voltage V_{ph}.

$$K = m_a \cdot sin(\omega t) \quad \textbf{(2.8)}$$

$$0 < m_a(Mod.Ratio) \leq 1 \quad \textbf{(2.9)}$$

$$V_{ph} = \frac{V_{DC} \cdot m_a \cdot sin(\omega t)}{2} \quad \textbf{(2.10)}$$

The bidirectional half-bridge converter is considered the building block of most VSC topologies [16]. Its switching is usually controlled by a PWM switching technique. There are many types of PWM techniques that can be used for VSCs. The simplest type to understand is the sine-triangle PWM. In this method the PWM signal is the output of a comparator that compares the instantaneous value of a generated pure triangle wave with the sinusoidal input reference signal. Using PWM control will provide the following advantages over indirect ac voltage control scheme [15, 17, 18]:

- It will provide an additional degree of freedom, allowing separate control of two quantities such as ac voltage amplitude and dc voltage.
- Lower order harmonics will be significantly reduced, especially if the switching frequency is high. This will result in less investment in harmonic filters.
- It provides a faster response time than six step phase control can provide.

On the other hand, using PWM will increase the power losses due to the frequent switching of the full dc line voltage. For this specific reason, all of the VSC-HVDC manufacturers are moving away from two-level bridges with PWM and going toward MMCs, which will be described in Section 2.2.4 [15, 17, 18].

2.2.2. Two-Level, Six-Pulse Bridge VSC

The two-level, six-pulse bridge is the simplest topology that can be used to build a three-phase VSC. The circuit diagram of this topology consists of three of the half bridge single-phase converters discussed in Section 2.2.1 connected in parallel. The circuit consists of six IGBTs which are driven to be either off or into full saturation mode, producing two voltage levels, which are 0.5 V_{DC} and -0.5 V_{DC}. Figure 2.6 shows a circuit diagram of a two-level, six-pulse bridge VSC.

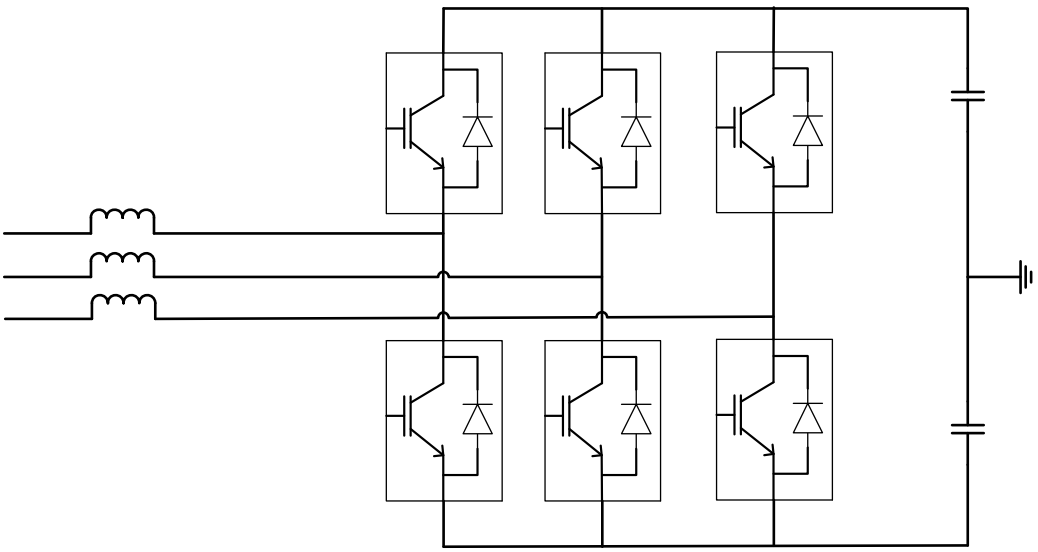

Figure 2.6 Two-Level VSC

Each IGBT in this topology is connected with an anti-parallel diode, which is inherent in the IGBT device package. These diodes provide a path for the current to flow in the opposite direction when the fundamental component of the resultant ac current is out of phase with

the fundamental components voltage produced by the converter. This is helpful in cases where the load is inductive [17, 18].

2.2.3. Three-Level Neutral Point Clamped VSC

The three phase, three-level neutral point clamped VSC shown in Figure 2.7 is a twelve-pulse VSC capable of generating three voltage levels; 0.5 VDC, 0, and -0.5 VDC. Each arm of the converter consists of 4 IGBT/diodes plus two additional clamp diodes that connect to the neutral of the capacitors. The NPC is the simplest topology out of the general family of multilevel converters.

Three-level NPC VSC has the following advantages over two-level VSC:

- For the same switching frequency, it will have twice the effective switching frequency and, thus, lower amplitudes of harmonics than an equivalent two-level VSC.
- The voltage across each individual switch in a three-level NPC VSC will be lower than that in a two-level VSC, reducing the need to connect devices in series.
- Lowering the voltage across each power electronic device also lowers the switching loss for each switching operation, improving converter efficiency.

On the other hand, three-level NPC VSCs are more complex and have more components than the ordinary two-level VSC. For example, one issue that adds complexity to the control in a three-level VSC is balancing dc voltages across the capacitors. Three-Level NPC VSCs are also more expensive than two-level VSCs, but the added capital cost is generally offset with lifetime savings in operating costs with reduced losses [17, 18]

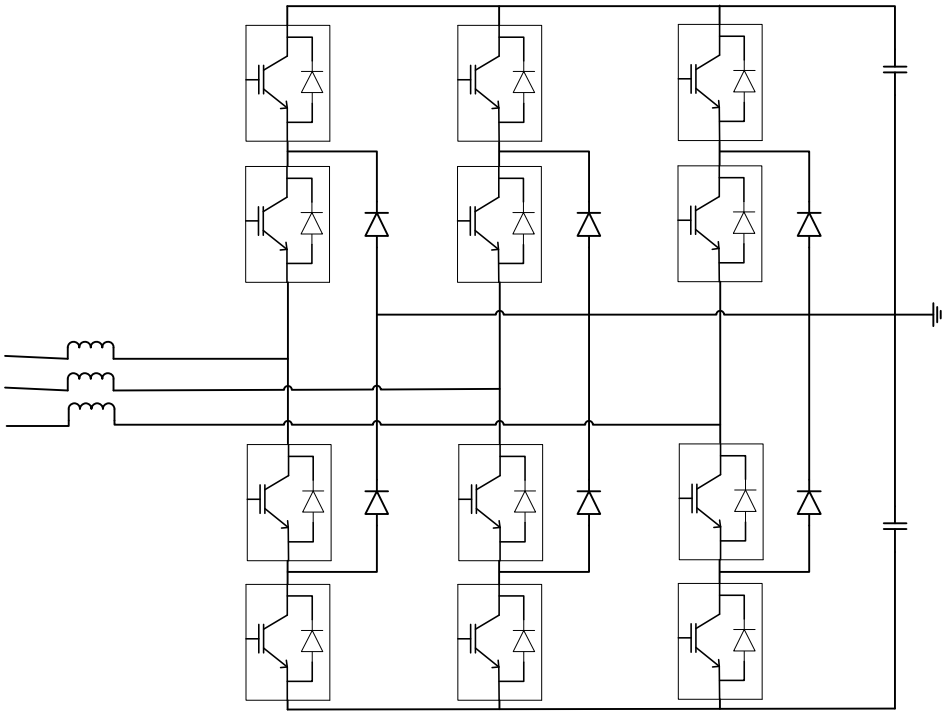

Figure 2.7 Three-Level Neutral Point Clamped VSC

2.2.4. Modular Multi-Level Converters

Modular Multi-level Converters (MMC) are the most commonly selected VSC topology in new orders or preliminary studies for new VSC HVDC systems. Figure 2.8 shows the circuit diagram of a half-bridge based sub-module. Figure 2.9 shows the circuit diagram of an MMC with 2 Sub-Modules.

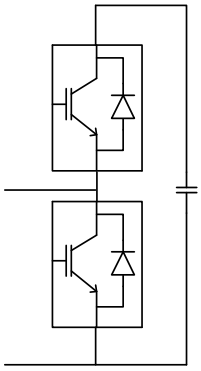

Figure 2.8 Half-Bridge Sub-Module Circuit Diagram

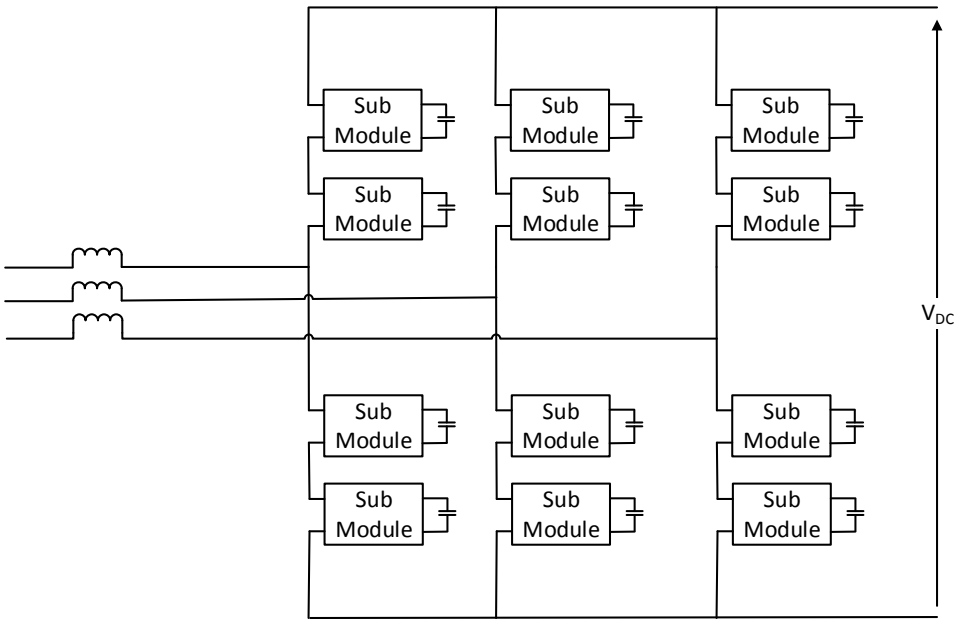

Figure 2.9 Two Sub-Modules MMC

Some manufacturers also offer full bridge modules for HVDC applications. MMCs have the following advantages [19]:

- They can operate with lower switching frequencies for individual sub-modules than two-level and three-level VSCs. PWM does not need to be used at all with a sufficient number of modules.
- The MMC can be scalable to higher voltage and power levels by changing the number of modules.
- The use of standardized modules allows the converter to be more easily customized to the application with less design effort than would be the case with two or three level converters or with LCC.
- With a sufficient number of modules, the ac voltage and current will have lower harmonic distortion than that from two-level and three-level VSCs.

- The MMC can have a very high efficiency that can reach up to 99% per converter when half-bridge sub-modules are used.

On the other hand, MCCs require more components than two-level and three-level VSCs. They are also more complex in terms of control. But from the point of view of steady-state closed-loop control behavior, the different VSC topologies have similar response. For this reason, the rest of the thesis will be based on two-level VSCs [19].

2.3. Control Objectives and Techniques

As mentioned earlier, one of the main advantages of VSC-HVDC is that it gives the ability to control active and reactive power independently. VSCs using PWM switching or multilevel converters have two degrees of freedom, i.e., they can control two different variables simultaneously. To improve response, the control will be done in the synchronous dq reference frame. Appendix A describes the method for transforming voltage or current parameters from the abc phase reference frame to the synchronous dq reference frame.

The following sub-sections will explain the control circuits for the grid side VSC (GSC) and the wind-power-plant VSC (WPPC) respectively.

2.3.1. Control Circuit of GSC

The grid side converter (GSC) will be used to control the dc line voltage at the grid converter terminals and the reactive power injected by the converter into the ac grid. In order to do this, the phase voltages and currents must be measured at the ac grid terminals. These measurements will then be transformed to the synchronous dq0 reference frame using the Park's transform explained in Appendix A.

2.3.1.1. Synchronization

In order to provide the frequency reference for the transformation, a phase locked loop (PLL) will be used to track the frequency of the system. The PLL will be designed to align the *d* component of the voltage with the phase *a* voltage. Figure 2.10 shows the block diagram of the PLL utilized in this work. The value of θ is the tracked phase angle that cycles from 0 to 2π radians and resets every cycle. The angle is fed back to the abc to dq transformation block [15, 18].

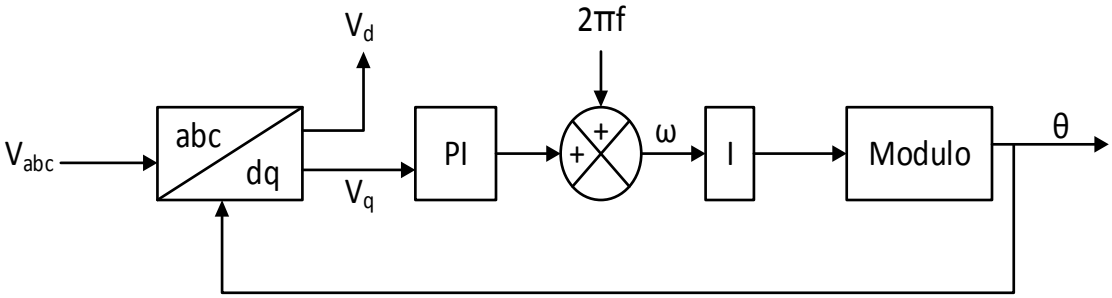

Figure 2.10 Block Diagram for PLL Implemented in this Study

The active and reactive power is calculated using the dq0 parameters with the following equations:

$$\mathbf{P = v_d \cdot i_d + v_q \cdot i_q + v_0 \cdot i_0} \quad \textbf{(2.11)}$$

$$\boldsymbol{Q = v_q i_d - v_d i_q} \quad \textbf{(2.12)}$$

However, for an ungrounded system, the zero sequence component of the current is equal to zero. Also, in steady-state, v_q is equal to zero since the PLL is aligning v_d to be in phase with v_a. Therefore, equations (2.11) and (2.12) can be rewritten as the following:

$$\mathbf{P = v_d \cdot i_d} \quad \textbf{(2.13)}$$

$$\boldsymbol{Q = -v_d \cdot i_q} \quad \textbf{(2.14)}$$

We can see that the active and reactive power equations are decoupled, which simplifies

the control scheme. Utilizing a feedback control in the PLL and in the inner control schemes will drive the error due to non-zero v_q values during a disturbance to zero [15, 20].

2.3.1.2. Inner Controller

The objective of the inner controller is to generate voltage reference values that will become the modulating functions for the converter starting from the current reference values. Figure 2.11 shows the block diagram of the inner controller.

The block diagram is derived from the following equations:

- Neglecting the ac side resistance, the measured voltage and the voltage across the converter are related by the following equation:

$$v_{meas} = L\frac{di}{dt} + v_{conv} \quad (2.15)$$

- Transforming the equation to Laplace domain:

$$v_{meas} = sLi + v_{conv} \quad (2.16)$$

- Transforming to the equation to dq reference frame:

$$v_{meas,d} = sLi_d - \omega Li_q + v_{conv,d} \quad (2.17)$$

$$v_{meas,q} = sLi_q + \omega Li_d + v_{conv,q} \quad (2.18)$$

The d and q components of the converter's reference voltage will be used to control the switching of the converters. In a triangle-sine PWM, for example, $v_{d,ref}$ and $v_{q,ref}$ will be transformed into $v_{a,ref}$, $v_{b,ref}$, and $v_{c,ref}$. These sinusoidal reference voltages will be compared with a pure triangle wave to generate the firing pulses of the converters [15, 20].

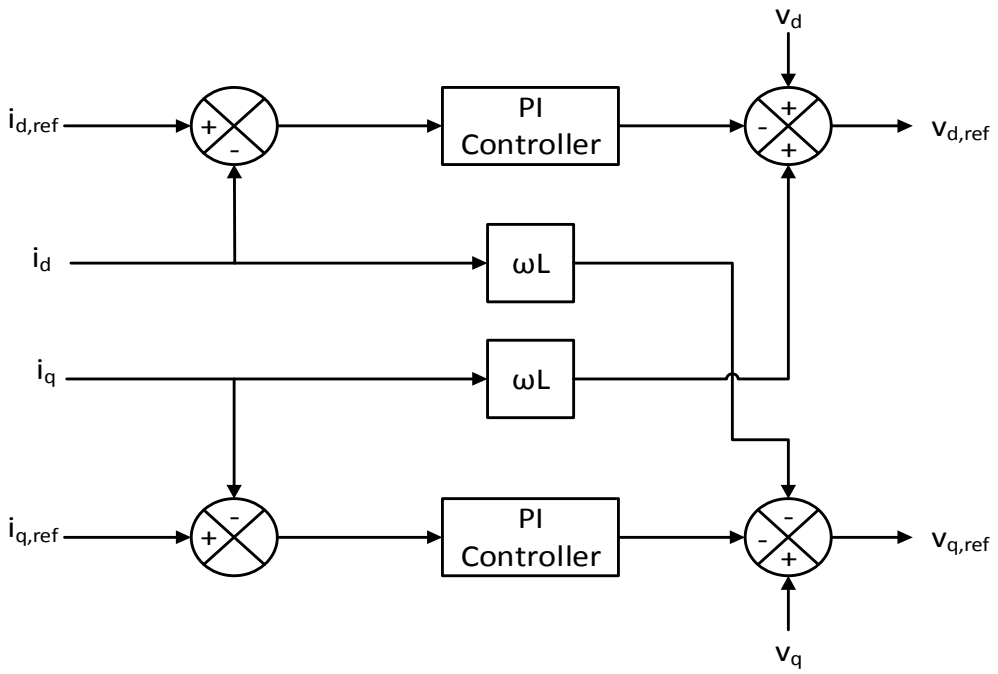

Figure 2.11 Inner Controller Block Diagram

2.3.1.3. DC Voltage Outer Controller

The objective of the dc voltage outer controller is to regulate the dc voltage of the dc line by modifying i_d. Figure 2.12 shows a block diagram of the dc voltage controller. The input of the PI controller is the error between the reference and measured dc voltage value. The output of the PI controller is the reference i_d value.

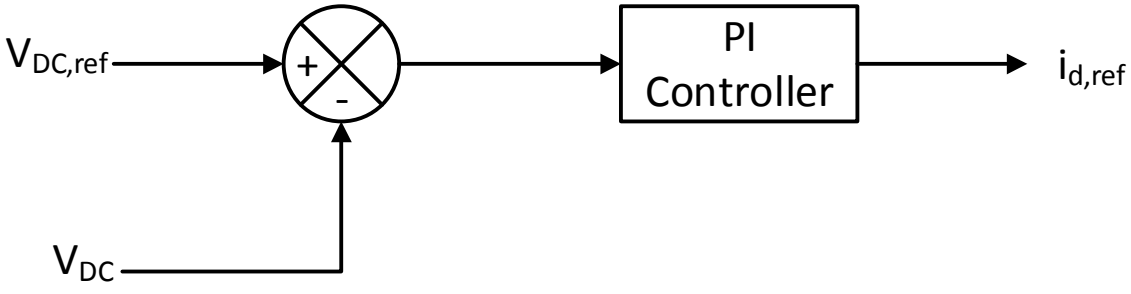

Figure 2.12 DC Voltage Controller Block Diagram

The control of the dc voltage at the GSC is important to ensure power balance between the converters. This will allow the WPPC to vary power injection to the dc line and, therefore, maximize wind power utilization [15, 20].

2.3.1.4. Reactive Power Outer Controller

The objective of the reactive power controller is to regulate the reactive power injection from the VSC to the ac grid. The reactive power controller determines the reference value of i_q sent to the inner controller. Since the relationship between the reactive power and i_q is linear, this can be controlled without a closed loop PI controller. Rearranging equation (2.14) results in the following:

$$i_{q,ref} = \frac{-Q_{ref}}{v_{d,ref}} \qquad (2.19)$$

This equation is used to determine the value of $i_{q,ref}$ [15, 20].

2.3.2. Control Circuit of WPPC

The WPPC will be used to control the active and the reactive power injection from the wind power plant converter to the dc transmission line. The control circuit of the reactive power transfer will be similar to the one used for the GSC. The only change will be in replacing the dc voltage controller with an active power controller, which will follow the output of the wind converter. The converter control will be based on inner controller similar to the one used in the GSC [15,20].

2.3.2.1. Active Power Outer Controller

The objective of the active power controller is to regulate the active power exchange between the wind power plant and the dc system based on the active power that the wind power plant can provide. This is done by determining the reference value of i_d. Similar to the

reactive power controller, the relationship between the active power and i_d is linear so a PI controller is not needed for this purpose. Equation (2.13) can be rearranged to look like the following:

$$i_{d,ref} = \frac{P_{ref}}{v_{d,ref}} \qquad \textbf{(2.20)}$$

This equation is used to determine the value of $i_{d,ref}$ [15, 20].

3. Chapter 3: Two-Terminal VSC-HVDC – Simulation Results

3.1. System Design

The simulation model for the two-terminal VSC-HVDC system described in Chapter 2 is implemented in the MATLAB/Simulink Simpower systems toolbox. The VSCs will be implemented as two-level switching converter models for simplicity in model implementation. The specific topology used has little impact on the steady-state and slow dynamic behaviors examined in this work. Table 3.1 lists the system parameters used.

Table 3.1 Parameters used in the system design[10]

Parameter	Value
AC Voltage – Grid Side	$V_{AC,LL} = 400\ kV$
AC Voltage – WPP Side	$V_{AC,LL} = 400\ kV$
Fundamental Frequency	$f = 50Hz$
Switching Frequency	$f_s = 1050Hz$
AC Line Resistance	$R_{AC} = 3.7853\Omega$
AC Line Inductance	$X_{AC} = 43.2658\Omega$ $L_{AC} = \frac{X_{AC}}{2\pi f} = 0.138H$
DC Line Nominal Voltage	$V_{DC,Pole\_to\_Ground} = 320\ kV$ $V_{DC,Pole\_to\_Pole} = 640kV$
Length of DC Transmission Line	$L = 400km$
DC Cable Resistance	$R_{DC} = 0.0121\frac{ohm}{km}$
DC Capacitors – Converter Filters	$C_{DC} = 47\mu F$

The following points were taken into consideration in building the system:

- The wind power plant is represented as an ac power source with a fixed voltage level equivalent to that in the ac grid. This is adequate for the scope of simulation presented in this thesis.
- Transformer turns ratios are neglected since voltage levels are fixed at values assumed to be suitable for the converter stations. Transformer leakage reactances are included in the ac system impedance.
- AC filters are not implemented since the ac systems are assumed stiff and harmonic behavior is not central to this work.
- The voltage feed forward presented in the inner current regulators in Figure 2.11 is neglected. This is acceptable in HVDC simulations since the current level is very small in comparison to the high voltage levels used, and therefore the cross-coupling terms have negligible impact on control performance.
- The capacity of the power electronics components and cables are assumed to be high enough to withstand the voltage and current levels used in the simulation.

Figure 3.1 shows the system built in Simulink. The system is configured as a symmetric monopole. The VSC station in the system is a two-level bridge converter built using six blocks of IGBTs and antiparallel diodes. Figure 3.2 shows the VSC station built in Simulink. The switching of the six IGBT/diode blocks is controlled by the firing pulses received from the control system. The WPP and ac grid control systems are an implementation of the control circuits explained in Section 2.3

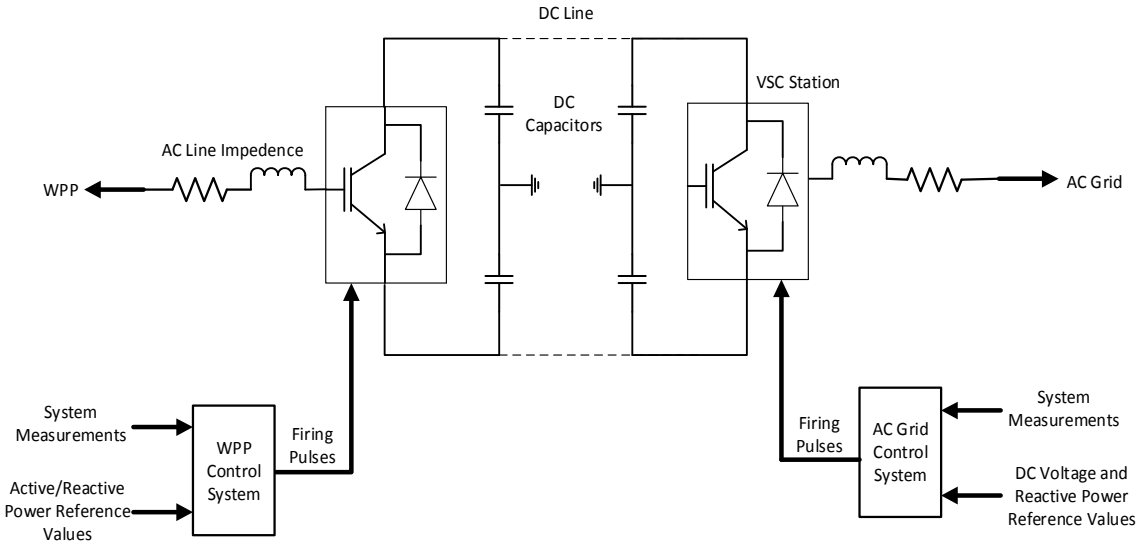

Figure 3.1 Two-Terminal VSC-HVDC system built in Simulink

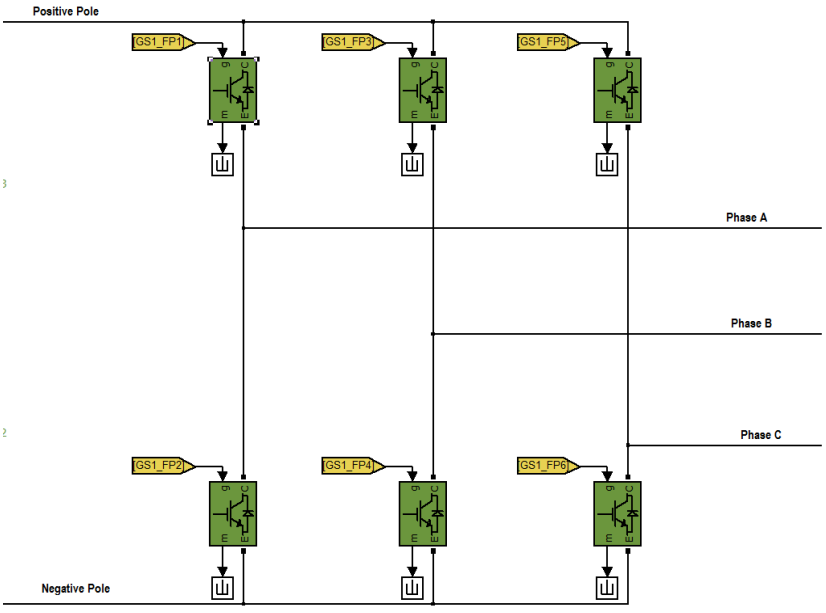

Figure 3.2 VSC Station – Snapshot from Simulink

3.2. Simulation Results

The following operating scenario will be used to run the simulation to test the model:

- Time interval = 9 seconds [1 sec to 10 sec]. The time from 0 sec to 1 sec is the simulation startup period, which is not emulating an actual start up scheme.

- AC Grid Control:
    - DC voltage = 640kV
    - Reactive power transfer = 0MVAr
- Wind Power Plant Control:
    - Reactive power transfer = 0MVAr
    - Active power transfer representing variations of the wind power plant output due to wind variations:

$$P = \begin{cases} 400MW & 1 \leq t < 4\ sec \\ 500MW & 4 \leq t < 7\ sec \\ 300MW & 7 \leq t < 10\ sec \end{cases}$$

Simulation of the above scenario results in the plots shown in Figure 3.3 which shows the active and reactive power delivered by the WPP to the offshore collector circuit versus time. Figure 3.4 shows the active and reactive power received by the ac grid versus time. We can observe the difference between the active power transferred by the WPP and that received by the ac grid. This power difference represents the losses in the dc line, ac collector system and transformer, and in the converter.

One important point to notice in the graphs is that the reactive power is not significantly affected by any change in the active power although we have neglected the feed forward in the inner control loop. As mentioned earlier, this is due to the fact that the current level in high voltage system is small relative to power levels.

Figures 3.5 and 3.6 shows the plots of I_d and I_q versus time in the WPP and GS respectively. As expected, these graphs are similar in shape to the graphs of the active and reactive power.

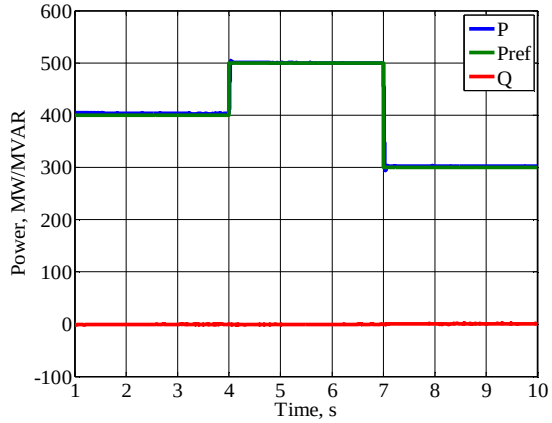

Figure 3.3 Graph of the active and reactive power delivered by WPP versus time

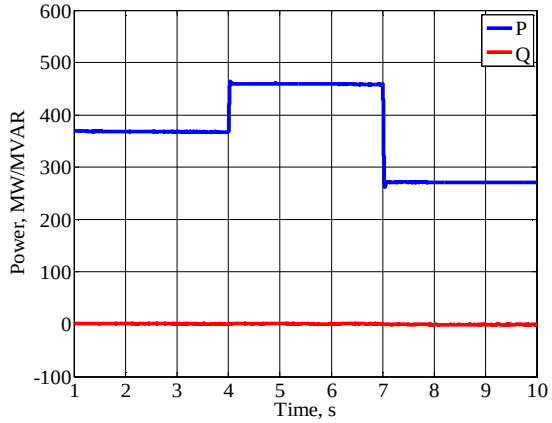

Figure 3.4 Graph of the active and reactive power received by the ac grid versus time

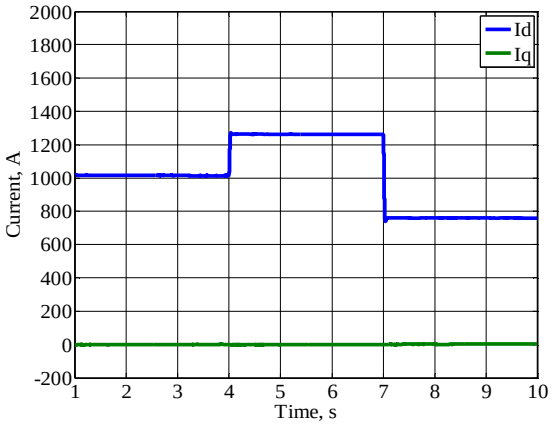

Figure 3.5 Graph of I_d and I_q transmitted from the WPP to the dc line.

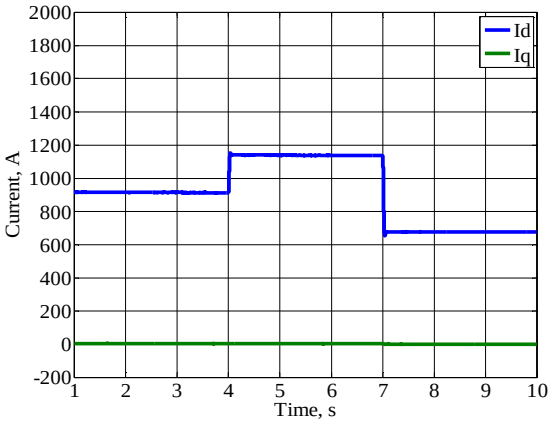

Figure 3.6 Graph of I_d and I_q received by ac grid from the dc line.

Figures 3.7 and 3.8 show the plot of the dc voltage at the terminal of the WPP and GS converters respectively.

The steady-state dc voltage at the GS converter's terminal matches the designed setting value, which is 640kV. This is expected since we are controlling the dc voltage at the grid side terminals. However, the steady-state dc voltage at the WPP converter's terminal is at a higher value. This difference is due to the voltage drop in the dc transmission line

resistance. The dc transmission system is represented by a simple dc circuit as shown in Figure 3.9 since the converters effectively regulate dc voltage and the transient response of the line RLC circuit is not of concern in these studies. The dc voltages at both terminals are related by the following equation:

$$v_{DC,WPP} = R_{DC} \cdot I_{DC} + v_{DC,GS} \quad \textbf{(2.20)}$$

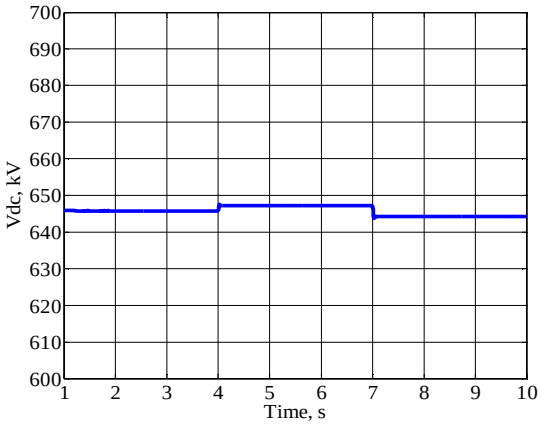

Figure 3.7 Graph of dc voltage at the WPP converter terminal versus time

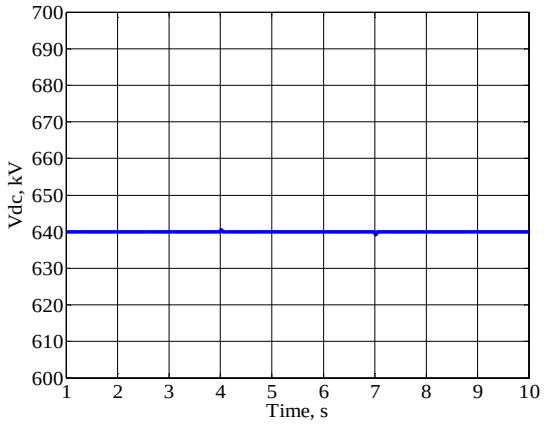

Figure 3.8 Graph of dc voltage at the GS converter terminal versus time

Figure 3.10 shows the graph of the dc current versus time.

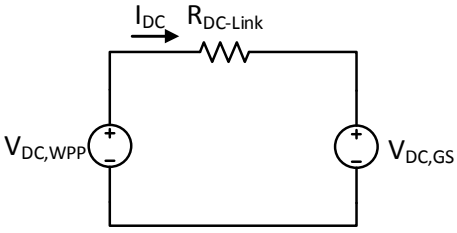

Figure 3.9 Equivalent dc circuit of the system

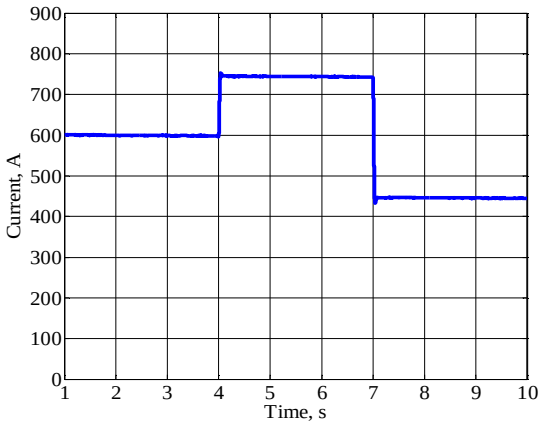

Figure 3.10 Graph of the current in the dc line versus time

Figures 3.11 and 3.12 show the ac phase voltages and line currents at the WPP for three cycles of the steady-state operating periods. We can clearly see from the graph the voltages and currents are in-phase.

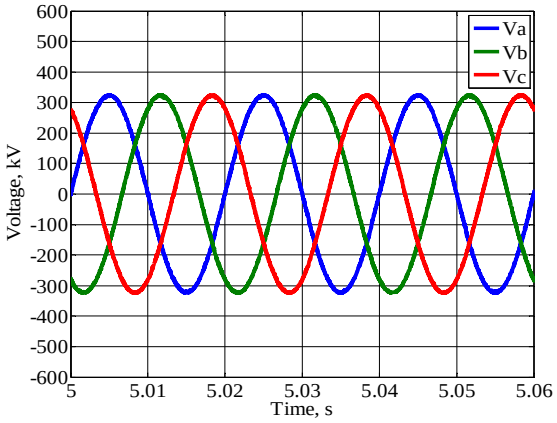

Figure 3.11 Graph of 3 cycles of the ac voltages of the WPP versus time

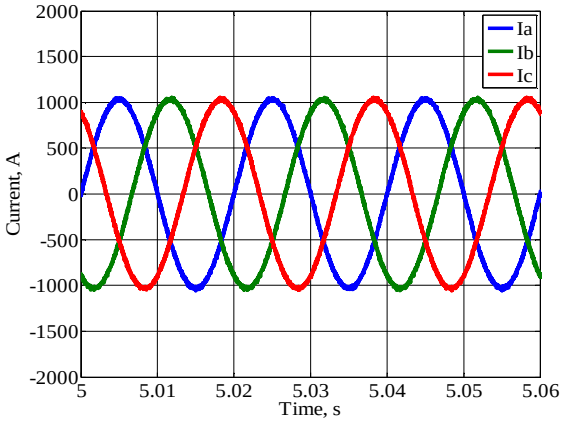

Figure 3.12 Graph of 3 cycles of the ac currents of the WPP versus time

Figures 3.13 and 3.14 show the ac phase voltages and currents of the ac grid respectively. The voltages and currents are out of phase by 180 degrees since the current direction is towards the ac grid.

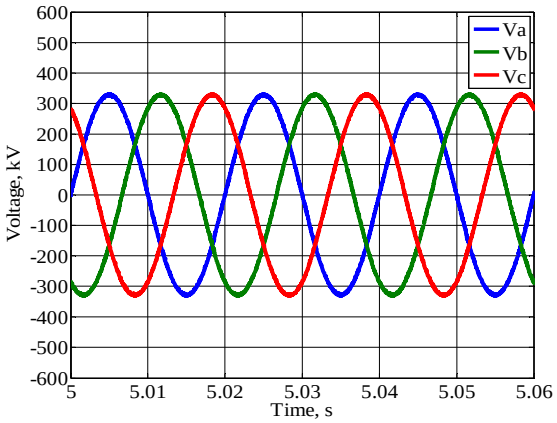

Figure 3.13 Graph of 3 cycles of the ac voltages of the ac grid versus time

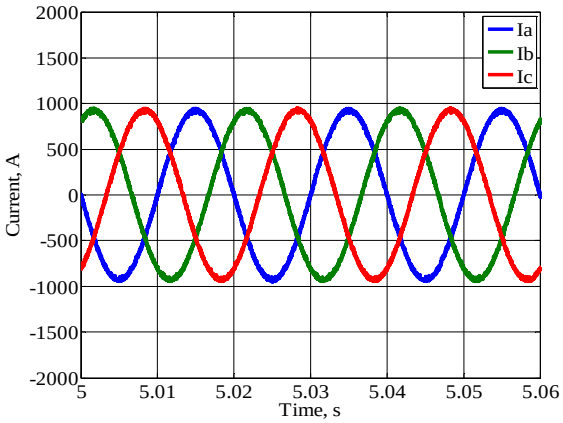

Figure 3.14 Graph of 3 cycles of the ac currents of the ac grid versus time

The converters demonstrated in this chapter is a building block towards the discussion of the MTDC systems in the next chapter. The results from the operating scenario proved that the system can correctly meet the steady-state operating points.

4. Chapter 4: Multi-Terminal VSC-HVDC

The concept of VSC-HVDC explained in Chapters 2 and 3 for a two-terminal setup can be extended to apply for multiterminal setups. Section 2 of this chapter will extend the concept into a three-terminal HVDC system consisting of two wind power plants and one ac grid, while Section 3 will extend the concept into a three-terminal HVDC system consisting of one wind power plant and two ac grids. In both sections the control methods of the different scenarios of active power transmission is described. Case studies are presented at the end of each section. Scalability of the approach presented in Sections 2 and 3 to larger systems will be discussed in Section 4.

4.1. Three-Terminal HVDC System Consisting of Two Wind Power Plants and One AC Grid

This section will explain the basic concept and block diagram of a three-terminal HVDC system connecting two wind power plants located at two different offshore locations to the ac grid located onshore. The different scenarios of active power sharing between the two wind plants based on droop characteristics and wind plant generation limits will be discussed. Finally, two case studies will be presented and simulated.

4.1.1. Basic Concept and System Diagram

Figure 4.1 shows a system diagram of a three-terminal VSC-HVDC system. The system consists of two wind power plants that are providing active power to the ac grid through the dc transmission lines.

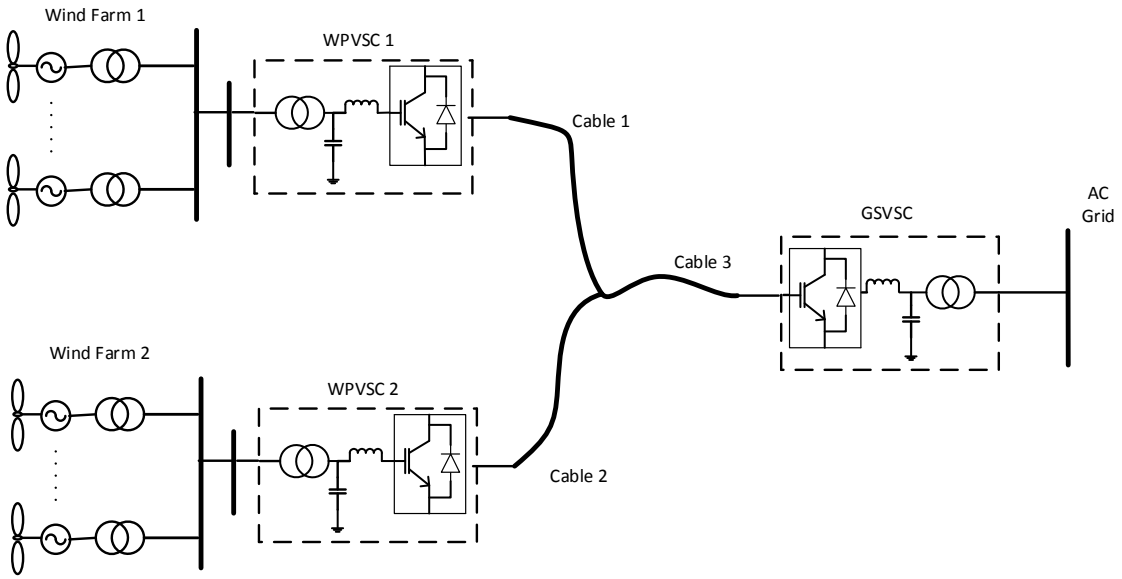

Figure 4.1 Three-Terminal VSC-HVDC System consisting of Two Wind Power Plants and One AC grid

The generation of the active power provided to the ac grid is shared between the two wind plants. Table 4.1 lists the different scenarios of how the two wind plants will share the active power. The control method used by the wind power plants is described in the upcoming sections.

Table 4.1 Operating Scenarios for active power sharing in a three-terminal HVDC system that consist of two wind power plants and one ac grid.

Case #	AC Grid	Wind Plant 1	Wind Plant 2	Active Power Sharing Method
1	(-ive) Receive Active Power	(+ive) Provide Active Power	(+ive) Provide Active Power	Droop Characteristics

2	**(-ive)** Receive Active Power	**(+ive) (Saturate)** Provide Active Power and saturate to its limit	**(+ive)** Provide Active Power	Droop Characteristics + Wind Plant Limit
3	**(-ive)** Receive Active Power	**(+ive)** Provide Active Power	**(+ive) (Saturate)** Provide Active Power and saturate to its limit	Droop Characteristics + Wind Plant Limit
4	**(-ive)** Receive Active Power	**(+ive) (Saturate)** Provide Active Power and saturate to its limit	**(+ive) (Saturate)** Provide Active Power and saturate to its limit	Wind Plant Limit

The objective of the method for distributing active power output between the two wind plants is to reduce the copper losses. Therefore, a controller based on the droop characteristics of the system will be used to generate the reference values of the active power controllers of both wind plants [22]. However, if the reference active power value is above the capacity of one of the wind plants, it will saturate. In this case, the other wind plant is expected to compensate for the difference. In case the required active power by the ac grid is above the capacity of both wind plants, they will both saturate to the maximum active power they can provide.

4.1.2. Droop Characteristics

Programmed droop characteristics are used to determine the ratio of active power that

each wind power plant is contracted to provide in order to have the minimum copper losses. Figure 4.2 shows the equivalent dc circuit of the three-terminal system presented in Figure 4.1.

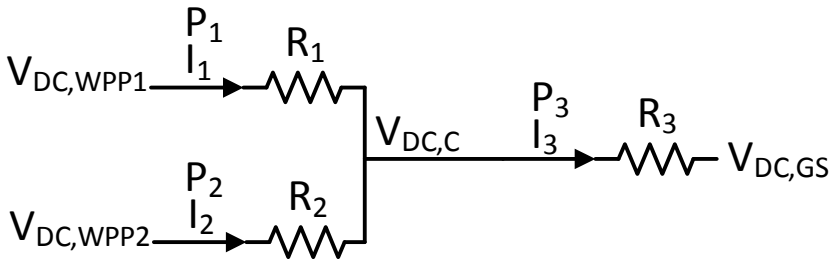

Figure 4.2 Equivalent DC circuit of the system

The currents in the circuit are related by Kirchhoff's law as shown in equation (4.1), where the value of I_3 can be calculated from the active power required by the grid side.

$$I_3 = I_1 + I_2 \tag{4.1}$$

Equations (4.2) and (4.3) represent the relation between the Voltage $V_{DC,C}$ and the dc voltages at WPP1 and WPP2 terminals respectively.

$$V_{DC,C} = V_{DC,WPP1} - I_1 \cdot R_1 \tag{4.2}$$

$$V_{DC,C} = V_{DC,WPP2} - I_2 \cdot R_2 \tag{4.3}$$

The copper losses in the dc transmission lines can be calculated using the following equation:

$$P_{Losses} = I_1^2 \cdot R_1 + (I_3 - I_1)^2 \cdot R_2 + I_3^2 \cdot R_3 \tag{4.4}$$

By differentiating equation (4.4) with respect to I_1 and equating to zero to determine a local minimum for losses, we will get the following equation representing the current through each dc transmission line that will result in the minimum copper losses:

$$I_1 = I_3\left(\frac{R_2}{R_1 + R_2}\right) \tag{4.5}$$

Using current division, I_2 will be calculated as:

$$I_2 = I_3\left(\frac{R_1}{R_1 + R_2}\right) \quad \textbf{(4.6)}$$

Equations (4.5) and (4.6) indicate that we will get the minimum copper losses when the voltages at the terminals of each wind plants are equal to each other. Therefore, the optimum set point for the active power delivered by each wind power plant to minimize transmission losses is determined by the following equations:

$$P_1 = P_3\left(\frac{R_2}{R_1 + R_2}\right) \quad \textbf{(4.7)}$$

$$P_2 = P_3\left(\frac{R_1}{R_1 + R_2}\right) \quad \textbf{(4.8)}$$

4.1.3. Logic Flowchart of Active Power Distribution Based on Droop characteristics and WPPs Generation Limits

To make sure that the system will run as required for all steady-state operating scenarios, a logic circuit that determines the reference active power delivered by each WPP needs to be designed. The inputs to this logic circuit will be the following:

- The active power required by the ac grid
- Droop characteristics of the system
- Wind Power Plants generation limits

Figure 4.3 shows a control logic flow chart to determine the reference active power to be delivered by WPP1.

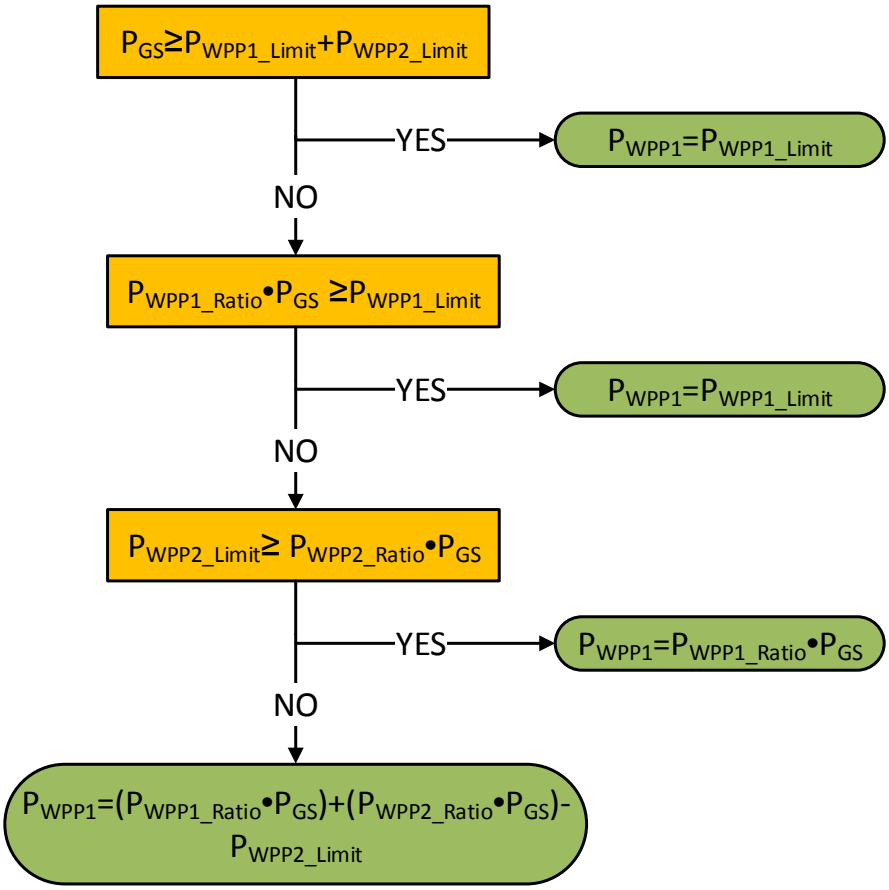

Figure 4.3 Logic Flowchart Determining the Active Power Provided by WPP1

Once the reference active power delivered by WPP1 is determined, we can determine the active power supplied by WPP2 using the flow chart shown in Figure 4.4. The output of the flowchart will be used as the reference active power in the WPP2 control circuit.

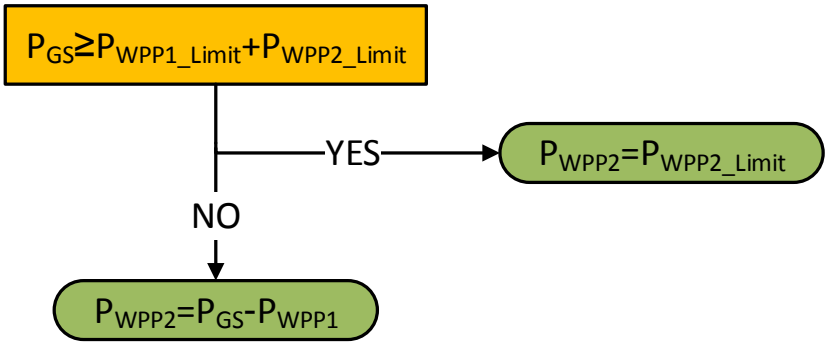

Figure 4.4 Logic Flowchart Determining the Active Power Provided by WPP2

4.1.4. Case Studies

The three-terminal HVDC system represented in Figure 4.1 was built in Matlab/Simulink. The same parameter values mentioned earlier in Table 3.1 are used in designing the system and converters were also built as a two-level switching model. The system holds similar assumptions as those used in the two-terminal HVDC system simulation. Wind speed is assumed to be constant throughout the simulation period and therefore a constant value can represent the generation limit of the wind power plants.

Two case studies will be simulated for this system to show its behavior at different scenarios and configurations.

4.1.4.1. Case A

The following case scenario will be used to run the simulation:

- Time interval = 9 seconds [1 sec to 10 sec]
- AC Grid Control:
    - DC voltage = 640kV
    - Reactive power transfer = 0MVAr
- Wind power plant 1 capacity = 500 MW
- Wind power plant 2 capacity = 400 MW
- DC transmission line resistances:
    - $R_1 = 0.0121\frac{ohm}{km} \cdot 100km = 1.21\Omega$
    - $R_2 = 0.0121\frac{ohm}{km} \cdot 300km = 3.63\Omega$
    - $R_3 = 0.0121\frac{ohm}{km} \cdot 200km = 2.42\Omega$
- Active power required by the ac grid (set points from ac grid operator):

$$P_3 = \begin{cases} 400MW & 1 \leq t < 4\ sec \\ 700MW & 4 \leq t < 7\ sec \\ 1000MW & 7 \leq t < 10\ sec \end{cases}$$

In this scenario, we can divide the active power reference value for each wind power plant into three parts:

- Part 1 – P_3=400MW: The requested active power is less than the combined rating of both wind plants. Therefore, we will follow the droop characteristics of the system.
  - $P_1 = P_3\left(\frac{R_2}{R_1+R_2}\right) = 400MW\left(\frac{3.63\Omega}{1.21\Omega+3.63\Omega}\right) = 300MW$
  - $P_2 = P_3\left(\frac{R_1}{R_1+R_2}\right) = 400MW\left(\frac{1.21\Omega}{1.21\Omega+3.63\Omega}\right) = 100MW$
- Part 2 – P_3=700MW: The requested active power is less than the combined rating of both wind plants. Therefore, we will follow the droop characteristics of the system.
  - $P_1 = P_3\left(\frac{R_2}{R_1+R_2}\right) = 700MW\left(\frac{3.63\Omega}{1.21\Omega+3.63\Omega}\right) = 525MW$
    - Since this exceeds the rating of wind power plant 1, it will saturate to 500MW and the difference will be compensated by the other wind power plants.
  - $P_2 = 200MW$
- Part 3 – P_3=1000MW: The requested active power is larger than the combined rating of both wind power plants. Therefore, both will provide their maximum capacity.
  - $P_1 = 500MW$
  - $P_2 = 400MW$

Figures 4.5 and 4.6 show plots representing the active and reactive power delivered by WPP1 and WPP2 respectively versus time. We can observe that the designed control circuit correctly determined the active power that should be delivered by each wind power plant.

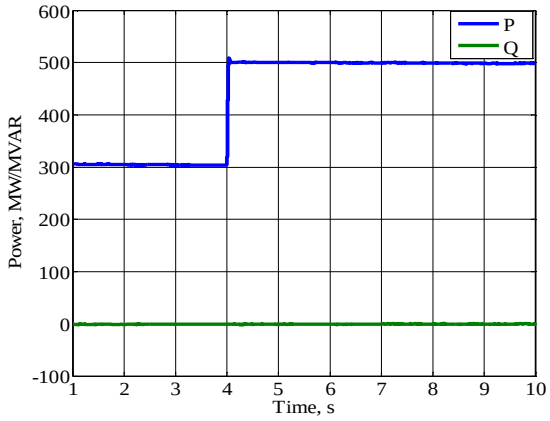

Figure 4.5 Graph of the Active and Reactive Power Delivered by WPP1 versus time

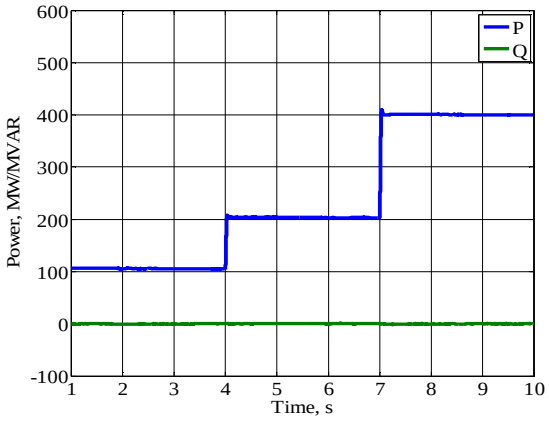

Figure 4.6 Graph of the Active and Reactive Power Delivered by WPP2 versus time

Figure 4.7 shows the plot of the active and reactive power received by the ac grid and the set points of active power from the ac grid operator versus time. The difference between the set points and the actual received active power in the time period $1 \leq t < 7\ sec$ represents the system losses. However, the difference in the time period $7 \leq t < 10\ sec$ is due to system losses and saturation of both wind power plants.

Figure 4.8 shows the plot of the dc voltage at the ac grid converter terminals versus time. As expected the value is regulated by the ac grid control circuit to 640kV.

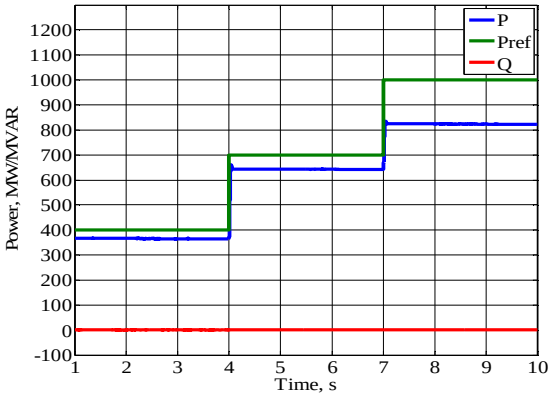

Figure 4.7 Graph of the Active and Reactive Power Received by the AC grid versus time

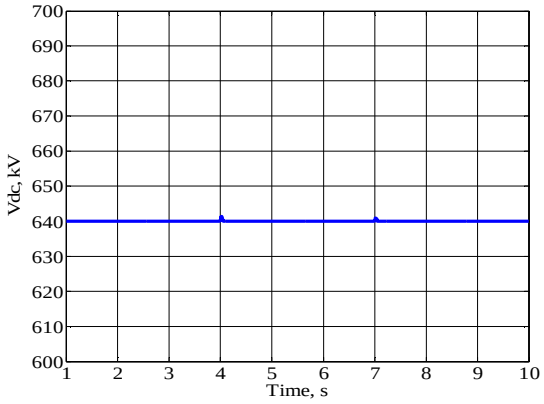

Figure 4.8 Graph of DC voltage at the GS converter terminal versus time

Figures 4.9 show plots of the variation of the dc voltage at the converter terminals of WPP1 and of WPP2 as the system operating points are changed. The value of dc voltage at each converter depends on the voltage drop in the dc transmission line resistance between each WPP converter terminal and the ac grid converter terminal. As expected in the first case, where both WPP are delivering power based on the system droop characteristics, the dc voltage at the terminals of each WPP converter are equal to each other.

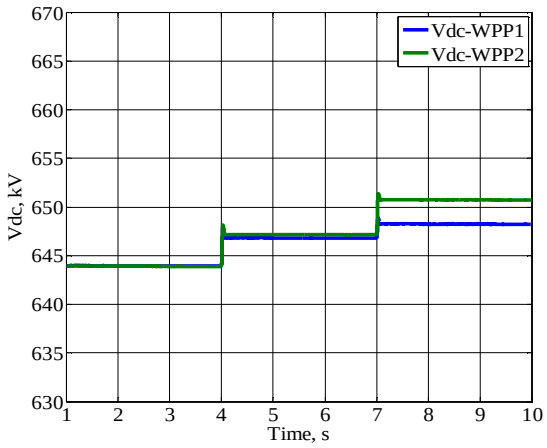

Figure 4.9 Graph of DC voltages at WPP1 and WPP2 converter terminals versus time

4.1.4.2. Case B

In this case, we will use the same scenario as in case A with the difference that WPP1 will be connected directly at the common coupling point of the MTDC, i.e. R_1 is equal to zero. The objective of this case is to observe the functionality of the droop characteristics control design on the system.

It is expected that WPP1 will provide all the power required by the ac grid unless it saturates to its limit. At that time, WPP2 will provide the rest of the power.

Figures 4.10 and 4.11 show plots representing the active and reactive power delivered by WPP1 and WPP2 respectively versus time. We can observe that WPP1 deliver all the active power required by the ac grid unless it reaches to its limit.

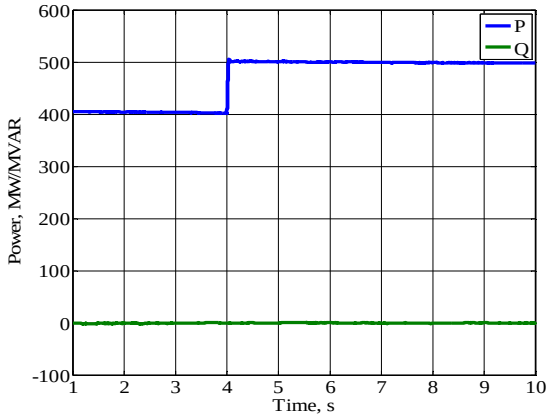

Figure 4.10 Graph of the Active and Reactive Power Delivered by WPP1 versus time

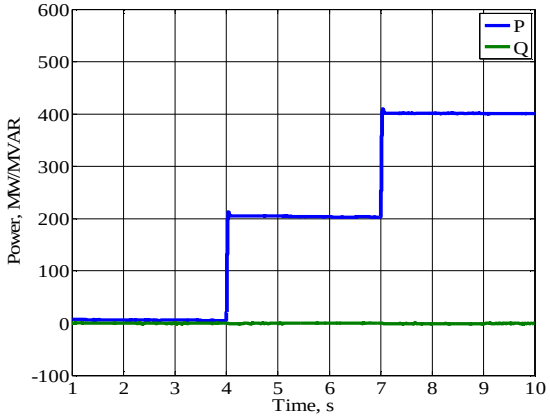

Figure 4.11 Graph of the Active and Reactive Power Delivered by WPP2 versus time

Figure 4.12 shows the plot of the active and reactive power received by the ac grid versus time. Figure 4.13 shows the plot of the dc voltage at the ac grid converter terminals versus time.

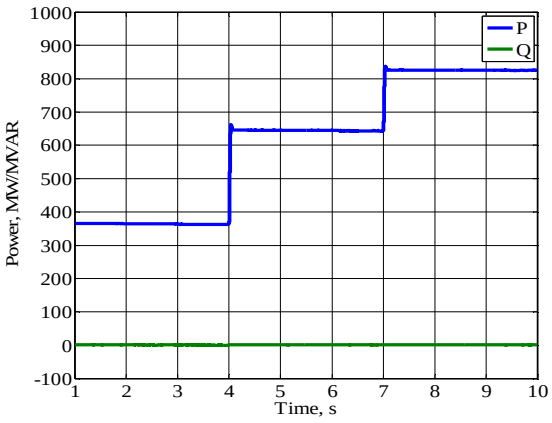

Figure 4.12 Graph of the Active and Reactive Power Received by the AC grid versus time

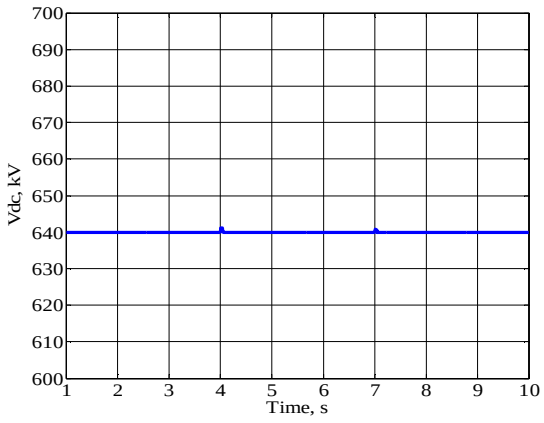

Figure 4.13 Graph of DC voltage at the GS converter terminal versus time

Figure 4.14 shows the plots of the variation of the dc voltage at the converter terminals of WPP1 and of WPP2 as the system operating points are changed. As expected, the dc voltage at the terminals of each WPP converter are equal to each other when no power is supplied by WPP2, which is the case in the time period $1 \leq t < 4\ sec$.

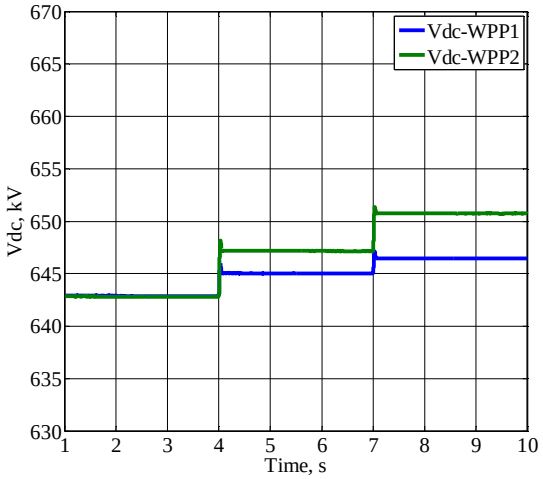

Figure 4.14 Graph of DC voltages at WPP1 and WPP2 converter terminals versus time

4.2. Three-Terminal HVDC System Consisting of One Wind Power Plant and Two AC Grids

In this section, the basic concept and block diagram of a three-terminal HVDC system connecting one wind power plant located at an offshore location into two ac grids located onshore will be explained. The different scenarios of active power distribution through the dc transmission system will be described. Finally, cases studies will be presented and simulated.

4.2.1. Basic Concept and Block Diagram

Figure 4.15 shows a block diagram of a three-terminal VSC-based HVDC system. The system consists of one wind power plant and two ac grids.

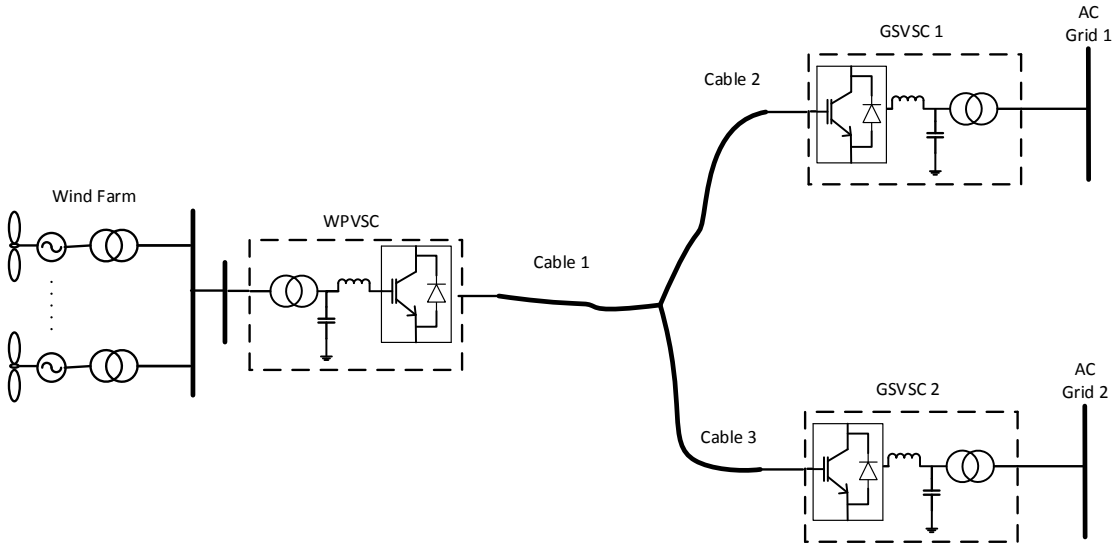

Figure 4.15 Three-Terminal VSC-HVDC System consisting of One Wind Power Plant and Two AC Grids

Figure 4.16 shows the dc equivalent circuit of the system shown in Figure 4.15.

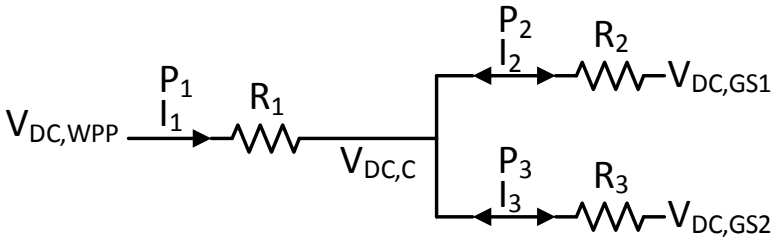

Figure 4.16 Equivalent DC circuit of the system

As seen in the figure, the currents I_2 and I_3 can be going to or from the two ac grids. The current values are dependent on the controlled dc voltage at the VSC terminals. The following equations show the relationship between the currents and the dc voltages assuming the current direction is from the dc transmission line to the GSVSCs:

$$V_{DC,GS1} = V_{DC,R} - I_2 \cdot R_2 \quad (4.8)$$

$$V_{DC,GS2} = V_{DC,R} - I_3 \cdot R_3 \quad (4.9)$$

Rearranging equations (4.8) and (4.9) will result in the following:

$$V_{DC,R} = V_{DC,GS1} + I_2 \cdot R_2 = V_{DC,GS2} + I_3 \cdot R_3 \quad (4.10)$$

$$V_{DC,GS2} = V_{DC,GS1} + I_2 \cdot R_2 - I_3 \cdot R_3 \quad (4.11)$$

The set of potential active power distribution scenarios for a configuration like the one in Figure 4.15 is more complex than that for the system explained in Section 4.1. This is mainly because each of the ac grids may provide or require active power from the dc transmission network. Table 4.2 lists the different scenarios of active power distribution through the dc transmission network.

Case 1 in Table 4.2 can be operated in three different modes. These modes differ in the way the active power provided by the wind power plant will be distributed between the two ac grids [23, 24]. Section 4.2.2 will explain these three modes in detail.

Table 4.2 Cases of active power distribution through the dc transmission system in a three-terminal HVDC system consisting of terminals for one wind power plant and two ac grids.

Case #	AC Grid 1	AC Grid 2	Wind Plant 2	Active Power Sharing Method
1	**(-ive)** Receive Active Power	**(-ive)** Receive Active Power	**(+ive)** Provide Active Power	Operation Modes 1-3
2	**(-ive)** Receive Active Power	**(+ive)** Provide Active Power	**(+ive)** Provide Active Power	Droop Characteristics / Saturation
3	**(+ive)** Provide Active Power	**(-ive)** Receive Active Power	**(+ive)** Provide Active Power	Droop Characteristics / Saturation

Cases 2 and 3 will operate in a manner similar to the one explained in Section 4.1 since we will have two sources of active power and one terminal receiving power. However, one of the active power sources will be an ac grid. In this case, the i_{d_ref} value of that ac grid can be determined either by a dc voltage outer controller or by an active power outer controller. Section 4.2.3 will explain the operation of cases 2 and 3 in detail.

4.2.2. Case 1 – Potential Modes of Operation

In case 1 of the three-terminal HVDC system shown in Figure 4.15, both ac grids require active power from the wind plant. The wind plant might not have sufficient capacity to

supply both ac grids with the required active power. The system can be operated in three different modes depending on how the generated active power will be distributed between the two GSVSCs when limits are reached [23, 24]. The following sub-sections will explain the three modes of operation and how the GSVSCs will be controlled in each mode.

4.2.2.1. Mode 1

In this mode of operation, one ac grid will have the priority of receiving active power over the other ac grid. The other ac grid will not start receiving active power until the active power received by the first ac grid reaches the set point [23, 24].

To operate the system in Mode 1, one option is to add a current limiter to the dc voltage control system. Figure 4.17 shows the block diagram of the dc voltage control circuit including the current limiter.

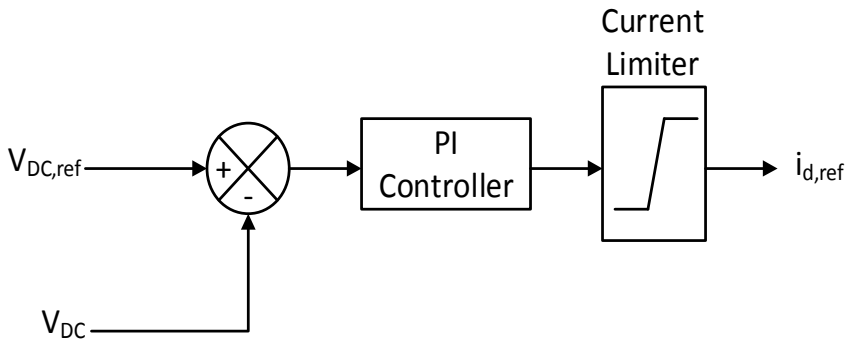

Figure 4.17 DC Voltage Controller with Converter Current Limiter Block

The dc voltage of GSVSC1 will be controlled at the set value as long as the active power received is below the set point. If the received active power reaches the limit, GSVSC1 will no longer control the dc voltage, and it will instead operate in current control mode set at the limit value. Figure 4.18 shows the VI characteristics of the GSVSC1 [23, 24].

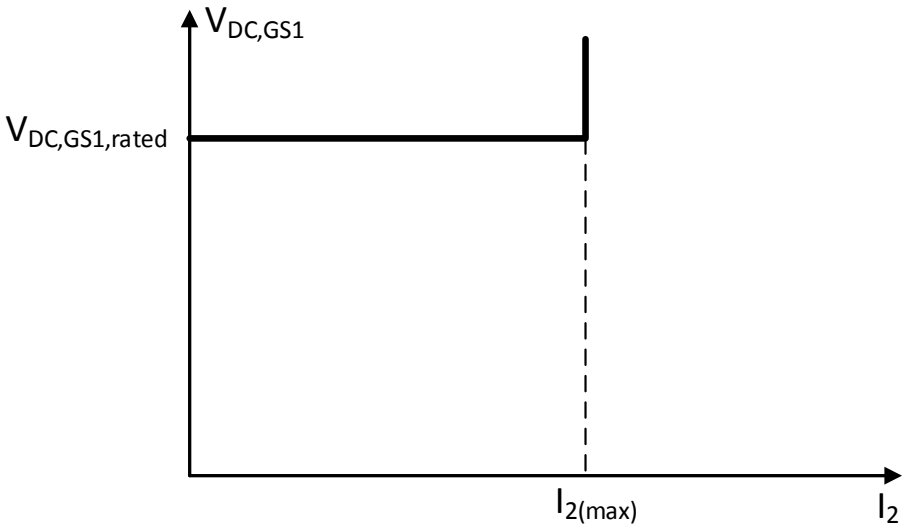

Figure 4.18 VI Characteristics for GSVSC1

On the other hand, the maximum voltage that $V_{DC,GS2}$ can reach before GSVSC1 reach its set point is calculated using the following equation:

$$\boldsymbol{V_{DC,GS2} = V_{DC,GS1} + I_{2(max)} \cdot R_2} \qquad \textbf{(4.12)}$$

GSVSC2 can be controlled at a voltage that is slightly larger than this calculated voltage. This will ensure that GSVSC2 will not start receiving active power unless GSVSC1 receives the required active power [23, 24]. A current controller could also be designed for GSVSC2 to ensure that it will not provide active power to the system.

4.2.2.2. Mode 2

In this mode of operation, both ac grids share the generated active power by set ratio [23, 24]. Again, this ratio is decided by the system operator and can be defined using:

$$\frac{\boldsymbol{P_2}}{\boldsymbol{P_3}} \approx \frac{\boldsymbol{I_2}}{\boldsymbol{I_3}} = \boldsymbol{n} \qquad \textbf{(4.13)}$$

To operate the system in Mode 2, a dc droop characteristic should be used for each of the GSVSCs. Figure 4.19 shows the definition of dc droop characteristics of both GSVSCs assuming both GSVSCs have the same dc voltage limit [23, 24]. Using the figure, we can

determine the following two equations:

$$I_2 = k_2 \cdot \Delta V_{DC,GS1} = k_2 \cdot (V_{DC,GS1} - V_{DC,GS1(min)}) \quad (4.14)$$

$$I_3 = k_3 \cdot \Delta V_{DC,GS2} = k_3 \cdot (V_{DC,GS2} - V_{DC,GS2(min)}) \quad (4.15)$$

The droop constants should be designed taking into consideration the maximum steady-state dc voltage the VSCs and cables can accept.

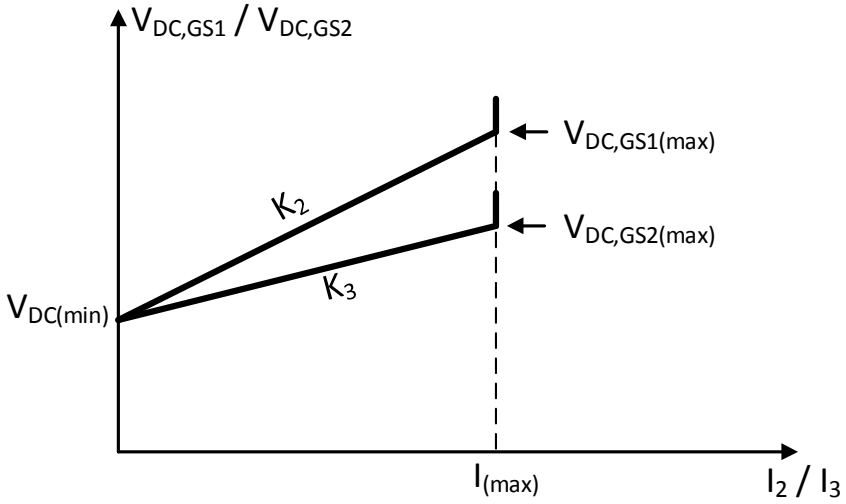

Figure 4.19 VI Characteristics of the Two GSVSCs

Rearranging equations (4.14) and (4.15) and substituting them in equation (4.11) will yield:

$$\frac{I_3}{k_3} - \frac{I_2}{k_2} = I_2 \cdot R_2 - I_3 \cdot R_3 \quad (4.16)$$

Therefore, the relationship between the two currents is:

$$\frac{I_2}{I_3} = \frac{R_3 + 1/k_3}{R_2 + 1/k_2} = n \quad (4.17)$$

And as a result, the relationship between the two droop constants should be:

$$k_3 = \frac{1}{n/k_2 + n \cdot R_2 - R_3} \quad (4.18)$$

Once the droop constants, total wind generated power, and $V_{DC(min)}$ parameters are known,

we can calculate the reference dc voltages of the GSVSCs. First of all, the active power received by each ac grid is calculated.

$$P_{GS2} = \frac{P_{wind}}{n+1} \quad (4.19)$$

$$P_{GS1} = P_{wind} - P_{GS2} \quad (4.20)$$

The reference dc voltage is related to the active power received by the following equation:

$$P_{GS1} = V_{DC\_GS1} \cdot I_{DC\_GS1} \quad (4.21)$$

Substituting the dc current from equation (4.14) into equation (4.21) and rearranging the equation will result in the following:

$$K_2 \cdot V_{DC\_GS1}^2 - K_2 \cdot V_{DC(min)} \cdot V_{DC\_GS1} - P_{GS1} = 0 \quad (4.22)$$

Solving the above equation will result in the reference value of the dc voltage controlled by the VSC in ac grid1. A similar approach should be followed to find the reference value of the dc voltage controlled by the VSC in ac grid2 [23, 24].

The reference values can also be approximated to ease the calculation process. This can be done by modifying equation (4.21) to be as follows:

$$P_{GS1} = V_{DC(min)} \cdot I_{DC\_GS1} \quad (4.23)$$

Therefore, we can easily calculate the dc voltage reference value using the following:

$$V_{DC\_GS1} = V_{DC(min)} + \frac{I_{DC\_GS1}}{K_7} \quad (4.24)$$

4.2.2.3. Mode 3

This mode of operation is a combination of the other two modes. One ac grid will have the priority of receiving active power over the other ac grid until a set point limit is reached. The remaining active power will be shared by both ac grids by a set ratio [23, 24].

Figures 4.20 and 4.21 show the block diagram of the dc voltage controllers for GSVSC1 and GSVSC2 respectively. Note that $V_{dc(min)}$ used in the droop characteristics design should be set higher that the reference dc voltage of GSVSC1 as discussed in the development of control Mode 1 [23, 24].

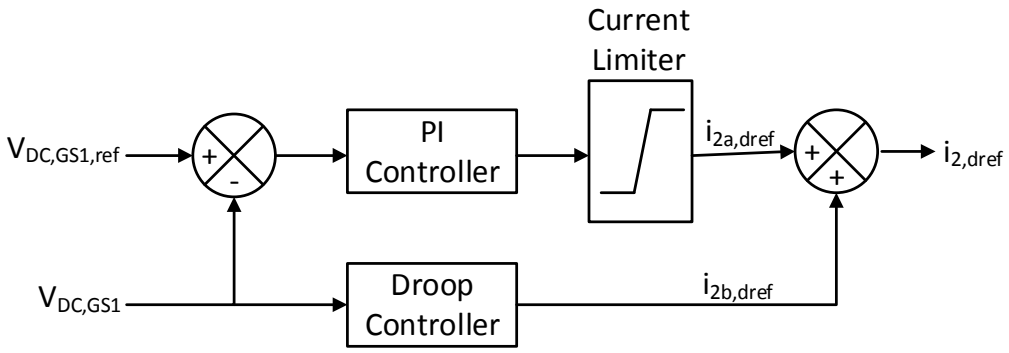

Figure 4.20 DC Voltage Controller of GSVSC1 operated in Mode3.

Figure 4.21 DC Voltage Controller of GSVSC2 operated in Mode3.

Figure 2.22 shows the VI characteristic curves of GSVSC 1 and 2 [23, 24].

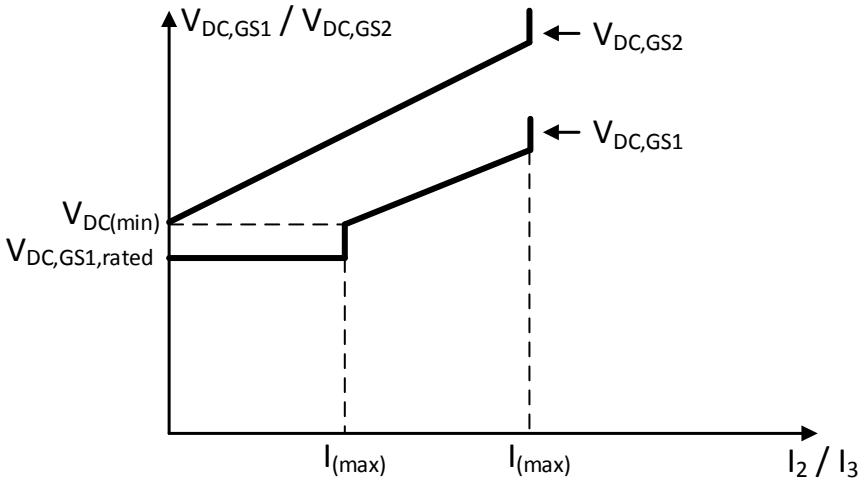

Figure 4.22 VI Characteristics of the Two GSVSCs

4.2.2 Cases 2 and 3 – Modes of Operation

Both cases 2 and 3 represent similar behavior in terms of operational modes. This section will consider case 3 where ac grid 2 is receiving active power, while ac grid 1 and the wind power plant are providing active power. A similar approach to the one used in Section 4.1 will be applied here. We will use the same direction of current assumed earlier, except we will assume the current I_2 to be flowing from the ac grid to the dc transmission line.

The currents in the circuit shown in Figure 4.16 are related by equation (4.25), where the value of I_3 can be calculated from the active power required by ac grid 2.

$$I_3 = I_1 + I_2 \tag{4.25}$$

Equations (4.26) and (4.27) represent the relation between the Voltage $V_{DC,C}$ and the dc voltages at the Wind Power Plant and ac grid 2 terminals respectively.

$$V_{DC,C} = V_{DC,WPP} - I_1 \cdot R_1 \tag{4.26}$$

$$V_{DC,C} = V_{DC,GS2} - I_3 \cdot R_3 \tag{4.27}$$

The copper losses in the dc line can be calculated using the following equation:

$$P_{Losses} = I_1^2 \cdot R_1 + (I_1 + I_3)^2 \cdot R_2 + I_3^2 \cdot R_3 \tag{4.28}$$

By differentiating equation (4.22) with respect to I_1 and equating to zero, we will get the following equation representing the current through each dc line that will result in the minimum copper losses:

$$I_1 = I_3\left(\frac{R_2}{R_1 + R_2}\right) \tag{4.29}$$

And therefore,

$$I_2 = I_3\left(\frac{R_1}{R_1 + R_2}\right) \tag{4.30}$$

Equations (4.23) and (4.24) indicate that we will get the minimum copper losses when the

voltages at the terminal of the wind power plant and ac grid 1 are equal to each other. Therefore, the active power levels delivered by the wind power plant and ac grid 1 are determined by the following equations:

$$P_1 = P_3\left(\frac{R_2}{R_1 + R_2}\right) \quad (4.31)$$

$$P_2 = P_3\left(\frac{R_1}{R_1 + R_2}\right) \quad (4.32)$$

The i_{d_ref} value of ac grid 1 can be determined either by a dc voltage outer controller or by an active power outer controller. For the dc voltage controller option, the dc voltage reference value can be calculated using the following equation:

$$V_{DC,GS1} = V_{DC,GS2} + I_2 \cdot R_2 + I_3 \cdot R_3 \quad (4.33)$$

For the active power controller option, the value calculated in equation (4.31) can be used as the active power reference value.

4.2.3. Case Studies

The three-terminal HVDC system represented in Figure 4.15 was built in Matlab/Simulink. The same parameter values and assumptions as those used in Section 4.1 are used in designing the system.

Two case studies will be simulated for this system to show its behavior at different scenarios and configurations.

4.2.3.1. Case A

In this case study, the system will be operated in Mode 1. The following case scenario will be used to run the simulation:

- Time interval = 9 seconds [1 sec to 10 sec]

- Resistances: We will assume that all the dc lines are using a dc cable similar to the one used previously.
  - $R_1 = 0.0121\frac{ohm}{km} \cdot 200km = 2.42\Omega$
  - $R_2 = 0.0121\frac{ohm}{km} \cdot 100km = 1.21\Omega$
  - $R_3 = 0.0121\frac{ohm}{km} \cdot 100km = 1.21\Omega$
- AC Grid 1 Control:
  - DC voltage = 640kV
  - Active Power set point of AC Grid 1 = 400MW
    - Id max = 1000A
  - Reactive power transfer = 0MVAr
- AC Grid 2 Control:
  - DC voltage:

$$V_{DC,GS2} \geq V_{DC,GS1} + I_{3(max)} \cdot R_3 = 640kV + 1000A \cdot 1.21\Omega = 641.21kV$$

    - Therefore, we will regulate the DC voltage at 642kV
  - Reactive power transfer = 0MVAr
- Active power generated by Wind Power Plant:

$$P_1 = \begin{cases} 300MW & 1 \leq t < 4\ sec \\ 425MW & 4 \leq t < 7\ sec \\ 600MW & 7 \leq t < 10\ sec \end{cases}$$

Figure 4.23 shows the plot of the active and reactive power delivered by WPP versus time. Figure 4.24 shows the plot of the dc voltage at the WPP converter terminal versus time.

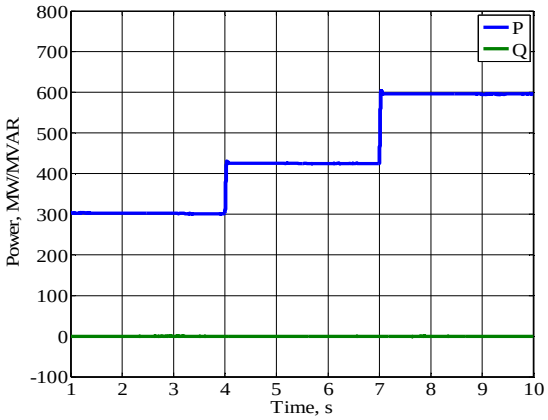

Figure 4.23 Graph of Active and Reactive Power Delivered by WPP versus time

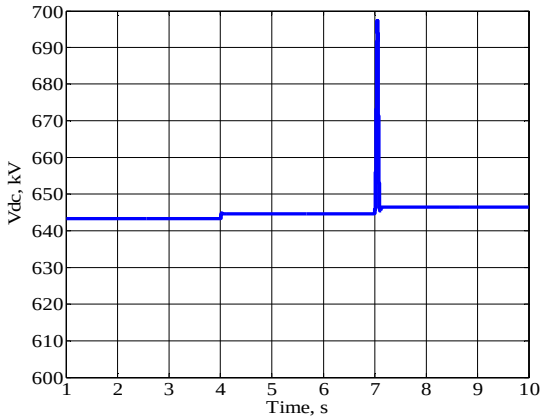

Figure 4.24 Graph of DC voltage at the WPP converter terminal versus time

Based on the case scenario, the active power received by each ac grid should be as follows:

- Time interval 1: $1 \leq t < 4\ sec$
    - The total generated active power by the wind plants is 250MW. Since this value is less than 400MW, it is expected that all the active power will go to the ac grid 1.
- Time interval 2: $4 \leq t < 7\ sec$
    - The total generated active power by the wind plants is 350MW. Since this value is less than 400MW, it is expected that all the active power will go to the ac grid 1.
- Time interval 3: $7 \leq t < 10\ sec$
    - The total generated active power by the wind plants is 600MW. Since this value is greater than 400MW, ac grid 1 will receive 400MW and ac grid 2 will receive the rest.

Figures 4.25 and 4.26 show plots representing the active and reactive power received by ac

grid 1 and ac grid 2 respectively versus time.

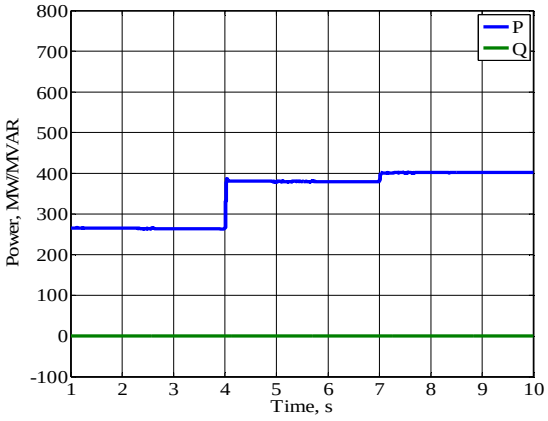

Figure 4.25 Graph of the Active and Reactive Power Received by AC grid 1 versus time

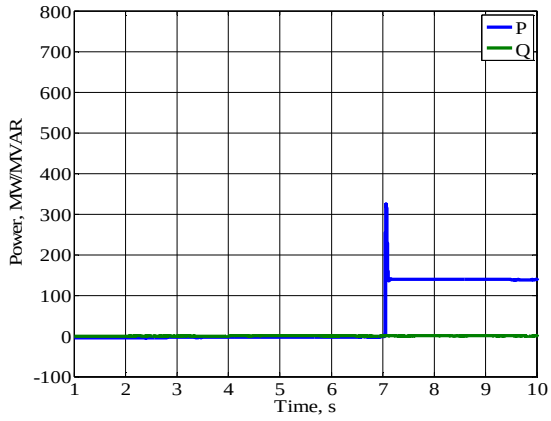

Figure 4.26 Graph of the Active and Reactive Power Received by AC grid 2 versus time

Figures 4.27 and 4.28 show plots of the dc voltages at the grid 1 and 2 converter terminals respectively versus time. As expected the plots match the characteristics plots. The dc voltage at the terminal of ac grid 1 converter is controlled at 640kV when the current is less than the limit. Once the current is above the limit, the dc voltage is higher since it is current controlled. The dc voltage at the terminal of ac grid 2 converter is controlled at 642kV.

The temporary overvoltage seen at t=7 seconds is a transient response due to ac grid 2 starting to receive active power. Note that this is not a completely accurate transient response due to model limitations.

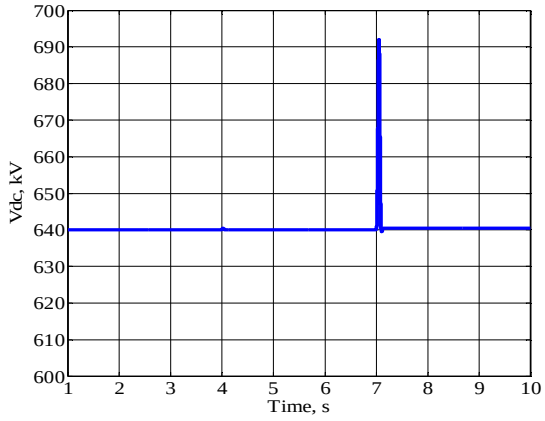

Figure 4.27 Graph of DC voltage at the AC grid 1 converter terminal versus time

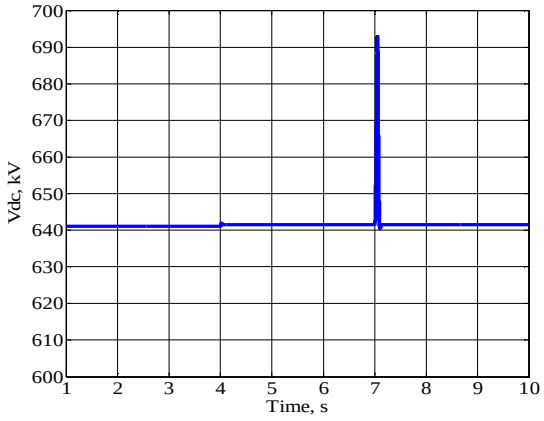

Figure 4.28 Graph of DC voltage at the AC grid 2 converter terminal versus time

4.2.3.2. Case B

In this case study, the system will be tested to operate in Mode 2. The following case scenario will be used to run the simulation:

- Time interval = 9 seconds [1 sec to 10 sec]
- Resistances: We will assume that all the dc lines are using a dc cable similar to the one used previously.
  - $R_1 = 0.0121\frac{ohm}{km} \cdot 200km = 2.42\Omega$
  - $R_2 = 0.0121\frac{ohm}{km} \cdot 100km = 1.21\Omega$
  - $R_3 = 0.0121\frac{ohm}{km} \cdot 100km = 1.21\Omega$
- Active power generated by Wind Power Plant:

$$P_1 = \begin{cases} 600MW & 1 \leq t < 4\ sec \\ 750MW & 4 \leq t < 7\ sec \\ 900MW & 7 \leq t < 10\ sec \end{cases}$$

- Droop constant, K_3=0.2
- Maximum voltage of both GSVSCs, V_{dc_max}=650kV

- Ratio of active power receiving between the two ac grids, n, is chosen to be equal to 2.

Figure 4.29 shows the generated plot representing the active and reactive power delivered by WPP.

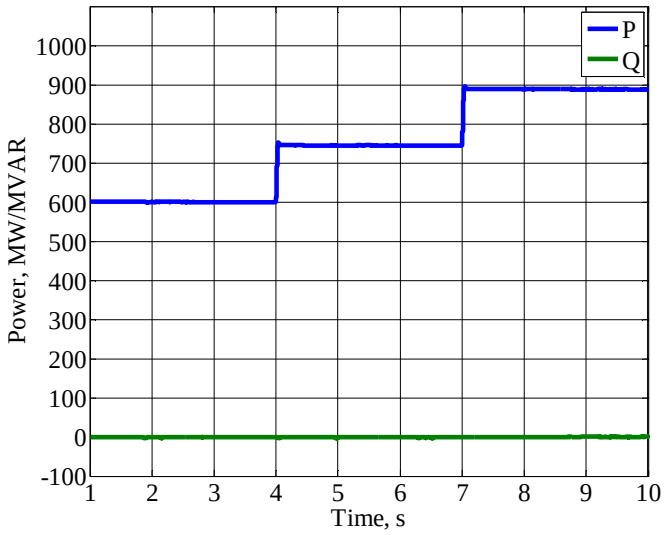

Figure 4.29 Graph of the Active and Reactive Power Delivered by WPP versus time

Figures 4.30 and 4.31 show plots representing the active and reactive power received by ac grid 1 and ac grid 2 respectively versus time. It can be seen that the received active power by ac grid 1 is almost double that received by ac grid 2 at all times. The ratio will not be accurate due to losses.

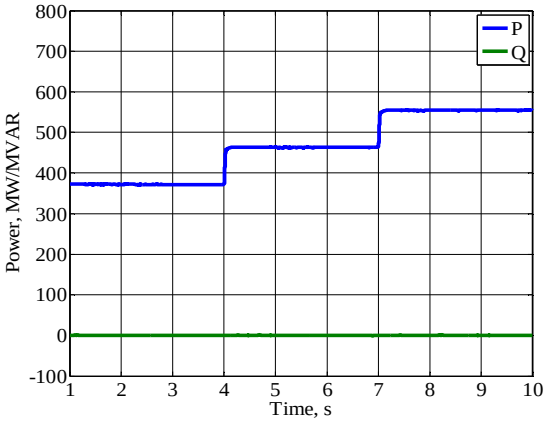

Figure 4.30 Graph of the Active and Reactive Power Received by AC grid 1 versus time

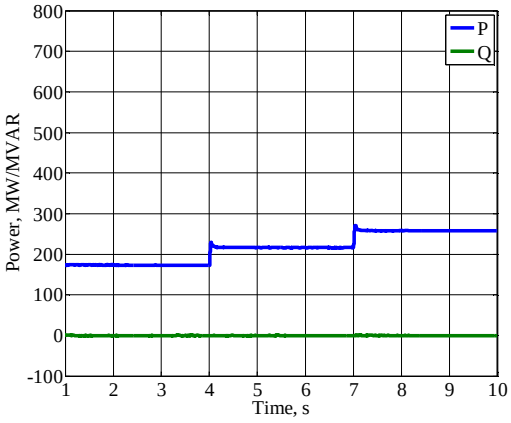

Figure 4.31 Graph of the Active and Reactive Power Received by AC grid 2 versus time

Figures 4.32 and 4.33 show plots of the dc voltages at the ac grid 1 and 2 converter terminals respectively versus time. The dc voltage at the terminals of both GSVSCs didn't reach the maximum set value and therefore the converters were voltage controlled throughout the simulation period.

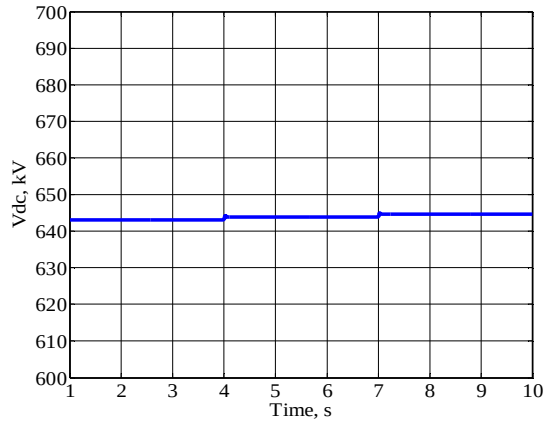

Figure 4.32 Graph of DC voltage at the AC grid 1 converter terminal versus time

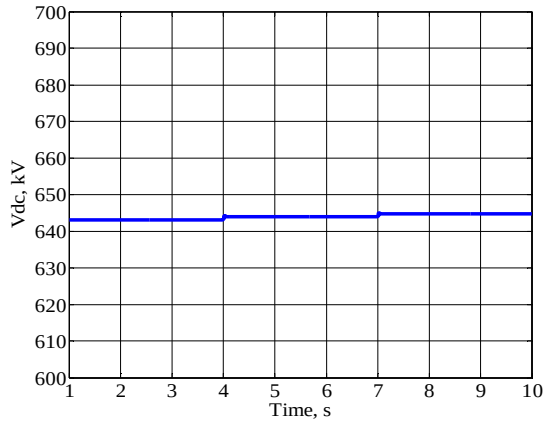

Figure 4.33 Graph of DC voltage at the AC grid 2 converter terminal versus time

4.3. General Control Approach for Multi-Terminal HVDC Systems

In this section, a general approach for controlling MTDC systems building from the methods from Sections 4.1 and 4.2 will be discussed and explained. Figure 4.34 shows a MTDC system consisting of n WPPs and m ac grids.

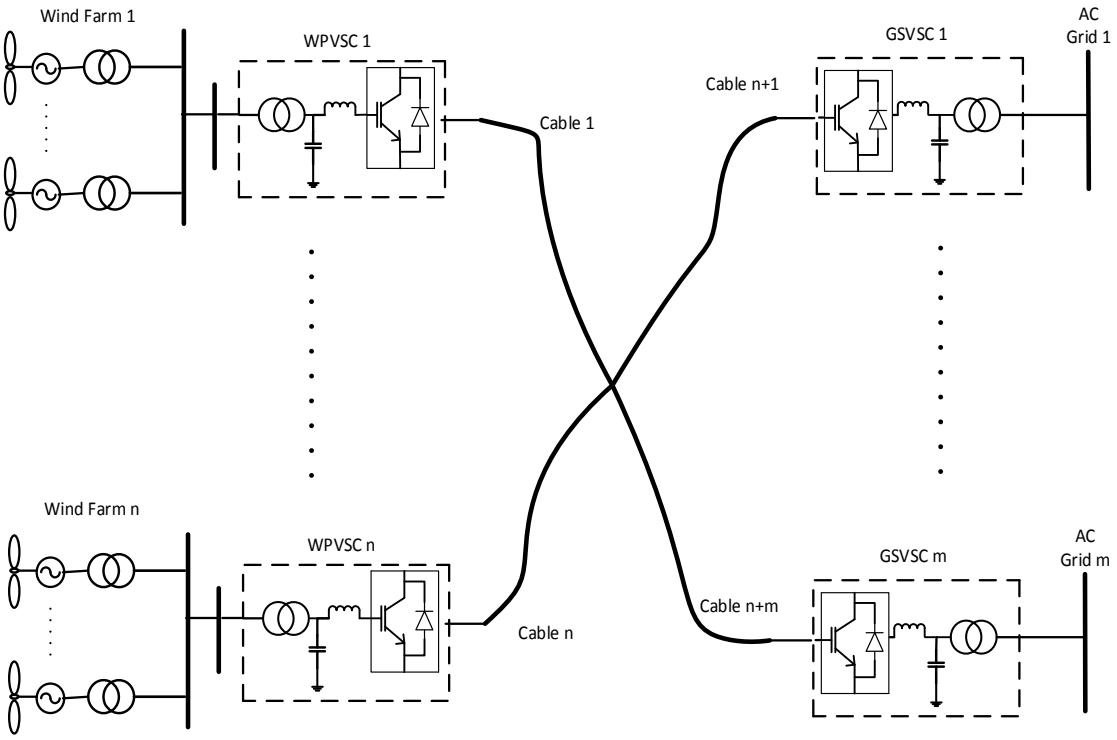

Figure 4.34 MTDC system consisting of n WPPs and m AC grids

The control approach can be divided into two parts:

- Control of VSCs that will provide active power. This will include all WPPs and ac grids that have surplus generation of power.
- Control of VSCs that will receive active power. This will include ac grids that have shortage in power.

Figure 4.35 shows the dc equivalent circuit of the MTDC system shown in Figure 4.34.

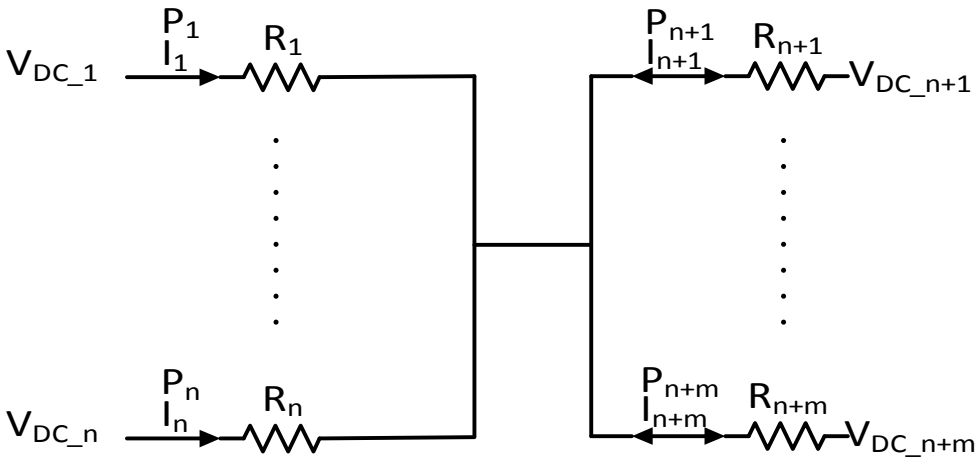

Figure 4.35 Equivalent DC circuit of the system

4.3.1. Control of VSCs that Provide Active Power in MTDC Systems

The general MTDC system configuration shown in Figure 4.34 consists of n+x VSCs that are providing active power to the system, where x represent the number of ac grids that have surplus generation of active power. As discussed earlier, the objective of the distribution of the supplied active power will be minimizing the copper losses [22]. Therefore, the controller will be designed based on the droop characteristics of the system taking into consideration the capacity of each WPP and ac grid.

The currents in the circuit shown in Figure 4.35 are related by the following equation, where I_T represents the total generated current:

$$I_T = I_1 + I_2 + \cdots + I_n + I_{n+1} + \cdots + I_{n+x} \qquad (4.34)$$

Note that the current direction of the ac grids VSC that are providing active power are assumed from the ac grid to the dc transmission line, while the current direction of the ac grids VSC that are taking active power are assumed from the dc transmission line to the ac grid.

The copper losses in the dc transmission line can be calculated using the following equation:

$$P_{Losses} = I_1^2 \cdot R_1 + I_2^2 \cdot R_2 + \cdots + I_{n+x}^2 \cdot R_{n+x} \quad (4.35)$$

Following a similar approach to the one used in Section 4.1, which is basically differentiating the copper losses equation with respect to each current and equating to zero to find the minimum point, we will get the following ratio relationship between the currents:

$$P_1 : P_2 : \ldots : P_{n+x} = \frac{1}{R_1} : \frac{1}{R_2} : \ldots : \frac{1}{R_{n+x}} \quad (4.36)$$

The voltages at the VSCs terminal will be equal to each other.

Once we have the droop characteristics of the system, total required active power, and the capacity of each WPP or ac grid that will provide active power, the control circuit can determine the amount of active power each unit will provide. The iterative logic flowchart shown in Figure 4.36 will be used to determine the reference active power values.

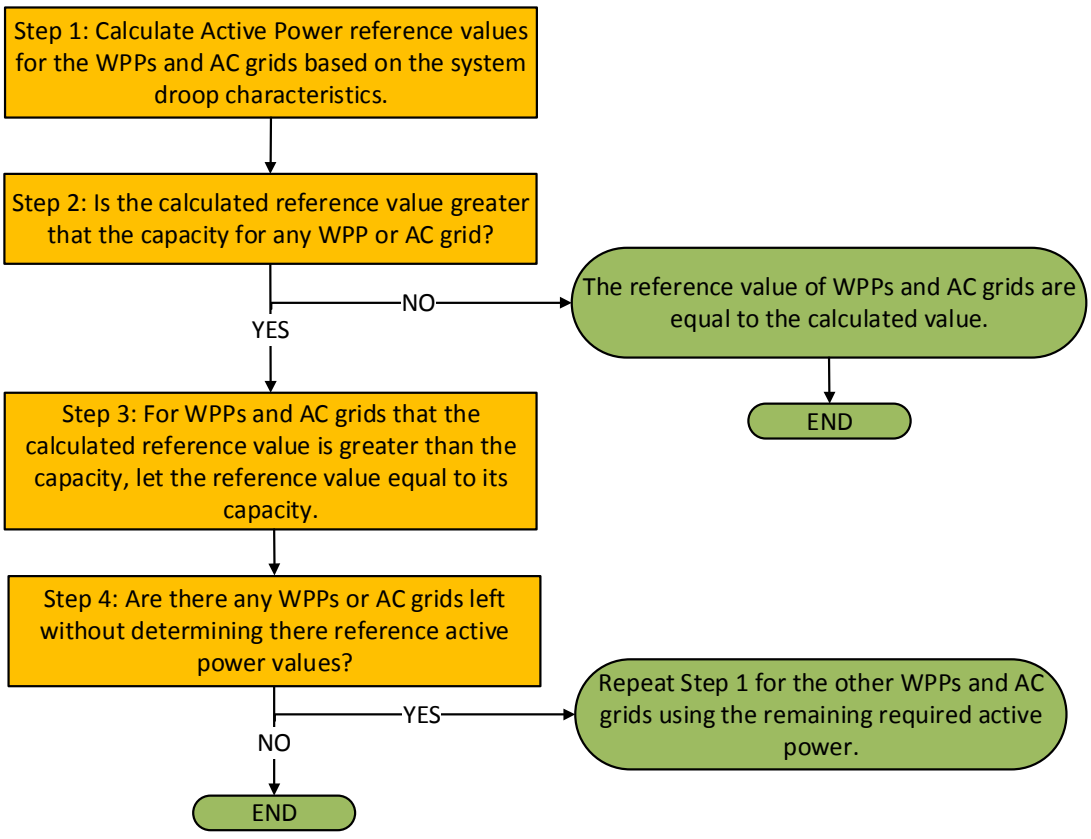

Figure 4.36 Logic Flowchart Determining the Active Power Provided WPPs and AC grids

4.3.2. Control of VSCs that Receive Active Power in MTDC Systems

4.3.2.1. Mode 1

In this mode of operation, we will set priority in receiving active power for each ac grid extending the method used in Mode 1 explained in Section 4.2.

The dc voltage of $GSVSC_{x+1}$ will be controlled at the set value as long as the active power received is below the set limit. If the received active power reaches the limit, $GSVSC_{x+1}$ will no longer control the dc voltage, but it will be current controlled at the limit value.

The dc voltage $GSVSC_{x+2}$ will be controlled at a voltage that is slightly larger than the maximum voltage that $V_{DC,C}$ can reach before $GSVSC_{x+1}$ reach its limits. This will ensure that $GSVSC_{x+2}$ will not receive active power unless $GSVSC_{x+1}$ is loaded at its required active power. A current limiter similar to the one shown in Figure 4.17 should also be designed for $GSVSC_{x+2}$ to ensure that it will not provide active power to the system and it will not receive more than its limit. The designed dc voltage that $GSVSC_{x+n}$ will be controlled at a value slightly larger than it can be calculated using the following equation.

$$V_{DC,GSx+2} = V_{DC,GSx+1} + I_{n+x+1(max)} \cdot R_{n+x+1} \qquad (4.37)$$

Similarly, this will be the case for $GSVSC_{x+3}$ to $GSVSC_m$. For example, the dc voltage that $GSVSC_{x+m}$ will be controlled at a value slightly larger than it can be calculated using the following equation.

$$V_{DC,GSm} = V_{DC,GSm-1} + I_{m+x-1(max)} \cdot R_{m+x-1} \qquad (4.38)$$

4.3.2.2. Mode 2

In this mode of operation, all ac grids will share the generated active power by a certain

ratio. The ratios can be defined as:

$$P_{x+1} : P_{x+2} : \dots : P_{n+m} = n_{x+1} : n_{x+2} : \dots : n_m \quad (4.39)$$

The currents and dc voltages will be related by the following equations:

$$I_{n+x+1} = k_{x+1} \cdot (V_{DC,GSx+1} - V_{DC,GS(min)}) \quad (4.40)$$

$$I_{n+x+2} = k_{x+2} \cdot (V_{DC,GSx+2} - V_{DC,GS(min)}) \quad (4.41)$$

Until we reach the last ac grid with the following equation:

$$I_{n+m} = k_m \cdot (V_{DC,GSm} - V_{DC,GS(min)}) \quad (4.42)$$

The droop constants will be designed in a similar way to that explained in Section 4.2. First of all K_{x+1} will be chosen. Then K_{x+2} will be calculated using the following equation:

$$k_{x+2} = \frac{1}{n_{x+1}/k_{x+1} + n_{x+1} \cdot R_{n+x+1} - R_{x+x+2}} \quad (4.43)$$

The same equation will hold for all droop constants until K_m which will be calculated using the following equation:

$$k_m = \frac{1}{n_{x+1}/k_{x+1} + n_{x+1} \cdot R_{n+x+1} - R_m} \quad (4.44)$$

Knowing total active power provided, we will first calculate P_{x+1}, P_{x+2}, etc., from the set ratios. Similar to the scheme described in Section 4.2, the reference dc voltage is related to the active power received by the following equation:

$$P_{GS1} = V_{DC\_GS1} \cdot I_{DC\_GS1} \quad (4.45)$$

Substituting the dc current from equation (4.39) in equation (4.42) and rearranging the equation will result in the following:

$$K_3 \cdot V_{DC\_GS1}^2 - K_3 \cdot V_{DC(min)} \cdot V_{DC\_GS1} - P_{GS1} = 0 \quad (4.46)$$

Solving the above equation will result in finding the reference value of the dc voltage

controlled by the VSC in ac grid 1. A similar approach should be followed to find the reference value of the dc voltage controlled by the VSC in ac grid 2.

4.3.2.3. Mode 3

This mode of operation is a combination of Modes 1 and 2. Some of the ac grids will be prioritized to receive active power over the other ac grids. When the set limit of an ac grid is reached, the remaining active power will be shared between all the ac grids by a set ratio.

4.4. Summary

In this chapter, the control methods of MTDC systems' VSCs for the different operational modes were explained. It was shown in the chapter that the active power sharing between the ac grids' VSCs can be controlled to meet the requirements set by the transmission operator. This was achieved by building a control system that can generate the reference dc voltage of each VSC. The equations to the control system depend on the MTDC system configuration.

5. Chapter 5: Adding Single Taps on Lines in Multiterminal HVDC Systems

5.1. Introduction

Tapping on HVDC lines is one of the applications of MTDC systems that can bring great benefits by providing power to small villages, isolated rural areas, offshore oil rigs, or any other areas that are close to HVDC lines. A tap can be defined as an additional terminal added to an MTDC system with a small power rating relative to the power transfer in the HVDC line. Therefore, the addition of the tap should not make a considerable change to the operation of the MTDC system. The definition of a tap is not restricted to receiving power from the HVDC line, but it also includes distributed generation with a relatively small power rating [25, 26]. In this chapter, however, taps are studied with the point of view that they receive power from HVDC lines.

The tap station steps down the high voltage level and converts the dc power to an ac power connecting the HVDC line to a small local ac network. Figure 5.1 shows a typical two-terminal HVDC system with a tap station.

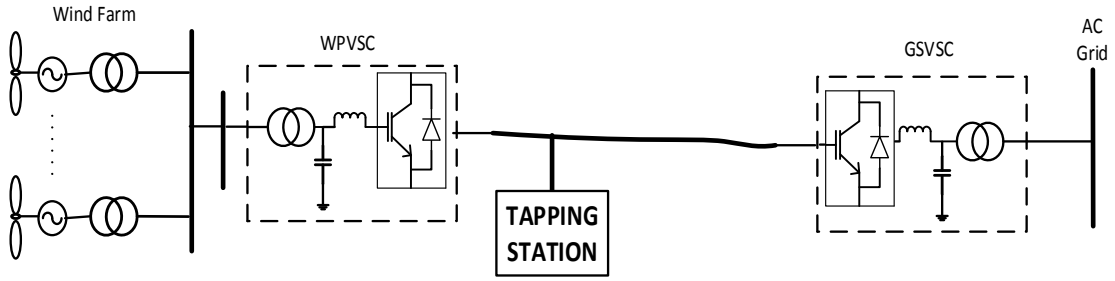

Figure 5.1 Two-Terminal HVDC System with an Inserted Tap Station.

Figure 5.2 shows the dc equivalent circuit of the system shown in Figure 5.1. It is important to note that the voltage sources represent VSCs that are basically dc current sources regulated to look like voltage sources.

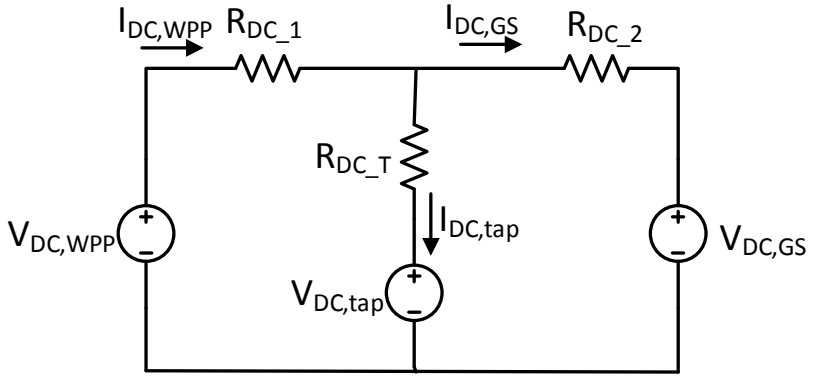

Figure 5.2 DC Equivalent Circuit of the Two-Terminal HVDC System with an Inserted Tap Station as shown in Figure 5.1.

There are many economical, technical, and operational concerns with tapping on HVDC lines. These concerns include [27]:

- The high cost of the tap station due to the high voltage insulation required by components rated for the HVDC line voltage.
- The impact the tap can have on the reliability of the HVDC system.
- The control of the tap station and its effect on the control of the HVDC system.
- Interaction with fault response.

When adding a tap on a HVDC line, a very high voltage step down is required. This is usually done using ac transformer. Recent studies proposed stepping down the voltage on the dc side using high frequency transformers interface via VSCs, but none have been deployed at full HVDC voltage levels in any project. The following are advantages of using dc transformers [27]:

- Only the dc transformer needs to be rated at the HVDC voltage and therefore reducing the cost of the tap station.

- DC transformer will reduce the effect of any disturbance in the tap system on the main HVDC line.

As mentioned earlier, when tapping on HVDC lines, the tap should not affect the control and operation of the MTDC system. In worst case scenarios, if the tap had to be isolated from the HVDC line by an ac circuit breaker due to a fault in the local ac network, for example, the operation of the MTDC system should stay stable. Similarly, if the tap is to be reconnected to the HVDC line after an ac or dc fault clearance, the operation of the MTDC system should stay stable. This might be an expected behavior in the case when only one tap is connected with a relatively low rating. However, the need of having multiple taps on lines in a HVDC grid raises the question of what is the total rating of, and number of tap stations that can be connected to an MTDC system without making a considerable effect on its control and operation. Chapter 6 will further discuss impacts of having multiple taps in MTDC systems.

In the next section of this chapter, two case studies of single tapping on an MTDC system will be presented.

5.2. Tapping on MTDC systems – Case Studies.

In this section, two case studies of single taps on an MTDC system will be presented. The same MTDC system from Section 4.1 will be used in both cases and it consists of two wind power plants and one ac grid. Figure 5.3 shows the configuration of the used MTDC system.

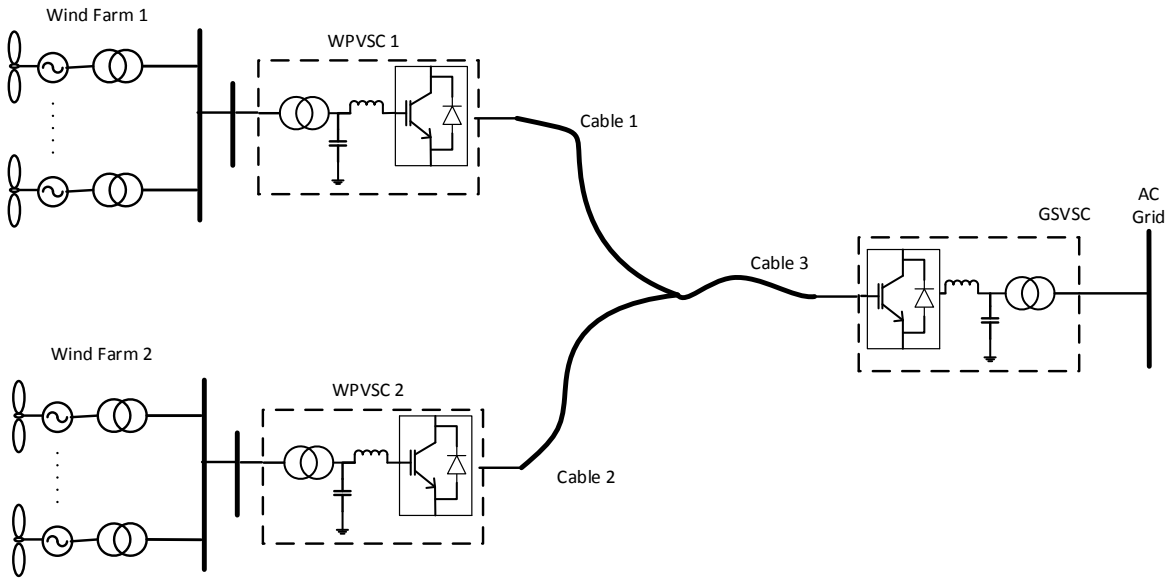

Figure 5.3 MTDS System consisting of Two Wind Power Plants and One AC Grid

The following parameter will be used for the cases simulation:

- Time interval = 9 seconds [1 sec to 10 sec]
- AC Grid Control:
    - DC voltage = 640kV
    - Reactive power transfer = 0MVAr
- Both wind power plants is considered to be identical with generation of 350 MW
- Resistances:
    - $R_1 = 0.0121\frac{ohm}{km} \cdot 50km = 0.605\Omega$
    - $R_2 = 0.0121\frac{ohm}{km} \cdot 50km = 0.605\Omega$
    - $R_3 = 0.0121\frac{ohm}{km} \cdot 250km = 3.025\Omega$
- Active power required by the ac grid:

$$P_3 = 700MW$$

Two case scenarios will be simulated where the substation of an offshore oil rig is to be fed

from an HVDC line. In the first scenario, the offshore oil rig will be located near the ac grid terminal, while in the second scenario it will be located near one of the wind power plants. For simplicity, the tap station will be represented as a dc current source from the positive pole to the negative pole and it will have an approximate rating of 2% of the 700 MW system rating.

$$I_{tap,rating} = 2\% \times \frac{700MW}{640kV} \approx 22A$$

To test the system response, the simulation will start with the tap connected online. After that, the tap will be isolated and finally restored to system.

$$I_{tap} = \begin{cases} I_{tap,rating} & 1 \leq t < 4\ sec \\ 0 & 4 \leq t < 7\ sec \\ I_{tap,rating} & 7 \leq t < 10\ sec \end{cases}$$

Note that the tap station is considered to be connected directly on the HVDC line, i.e. R_{DC_T} is equal to zero.

5.2.1. Case A – Offshore Oil Rig Located near AC Grid

In this case, the tap station will be located halfway between the ac grid VSC station and the point of intersection of cables 1, 2, and 3. Figure 5.4 shows case A system diagram. The case will also be simulated completely without the tap station to compare the results and see the effect of the tap station on the MTDC system operation.

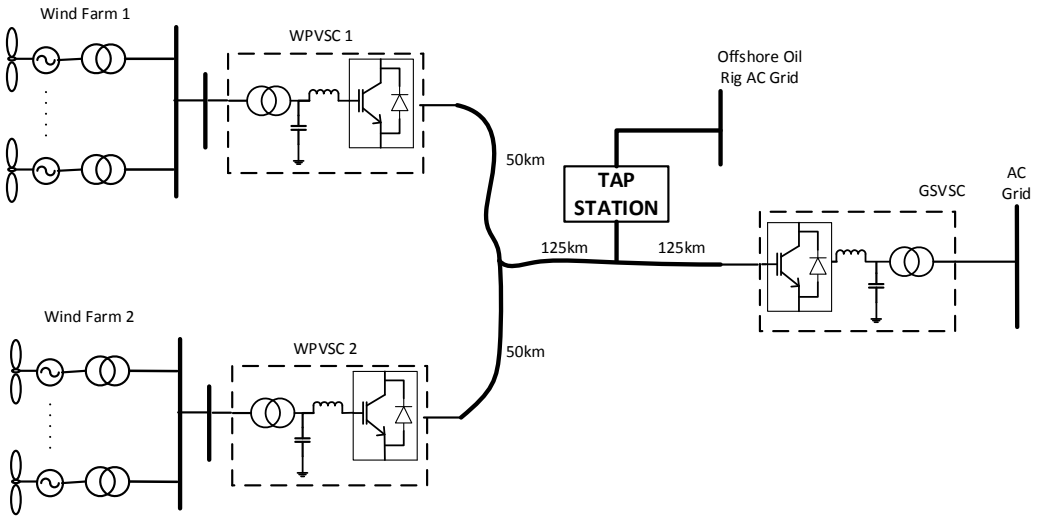

Figure 5.4 Case A System Diagram

Figures 5.5 and 5.6 show plots representing the active and reactive power received by the ac grid versus time for the cases with and without the tap station respectively. Observe that the power received by the grid side in the case with the tap station is stable. The only change in the case with the tap station is the difference in the active power received by the ac grid in the time when the tap station is online.

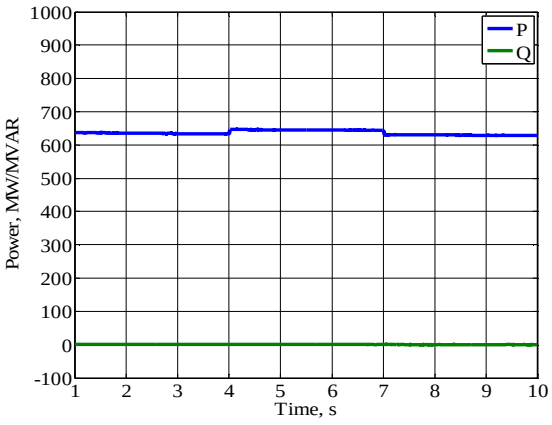

Figure 5.5 Graph of the Active and Reactive Power Received by the AC grid versus time for the case with a tap station.

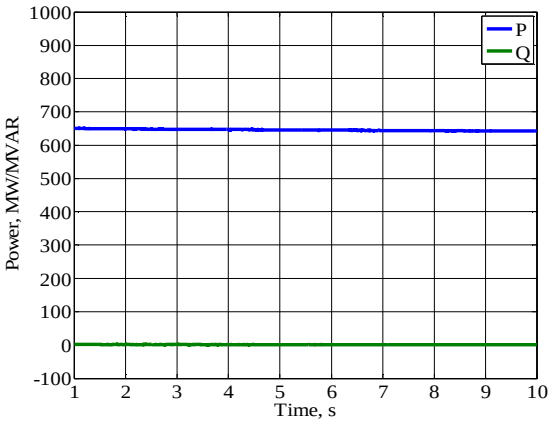

Figure 5.6 Graph of Active and Reactive Power Received by the AC grid versus time for the case without a tap station.

Figures 5.7 and 5.8 show plots representing the dc voltage at the ac grid VSC terminals versus time for the cases with and without the tap station respectively. It can be seen that the dc voltage is always stable and regulated at 640kV, which is expected since the ac grid VSC is controlling the dc voltage at a fixed value.

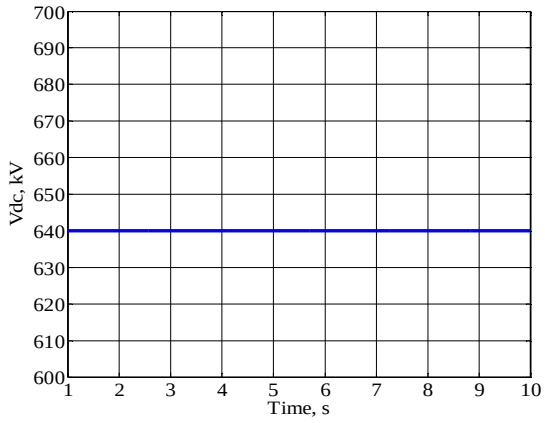

Figure 5.7 Graph of DC voltage at the AC grid converter terminal versus time for the case with a tap station

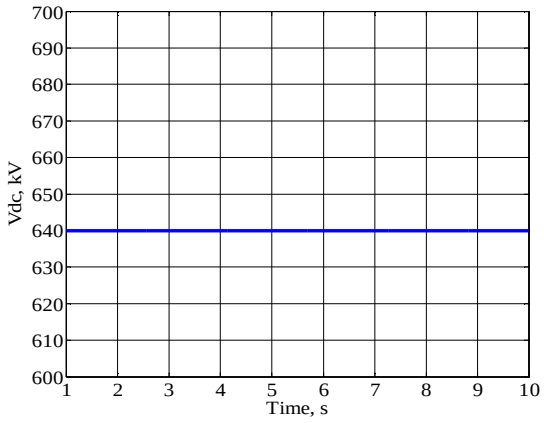

Figure 5.8 Graph of DC voltage at the AC grid converter terminal versus time for the case without a tap station

Figures 5.9 and 5.10 show plots representing the dc voltage at the WPP1 VSC terminals versus time for the cases with and without the tap station respectively. Notice that in the case with a tap station, the change in dc voltage at the WPP1 VSC terminal to isolating or reconnecting the tap station is very small. This is primarily because the rating of the tap station is as small as 2% of the power through the HVDC lines.

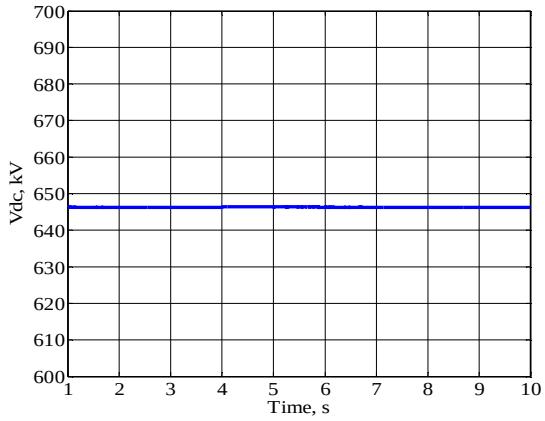

Figure 5.9 Graph of DC voltage at the WPP1 converter terminal versus time for the case with a tap station

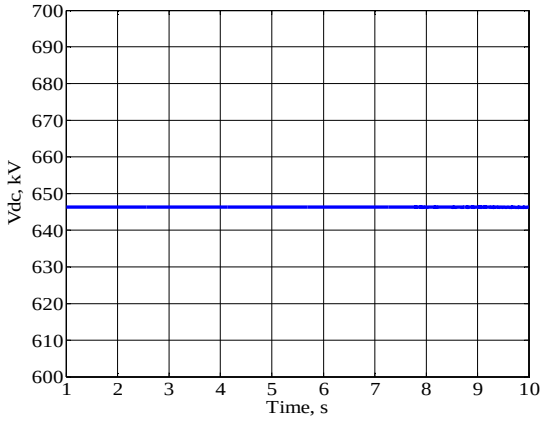

Figure 5.10 Graph of DC voltage at the WPP1 converter terminal versus time for the case without a tap station

5.2.2. Case B – Offshore Oil Rig Located near Wind Power Plant 1

In this case, the tap station will be located halfway between the WPP1 VSC station and the point of intersection of cables 1, 2, and 3. Figure 5.11 shows case B system diagram.

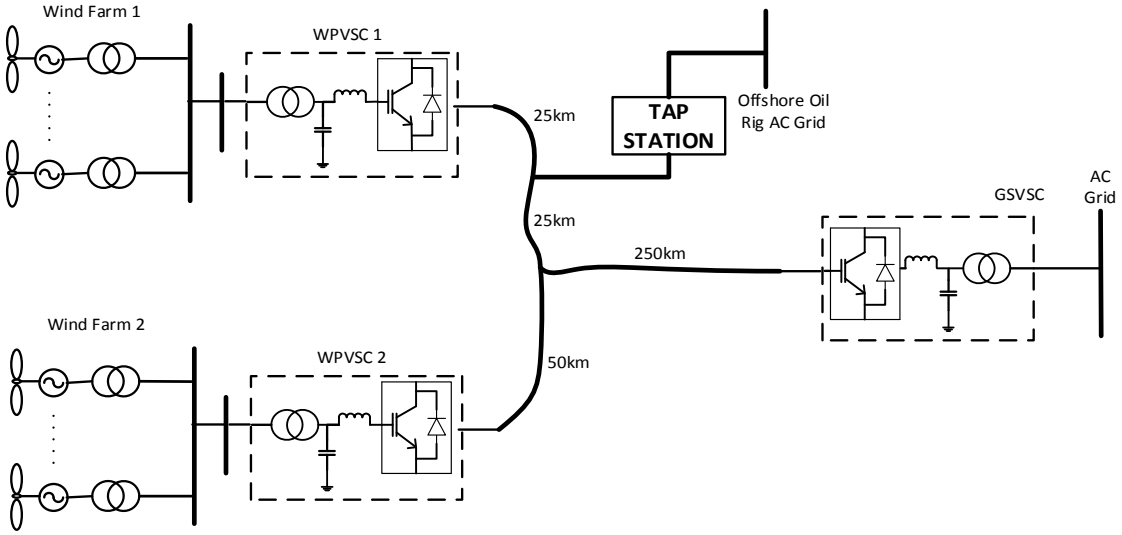

Figure 5.11 Case B System Diagram

Figure 5.12 shows a plot representing the active and reactive power received by the ac grid versus time. Similar to case A, we can observe that the power received by the ac grid is

stable.

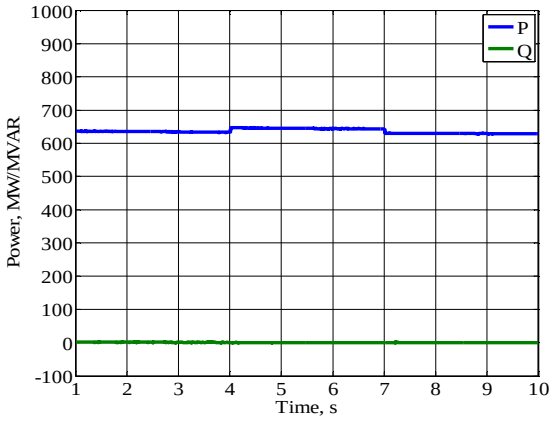

Figure 5.12 Graph of the Active and Reactive Power Received by the AC grid versus time for case B simulation

Figures 5.13 and 5.14 show plots representing the dc voltage at the ac grid VSC terminals and WPP1 VSC terminal versus time. It can be observed that the dc voltage at the WPP terminals is stable in the presence of a tap station near the WPP converter station.

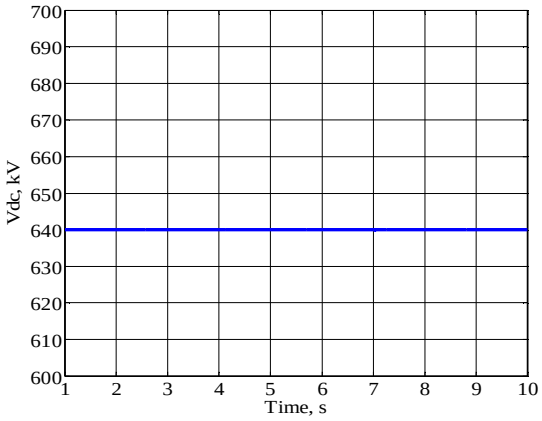

Figure 5.13 Graph of DC voltage at the AC grid converter terminal versus time for case B simulation

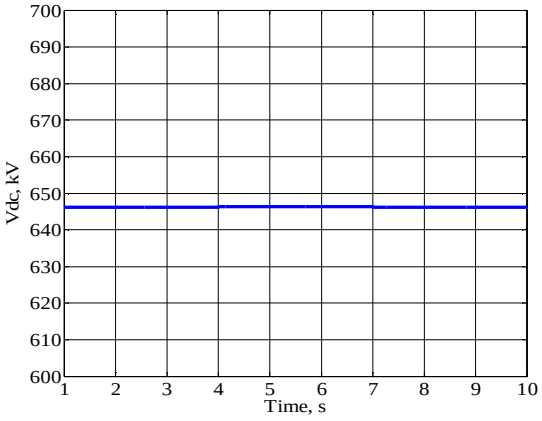

Figure 5.14 Graph of DC voltage at the WPP1 converter terminal versus time for case B simulation

Adding single taps on lines in MTDC systems was presented in this chapter. General

concerns with tapping on HVDC lines were discussed. Two case studies of adding a single tap in a MTDC system were simulated. Adding multiple taps in MTDC systems was introduced and will be discussed in more details in Chapter 6.

6. Chapter 6: Multi-Tapping on HVDC Lines in MTDC Systems

6.1. Introduction

As discussed in Chapter 5, tapping on HVDC lines is a beneficial application that provides power to areas that are located close to the HVDC lines. The need of having multiple taps on HVDC lines and the effects this practice can have on MTDC systems have been the focus of many researchers. One important point to take into consideration is determining the number and the rating of tap stations that can be connected to an MTDC system without having a considerable effect on its control and operation. Developing an analytical method to determine the tapping limit of an MTDC system is not within the scope of this thesis work. However, any method of determining the tapping limit will depend on many factors including [27, 28]:

- Voltage rating of power electronics used in the MTDC system. This is important since the voltage drop in the HVDC line will be changed due to changes in power transfers to or from the tap stations.
- Power stability of the MTDC system.
- Control parameters of the MTDC system
- Length and resistance of the HVDC lines
- Locations of the tapping stations

In Section 6.2, a breakdown of the different control schemes for multi-tapping in MTDC system will be presented. Section 3 of this chapter will present different case studies of multi-tapping in MTDC system.

6.2. Control Schemes of Multi-Tapping in MTDC Systems

6.2.1. Approach Description

To address possible control schemes for multi-tapping in MTDC systems, let us begin by looking at the system shown in Figure 6.1. This system consists of 1 WPP, 1 ac grid, and 2 tap stations.

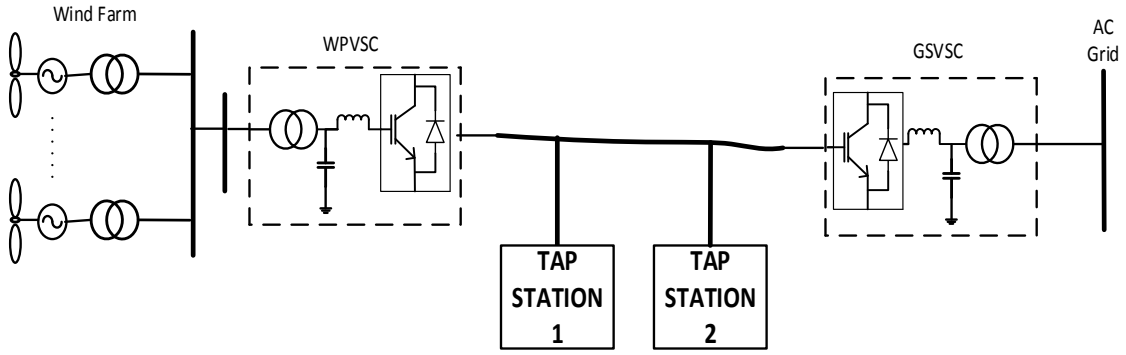

Figure 6.1 Two-Terminal HVDC System with Two Tapping Stations.

Figure 6.2 shows the dc equivalent circuit of the system shown in Figure 6.1. It is important to remember here that the power flow through the tap station can be bi-directional, i.e. a tap station could be a distributed generation that is providing power to the MTDC system or a load subsystem. However, tap stations in this section are assumed to be receiving power from the MTDC system.

In such a system, determining the control scheme strategy used for power distribution between the terminals and taps depends on the following factors:

- The percentage of the total power received by both tapping stations relative to the total power transfer in the HVDC transmission system. This value will determine whether or not the control circuits of the tap stations need to be considered by the control circuit of the MTDC system. This decision also depends on the total tapped

power limit of the MTDC system. In [29], an analytical method is presented to determine the total tapped limit of an MTDC system.

- The method of distributing the tapped-off power between the tap stations. This can be done using constant values or droop characteristics.

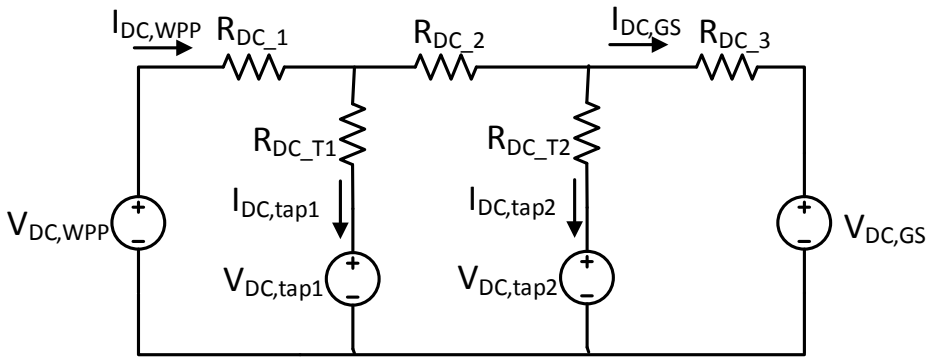

Figure 6.2 DC Equivalent Circuit of the System in Figure 6.1.

Expanding the system shown in Figure 6.1 into a general MTDC system with multiple tapping points (multi-tapping) will result in more complexity in determining the control strategy to be used for power distribution.

A general MTDC system with multi-tapping will consist of the following:

1. ***n*** terminals that are providing power to the MTDC network.
2. ***m*** terminals that are receiving power from the MTDC network.
3. ***r*** tap stations that are receiving power from the MTDC network.

For the ***n*** terminals that are providing power to the MTDC network, the objective of the distribution of the supplying of active power will be minimizing the copper losses. Therefore, the droop characteristics discussion in Section 4.3.1 for terminals providing power in an MTDC network is valid for this general case and it will not be repeated here.

For the ***m*** terminals and ***r*** tap stations that are receiving power from the MTDC network,

several strategies can be applied and they are introduced in the next subsections.

6.2.2. Control Scheme A

The control scheme of the tap stations falls into category A if:

1. The power tapped off the HVDC lines by all tap stations is within the tapping limit of the MTDC system.
2. The amount of power received by each tap is a constant value determined by an operator or a higher control system.

A constant amount of power is required by the tap if the HVDC line is the only source of power for the local ac system connected through the tap station. In some cases, the local ac system might have internal power generation, such as diesel generators, but they cannot provide the required power and, therefore, a constant amount of power should be tapped off the HVDC line.

Figure 6.3 shows an MTDC system consisting of 1 WPP, 1 ac grid, and ***r*** tap stations. Only 1 ac grid and 1 WPP is presented to simplify the figure. However, a system with more WPPs and ac grids falls into this category if points 1 and 2 are satisfied.

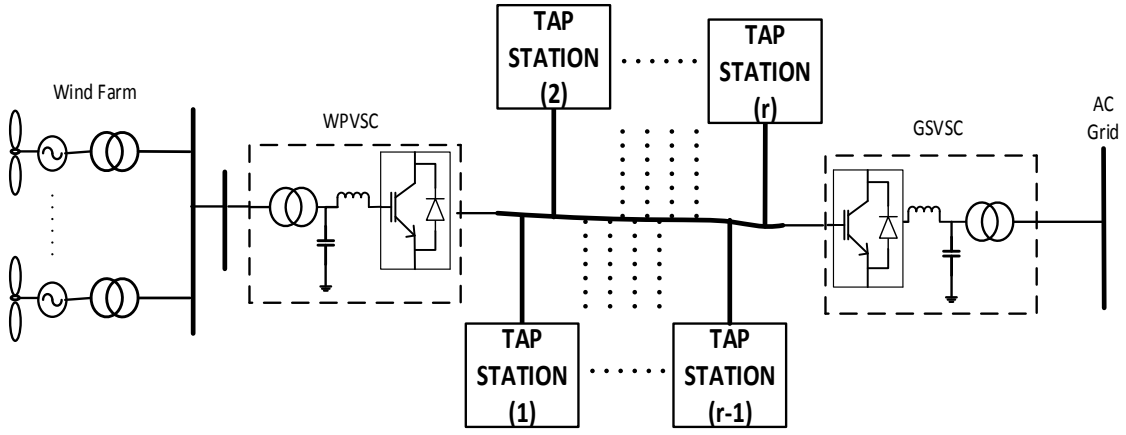

Figure 6.3 MTDC system consisting of 1 WPP, 1 AC grid, and ***r*** tap stations.

Figure 6.4 shows the dc equivalent circuit of the system shown in Figure 6.3.

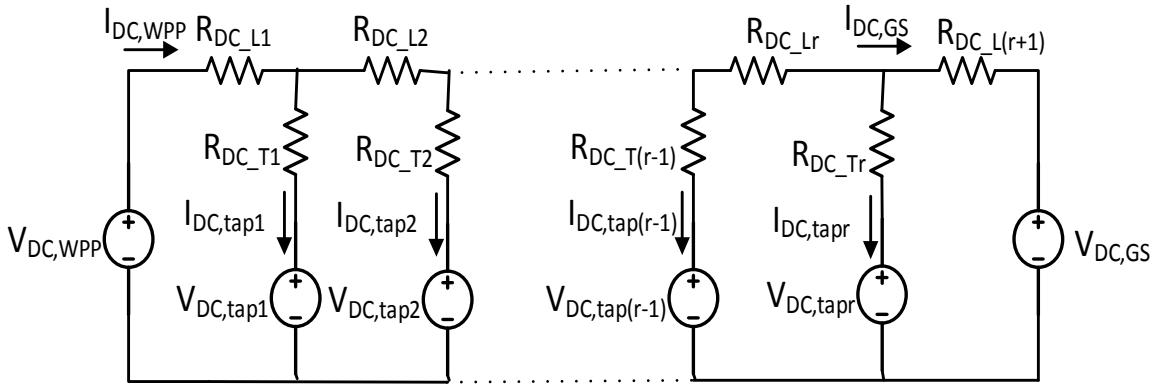

Figure 6.4 DC Equivalent Circuit of the System shown in Figure 6.3.

In this category, the control of each individual tap station is independent of the control of the MTDC system and other tap stations. Depending on the tap stations' configuration, the amount of power delivered to each tap is constant and these objectives are achieved by controlling either the dc voltage at the dc terminals of each tap station using a dc voltage controller or the power received by each tap station using an active power controller.

6.2.3. Control Scheme B

The control scheme of the tap stations falls into category B if:

1. The power tapped off the HVDC lines by all tap stations is within the tapping limit of the MTDC system.
2. The amount of power received by each tap is determined by droop characteristics analysis performed on the tap stations.

In this category, the total cumulative power tapped-off the MTDC system by all the tapping stations is a constant value that is below the tapping limit of the MTDC system. The ratio of power each tap will receive from the total cumulative power is determined by droop

characteristics of all the tap stations similar to the method discussed in Section 4.2.

The above characteristics show that the control systems of the tap stations are also independent and isolated from the MTDC network control system.

6.2.4. Control Scheme C

The control scheme of the tap stations falls into category C if:

1. The power tapped off the HVDC lines by all the tap stations is above the tapping limit of the MTDC system.
2. As a group, the tap stations are considered as a virtual terminal that receives power from the MTDC network.

Since the power tapped off the HVDC lines by all tap stations is above the tapping limit of the MTDC system, the control system of the MTDC system should take into consideration the power requirements of the tapping stations. The proposed method is to combine the tapping stations into one or more groups and then represented each group as a terminal in the MTDC network. The grouping of tapping stations is based on factors such as the ratings of the terminals and their location in the MTDC system.

Once the taps are grouped and represented as a terminal, power distribution between all the terminals can be done using any of the modes discussed in Section 4.3.2. Within a terminal consisting of a group of tapping stations, power distribution between the tap stations can be determined using either control scheme A or scheme B.

6.3. Case Studies of Multi-Tapping in MTDC Systems

6.3.1. MTDC System Configuration

Three case studies of multi-tapping will be presented in the next sub-sections. The MTDC system used for all case studies will consist of 1 ac grid and 1 WPP. The general simulation parameters are as follows:

- Time interval = 5 seconds [1 sec to 6 sec]
- MTDC system tapping limits = 25%
- Length of HVDC line = 300 km
- Resistance of HVDC line, $R_{DC} = 0.0121 \frac{ohm}{km}$
- AC Grid Control:
    - DC voltage = 640kV
    - Reactive power transfer = 0MVAr
- Required power by the ac grid = 500MW
- WPP Control:
    - For the sake of explaining the different control schemes, it will be assumed that the WPP is capable of delivering any amount of active power required.
    - Reactive power transfer = 0MVAr

6.3.2. Case A

In this case, two tap stations are connected to the HVDC line of the MTDC system and are feeding two offshore oil rigs. Offshore oil rig 1 does not have any local power generation and require 50 MW to be fed to its local ac network. Offshore oil rig 2 has diesel generators that are feeding its local ac network, but this subsystem will have a shortage of 25 MW that

is required to be fed from the HVDC line. Since the tapping stations require a constant amount of power that is below the tapping limit of the MTDC system of 125 MW, this case falls under control scheme A. Figure 6.5 shows the system diagram.

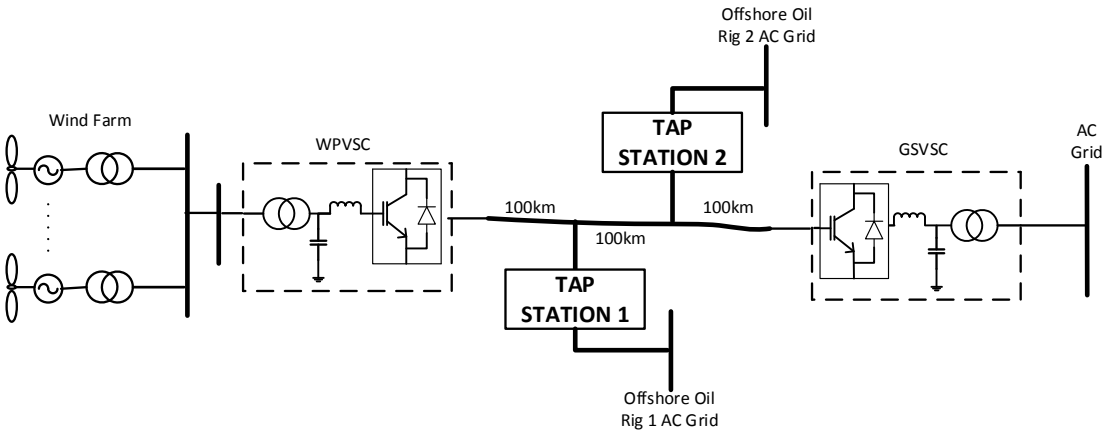

Figure 6.5 Case A System Diagram.

The location and details of the tap stations are as follows:

- Tap Station 1:
    - Location: 100 km from the WPP
    - Required Active Power = 50MW = 10% of power transfer in the HVDC line.
    - $R_{DC\_T1} = 0.2\Omega$
- Tap Station 2:
    - Location: 200 km from the WPP
    - Required Active Power = 25MW = 5% of power transfer in the HVDC line.
    - $R_{DC_{T2}} = 0.1\Omega$

Since the control circuit of the MTDC system is not affected by the tap station, the WPP will be controlled to deliver 500 MW, which is required by the ac grid.

Figures 6.6 and 6.7 show the active and reactive power delivered by the WPP grid and

received by the ac grid respectively versus time. It can be observed that the ac grid is not receiving the required 500 MW due to the active power tapped off by the tap stations and the transmission system losses.

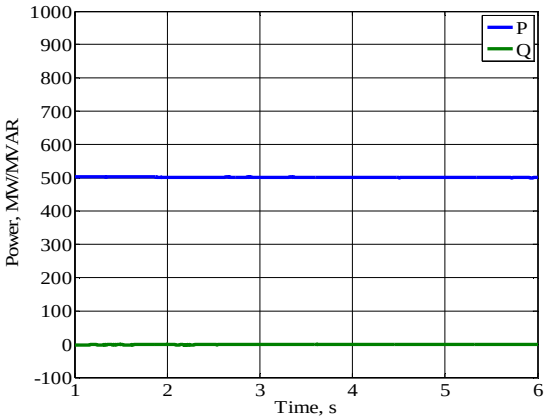

Figure 6.6 Graph of the Active and Reactive Power Delivered by WPP versus time

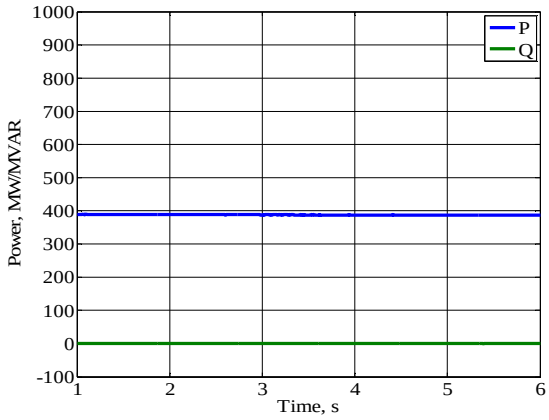

Figure 6.7 Graph of the Active and Reactive Power Received by the AC grid versus time

Figure 6.8 shows the dc voltages at the WPP converter terminals, point of tapping of tap station 1, point of tapping of tap station 2, and ac grid converter terminals.

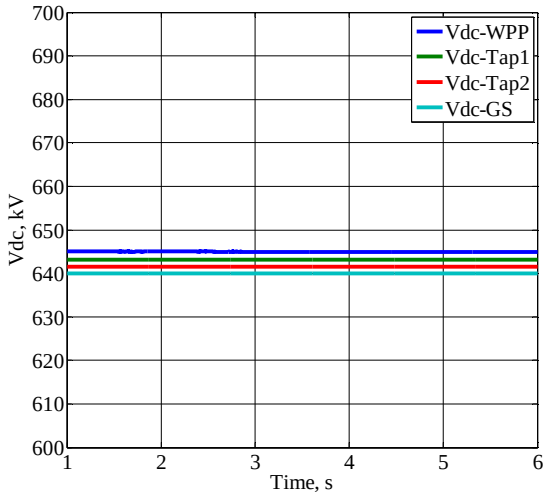

Figure 6.8 Graph of the DC voltages at Different Locations in the HVDC Line.

As designed, the dc voltage at the ac grid converter terminals is controlled at the nominal voltage 640kV. The dc voltage increases toward the WPP terminals.

Figure 6.9 shows the plot of the dc currents through the HVDC line at different locations.

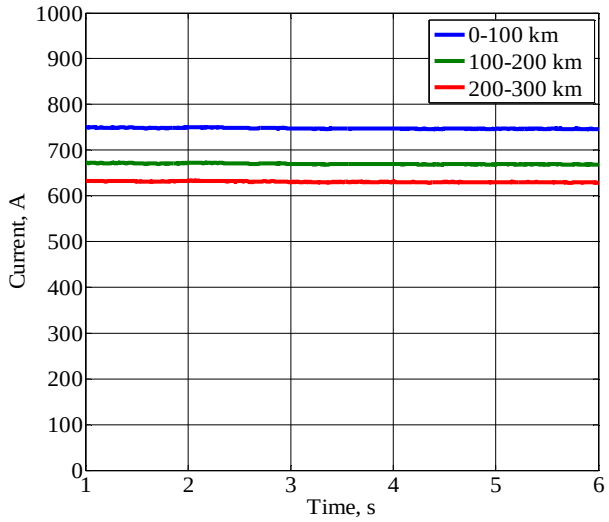

Figure 6.9 Graph of the DC currents through the HVDC line at different locations.

6.3.3. Case B

In this case, two tap stations are again connected to the HVDC line of the MTDC system and are feeding two offshore oil rigs. The system diagram and the location of the tapping stations are similar to case A. The two offshore oil rigs will receive a total of 75 MW from the HVDC line and the distribution of power between them will be based on droop characteristics. The tap stations location and dc resistance values are similar to case A. The power received by each tap station is calculated based on droop characteristics to minimize the losses assuming that the two systems have an internal power generation. The power calculations are as follows:

$$P_{tap1} = P_{tap_{total}} \left(\frac{R_{DC_2} + R_{DC_{T2}}}{R_{DC_{T1}} + R_{DC_2} + R_{DC_{T2}}} \right)$$

$$P_{tap1} = 75MW\left(\frac{1.21\Omega + 0.1\Omega}{0.2\Omega + 1.21\Omega + 0.1\Omega}\right) \approx 65MW$$

$$P_{tap2} = P_{tap_{total}}\left(\frac{R_{DC_{T1}}}{R_{DC_{T1}} + R_{DC_2} + R_{DC_{T2}}}\right)$$

$$P_{tap2} = 75MW\left(\frac{0.2\Omega}{0.2\Omega + 1.21\Omega + 0.1\Omega}\right) \approx 10MW$$

Similar to the previous case, the control circuit of the MTDC system is not affected by the tap station and the WPP will be controlled to deliver 500 MW, which is required by the ac grid.

Figures 6.10 and 6.11 show the active and reactive power delivered by the WPP grid and received by the ac grid respectively versus time. Similar to case A, the ac grid is not receiving the required 500 MW due to the active power tapped off by the tap stations and the transmission system losses.

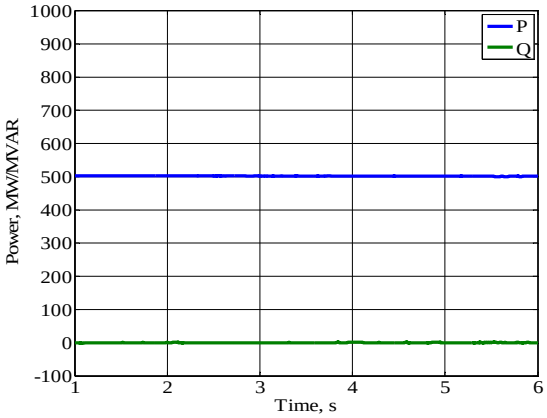

Figure 6.10 Graph of the Active and Reactive Power Delivered by WPP versus time

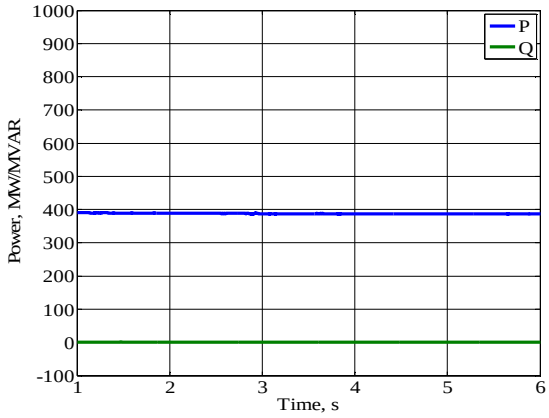

Figure 6.11 Graph of the Active and Reactive Power Received by the AC grid versus time

Figure 6.12 shows the dc voltages at the WPP converter terminals, point of tapping of tap station 1, point of tapping of tap station 2, and ac grid converter terminals.

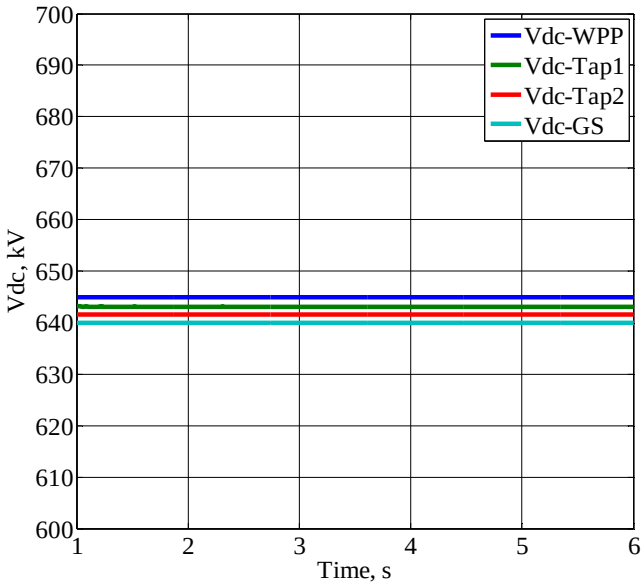

Figure 6.12 Graph of the DC voltages at Different Locations in the HVDC Line.

Figure 6.13 shows the dc currents through the HVDC line at different locations. The difference in currents through the HVDC line at the different locations represents the amount of power received by the individual tap stations.

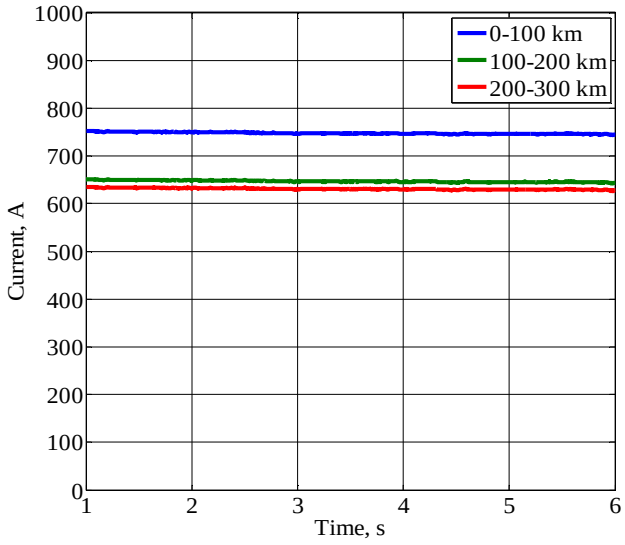

Figure 6.13 Graph of the DC currents through the HVDC line at different locations.

6.3.4. Case C

In this case, four tap stations are connected to the HVDC line of the MTDC system feeding two offshore oil rigs and two isolated small villages. Figure 6.14 shows the system diagram.

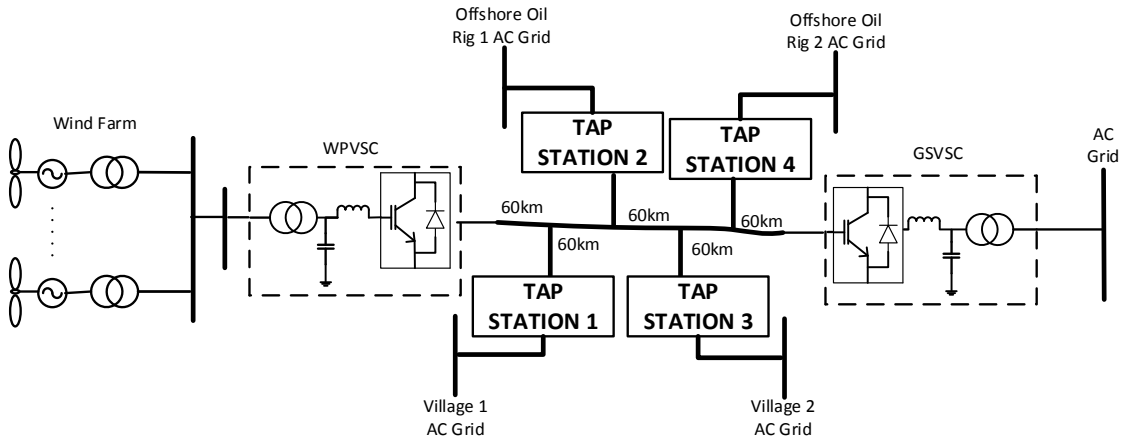

Figure 6.14 Case C System Diagram.

The tap station details are as follows:

- Tap Station 1 (Village 1)
    - Location: 60 km from the WPP
    - Require Active Power = 75MW = 15% of power transfer in the HVDC line.
    - $R_{DC\_T1} = 0.1\Omega$
- Tap Station 2 (Oil Rig 1)
    - Location: 120 km from the WPP
    - Require Active Power = 50MW = 10% of power transfer in the HVDC line.
    - $R_{DC_{T_2}} = 0.2\Omega$
- Tap Station 3 (Village 2)
    - Location: 180 km from the WPP
    - Require Active Power = 100MW = 25% of power transfer in the HVDC line.
    - $R_{DC\_T1} = 0.15\Omega$

- Tap Station 4 (Oil Rig 1)
    - Location: 240 km from the WPP
    - Require Active Power = 25MW = 5% of power transfer in the HVDC line.
    - $R_{DC_{T_4}} = 0.15\Omega$

Since the total cumulative power required by all taps is above the tapping limit of the MTDC system, the tap stations will be represented as a terminal in the MTDC system control system. Since the WPP is assumed to be capable of delivering any amount of active power required, the WPP will be controlled to provide 750 MW and the tap stations will be controlled to receive a constant amount of power equal to the required value of each individual tapping station.

Figures 6.15 and 6.16 show the active and reactive power delivered by the WPP grid and received by the ac grid respectively versus time. It can be observed that the active power received by the ac grid is closer to 500 MW in comparison to the previous two cases studies.

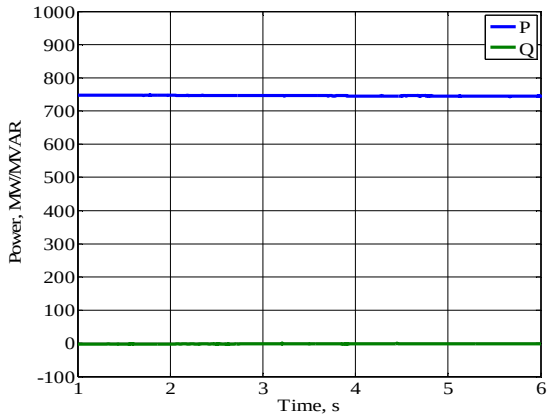

Figure 6.15 Graph of the Active and Reactive Power Delivered by WPP versus time

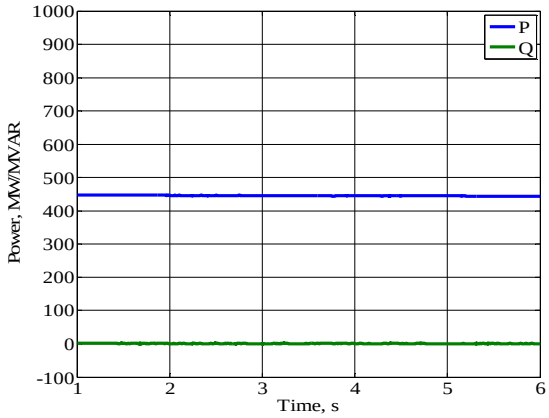

Figure 6.16 Graph of the Active and Reactive Power Received by the AC grid versus time

Figure 6.17 shows the dc voltages at the WPP converter terminals, ac grid converter terminals, and all points of tapping. Again, the DC voltage at the ac grid converter terminals is controlled at 640 kV.

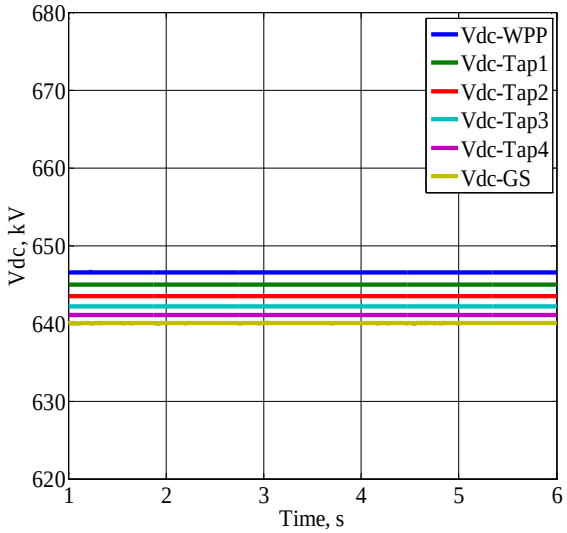

Figure 6.17 Graph of the DC voltages at Different Locations in the HVDC Line.

Figure 6.18 shows the plot of the dc currents through the HVDC line at different locations.

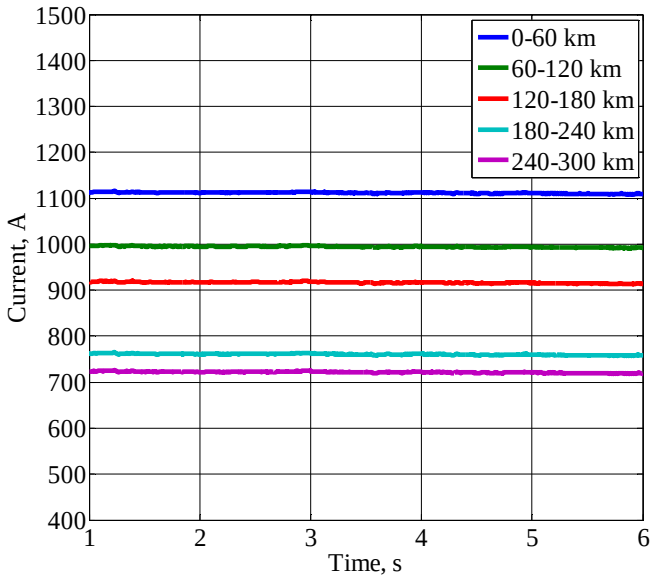

Figure 6.18 Graph of the DC currents through the HVDC line at different locations.

6.4. Summary

In this chapter, a control scheme approach for adding multiple taps on HVDC lines in MTDC systems was presented. The control scheme presented depends on factors such as the tapping limits of the MTDC system and the method of distributing the tapped power between the tap stations. Various case studies were simulated to test the control schemes and the operation of MTDC systems in the presence of multiple tap stations.

7. Chapter 7: Summary, Conclusion, and Future Work

7.1. Summary

The control and normal operation of VSC-based MTDC systems have been studied in this thesis. The typical architectures and components of a two-terminal VSC-based HVDC transmission system were initially introduced as building blocks for the discussion. A switching VSC model of the system was built in Matlab/Simulink software and a case study was simulated to validate the system control and operation.

The concept of two-terminal VSC-based HVDC system was then extended to a three-terminal HVDC system consisting of one ac grid and two WPPs. The different scenarios of active power sharing between the two wind plants based on droop characteristics were discussed. The wind plants generation limits were taken into consideration in designing the control topology. Also discussed was a three-terminal HVDC system consisting of two ac grids and one WPP. A control scheme of the active power sharing between ac grids was presented. The control methodology was based on the design of the droop constants to control the grid side VSCs for three different operational modes. The three operational modes differ in how the generated wind power is distributed between the ac grids in the MTDC system.

In addition, a generalized control scheme for an MTDC system with an arbitrary number of WPPs and ac grids was presented. The control scheme was also based on droop characteristics taking into consideration the varying nature of wind power generation output.

The difficulties and challenges of adding tap stations on HVDC lines in MTDC systems were also discussed in the thesis. A new control scheme approach for adding multiple taps on

HVDC lines in MTDC systems was presented. Several case scenarios were simulated to verify the control scheme approach and the operation of MTDC systems in the presence of tap stations.

7.2. Conclusion

The below points represent the important conclusions of the thesis:

- In a MTDC system, the output power of the WPPs can be controlled to minimize the copper losses on a system wide base. This was achieved by developing a control system based on droop characteristics to determine the reference active power of each WPP.
- In a MTDC system, the operational requirements of the DC grid can be met by controlling the DC voltage at the terminals of each GSVSC. This was achieved by developing a control system that determine the reference dc voltage of each GSVSC and adding current limiters to the DC voltage outer controllers.
- The discussion in Chapter 6 on multiple taps in MTDC systems demonstrated an approach for determining the control method of the multiple taps. It showed that the taps can be controlled independently from the MTDC system if the tapped-off power is within the tapping limit of the MTDC system. It also suggested that in the case when the tapped-off power is above the tapping limit of the MTDC systems, the tap stations can be combined into one or more groups, where each group is represented as a terminal in the MTDC system

7.3. Future Work

The MTDC systems presented in this thesis were studied from the normal operation point of view. However, studying the behavior of MTDC systems in abnormal operation is equally

important and can be the direction of future research work. Some of the topics that can be studied include:

- It is very important to study the response of the MTDC systems in the case of faults. This includes faults in the dc transmission lines, faults in the ac system of the ac grids or WPPs, and internal faults in the converters.
- Methods of fault detection to identify and classify faults is important for a safe and reliable operation of the MTDC system. In addition to that, protection methods of the MTDC systems against disturbances can also be a part of a future work.
- The control systems used in this thesis didn't account for the system losses characterized by the converter losses, dc transmission line losses, and the ac collector system losses. The system losses can be tabulated and included in the control system design.
- The objective of the control scheme of wind power plants in this thesis was to minimize the copper losses. The control presented in this research assumed that the outputs of all wind power plants are controllable. A possible research work can focus on how the objective of minimizing copper losses can be achieved if the outputs of some of the wind power plants are not controllable.
- In this thesis, a control scheme approach was presented for multiple taps on HVDC lines in MTDC systems. The approach relies on knowing the tapped-off power limit of the MTDC system. There has been very little research work created that has analytically discussed this limit. Since MTDC systems are expected to be built soon, it is really important to analytically determine the power tapping limit of MTDC systems.

References

[1] EWEA, *"The European Offshore Wind Industry – Key Trends and Statistics 1st Half 2013,"* July 2013. Accessed (2014, May 1).

[2] Craciun, B.-I.; da Silva, R.; Teodorescu, R.; Rodriguez, P., "Multilink DC transmission for offshore Wind Power integration," *Industrial Electronics (ISIE), 2012 IEEE International Symposium on* , vol., no., pp.1894,1899, 28-31 May 2012.

[3] EWEA, *"Pure Power – Wind Energy Targets for 2020 and 2030,"* 2009. Accessed (2014, May 1).

[4] Bahrman, M.P.; Johnson, B.K., "The ABCs of HVDC transmission technologies," *Power and Energy Magazine, IEEE* , vol.5, no.2, pp.32-44, March-April 2007.

[5] Mossadegh, N.; Aggarwal, R.K., "Management and viability of Multi-Terminal HVDC for offshore renewable energy networking," *Universities Power Engineering Conference (UPEC), 2010 45th International* , vol., no., pp.1,6, Aug. 31 2010-Sept. 3 2010.

[6] Flourentzou, N.; Agelidis, V.G.; Demetriades, G.D., "VSC-Based HVDC Power Transmission Systems: An Overview," *Power Electronics, IEEE Transactions on* , vol.24, no.3, pp.592-602, March 2009.

[7] Weimers, L., "New markets need new technology," in *Proc. of 2000 International Conference on Power System Technology*, vol. 2, Perth, Australia, December 2000, pp. 873–877.

[8] IEEE HVDC and FACTS Subcommittee, *"HVDC Projects List,"* April 2014. Available: http://www.ece.uidaho.edu/hvdcfacts. Accessed (2014, May 1).

[9] Long, W. F.; Reeve, J.; McNichol, J.R.; Harrison, R. E.; Fletcher, D. E.; Bowles, J.P., "Consideration for Implementing Multiterminal DC Systems," *Power Apparatus and Systems, IEEE Transactions on* , vol.PAS-104, no.9, pp.2521-2530, Sept. 1985.

[10] Biggs, R. B.; Jewell, W. T., *Summary of Multiterminal High-Voltage Direct Current Transmission Technology.* Oklahoma State University, 1984.

[11] Callavik M.; Blomberg A.; Hafner J.; Jacobson B., "The Hybrid HVDC Breaker – An innovation breakthrough enabling reliable HVDC grids," *ABB Grid Systems, Technical Paper*, Nov 2012.

[12] Prieto-Araujo, E.; Bianchi, F.D.; Junyent-Ferré, A.; Gomis-Bellmunt, O., "Methodology for Droop Control Dynamic Analysis of Multiterminal VSC-HVDC Grids for Offshore Wind Farms," *Power Delivery, IEEE Transactions on* , vol.26, no.4, pp.2476,2485, Oct. 2011.

[13] Egea-Alvarez, A.; Bianchi, F.; Junyent-Ferre, A.; Gross, G.; Gomis-Bellmunt, O., "Voltage Control of Multiterminal VSC-HVDC Transmission Systems for Offshore Wind Power Plants: Design and Implementation in a Scaled Platform," *Industrial Electronics, IEEE Transactions on* , vol.60, no.6, pp.2381,2391, June 2013.

[14] Asplund, G.; Eriksson, K.; Jiang, H.; Lindberg, J.; Palsson, R.; Svensson, K., "DC transmission based on voltage source converters," in *International Conference on Large High Voltage Electric Systems. CIGR´E 98*, vol. 4, Paris, France, 1998.

[15] Cuiqing Du, *VSC-HVDC for Industrial Power Systems*. PHD Thesis, Chalmers University, 2007, Goteborg, Sweden.

[16] Mohan, N.; Undeland, T. M.; Robbins, W. P., *Power Electronics: Converters, Applications and Design, 3rd ed.* New York, NY: John Wiley & Sons, 2003.

[17] Arrillaga, J.; Liu, Y. H.; Watson, N. R., Flexible Power Transmission: The HVDC Options. England: John Wiley & Sons, 2007.

[18] Yazdani, A.; Iravani, R., *Voltage-Sourced Converters in Power Systems,* New Jersey, NJ: John Wiley & Sons, 2010.

[19] SKM, *"Review of Worldwide Experience of Voltage Source Convertor (VSC) High Voltage Direct Current Technology (HVDC) Installations,"* March 2013. Accessed (2014, May 1).

[20] Peralta, J.; Saad, H.; Dennetiere, S.; Mahseredjian, J., "Dynamic performance of average-value models for multi-terminal VSC-HVDC systems," *2012 IEEE Power and Energy Society General Meeting,* , vol., no., pp.1,8, 22-26 July 2012.

[21] De Kerf, K.; Srivastava, K.; Reza, M.; Bekaert, D.; Cole, S.; Van Hertem, D.; Belmans, R., "Wavelet-based protection strategy for DC faults in multi-terminal VSC HVDC systems," *Generation, Transmission & Distribution, IET* , vol.5, no.4, pp.496,503, April 2011.

[22] Abdel-Khalik, A.S.; Massoud, A.M.; Elserougi, A.A.; Ahmed, S., "Optimum Power Transmission-Based Droop Control Design for Multi-Terminal HVDC of Offshore Wind Farms," *Power Systems, IEEE Transactions on*, vol.28, no.3, pp.3401,3409, Aug. 2013.

[23] Lie Xu; Liangzhong Yao; Bazargan, M., "DC grid management of a multi-terminal HVDC transmission system for large offshore wind farms," *Sustainable Power Generation and Supply, 2009. SUPERGEN '09. International Conference on* , vol., no., pp.1,7, 6-7 April 2009.

[24] Xu, L.; Yao, L., "DC voltage control and power dispatch of a multi-terminal HVDC system for integrating large offshore wind farms," *Renewable Power Generation, IET*. vol.5, no.3, pp.223,233, May 2011.

[25] Ekstrom, A.; Lamell, P., "HVDC tapping station: power tapping from a DC transmission line to a local AC network," *AC and DC Power Transmission, 1991., International Conference on* , vol., no., pp.126,131, 17-20 Sep 1991.

[26] Aredes, M.; Portela, C.; Machado, F.C., "A 25-MW soft-switching HVDC tap for ±500-kV transmission lines," *Power Delivery, IEEE Transactions on* , vol.19, no.4, pp.1835,1842, Oct. 2004.

[27] Jovcic, D.; Ooi, B.T., "Tapping on HVDC lines using DC transformers," *Electric Power Systems Research,* vol. 81 (2), Feb 2011, p.561-56.

[28] Krishnayya, P. C S; Lefebvre, S.; Sood, V.K.; Balu, N.J., "Simulator Study of Multiterminal HVDC System with Small Parallel Tap and Weak AC Systems," *Power Engineering Review, IEEE* , vol.PER-4, no.10, pp.65,66, Oct. 1984.

[29] Nnachi, A.F.; Munda, J.L.; Nicolae, D.V.; Mabwe, A.M., "Small power tapping limit on dc-link of VSC HVDC transmission system," *Industrial Electronics Society, IECON 2013 - 39th Annual Conference of the IEEE* , vol., no., pp.2175,2179, 10-13 Nov. 2013.

Appendix A

Park's Transformation

The Park's transformation can be used to transform a set of three phase voltages or currents to an orthogonal dqo reference frame that is synchronized to the power system frequency. Applying this transformation will simplify the design of controllers for power converters applied to three-phase systems. In steady-state, the abc phase domain currents as a function of time will appear as constant "dc" variables. The dq reference frame is based on the dq axis, which are orthogonal to each other, rotating at frequency ω, and placed at the angular position θ= ωt on the αβ plane. The transformation is illustrated in the following two steps:

- Transforming abc to stationary αβ0 reference frame.
    - Note that sqrt is assuming peak quantities.

$$\begin{bmatrix} v_\alpha \\ v_\beta \\ v_0 \end{bmatrix} = \sqrt{\frac{2}{3}} \times \begin{bmatrix} 1 & -\frac{1}{2} & -\frac{1}{2} \\ 0 & \frac{\sqrt{3}}{2} & -\frac{\sqrt{3}}{2} \\ \frac{1}{\sqrt{2}} & \frac{1}{\sqrt{2}} & \frac{1}{\sqrt{2}} \end{bmatrix} \begin{bmatrix} v_a \\ v_b \\ v_c \end{bmatrix} \qquad \textbf{A.1}$$

- Transforming stationary αβ0 reference frame to synchronous dq0 reference frame. This is called Park's transformation.

$$\begin{bmatrix} v_d \\ v_q \\ v_0 \end{bmatrix} = \begin{bmatrix} cos(\theta) & sin(\theta) & 0 \\ -sin(\theta) & cos(\theta) & 0 \\ 0 & 0 & 1 \end{bmatrix} \begin{bmatrix} v_\alpha \\ v_\beta \\ v_0 \end{bmatrix} \qquad \textbf{A.2}$$

Therefore, the transformation from abc to dq can be done using this equation:

$$\begin{bmatrix} v_d \\ v_q \\ v_0 \end{bmatrix} = \sqrt{\frac{2}{3}} \times \begin{bmatrix} cos(\theta) & cos(\theta - \frac{2\pi}{3}) & cos(\theta + \frac{2\pi}{3}) \\ -sin(\theta) & -sin(\theta - \frac{2\pi}{3}) & -sin(\theta + \frac{2\pi}{3}) \\ \frac{1}{\sqrt{2}} & \frac{1}{\sqrt{2}} & \frac{1}{\sqrt{2}} \end{bmatrix} \begin{bmatrix} v_a \\ v_b \\ v_c \end{bmatrix} \qquad \textbf{A.3}$$